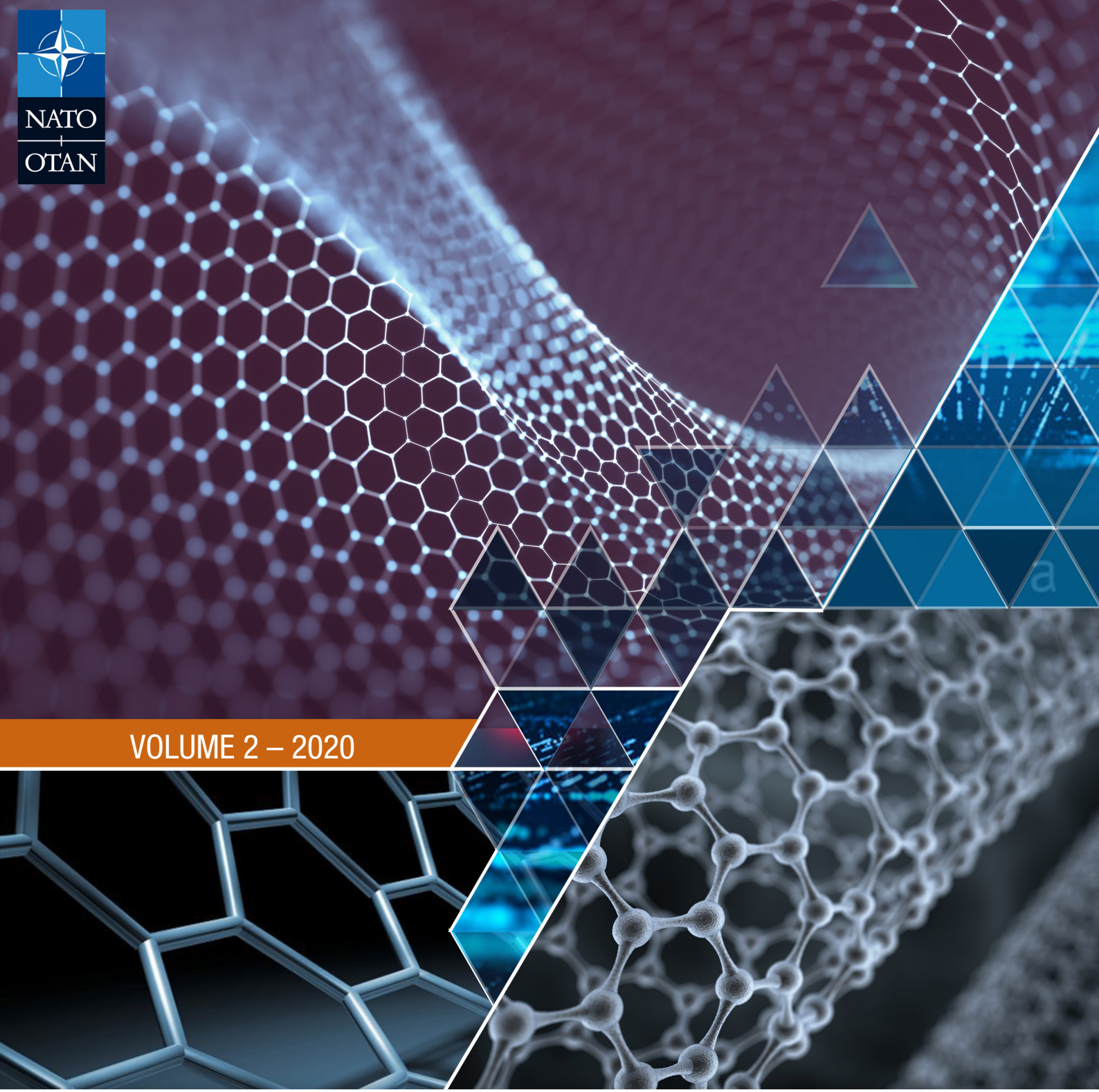

Journal of the NATO Science and Technology Organization

Applied Vehicle Technology Panel

2020 Peer Reviewed Conference Proceedings

xxx xxxxx xxxx
DOI:xx.xxxxx/STO-x-xx

Table of Contents

Content Imprint

The Journal of the Science and Technology Organization

Applied Vehicle Technology Panel

Chairman
Applied Vehicle Technology Panel
Prof Dr David Lecompte

Vice-Chairman
Applied Vehicle Technology Panel
Mr Stanley Cole

Editor
Prof Dr David Lecompte

Associate Editor
Dr Steven Savage

Editorial Team
Dr Tom Thorvaldsen
Mr Christoph Müller
Mr Donatas Rondomanskas

Purpose

By presenting the individual foci of its expert panels and by serving as a forum for its peer reviewed work, the STO Journal strives to promote the achievements emerging out of the Collaborative Programme of Work.

Disclaimer

The view and opinions expressed or implied in the AVT Panel Edition are those of the authors concerned and should not be construed as carrying the official sanction of NATO.

Terms of Use

NATO STO Collaboration Support Office (CSO) Director's Foreword

Dear Readers,

This first peer reviewed Journal of the NATO Science and Technology Organization, devoted to the topic of the Graphene research and development applications in defence, is a small sample of the intellectual strength and knowledge drawn from the NATO Collaborative S&T community. That community has been active and developing within NATO for more than 70 years, supporting NATO and the Nations in the field of Defence and Security R&D.

NATO and Nations are currently concerned about the revolutionary and rapid scientific discoveries within the civilian sphere, with the understanding that most of those discoveries will have a dual use. The most important new discoveries have been framed by NATO as Emerging Disruptive Technologies, highlighting the fact that they might have a game-changing impact on the future of warfighting and on the balance of military power.

The Graphene technologies highlighted here can be categorized within the New Materials discoveries and application EDTs framework. With this introductory volume of the NATO STO Journal, our goal is to share selected knowledge from the expert community to promote further research and development and to highlight graphene's future impact on our defence, security, deterrence, and crisis management.

Dr Pavel Zůna
Director
NATO STO Collaboration Support Office

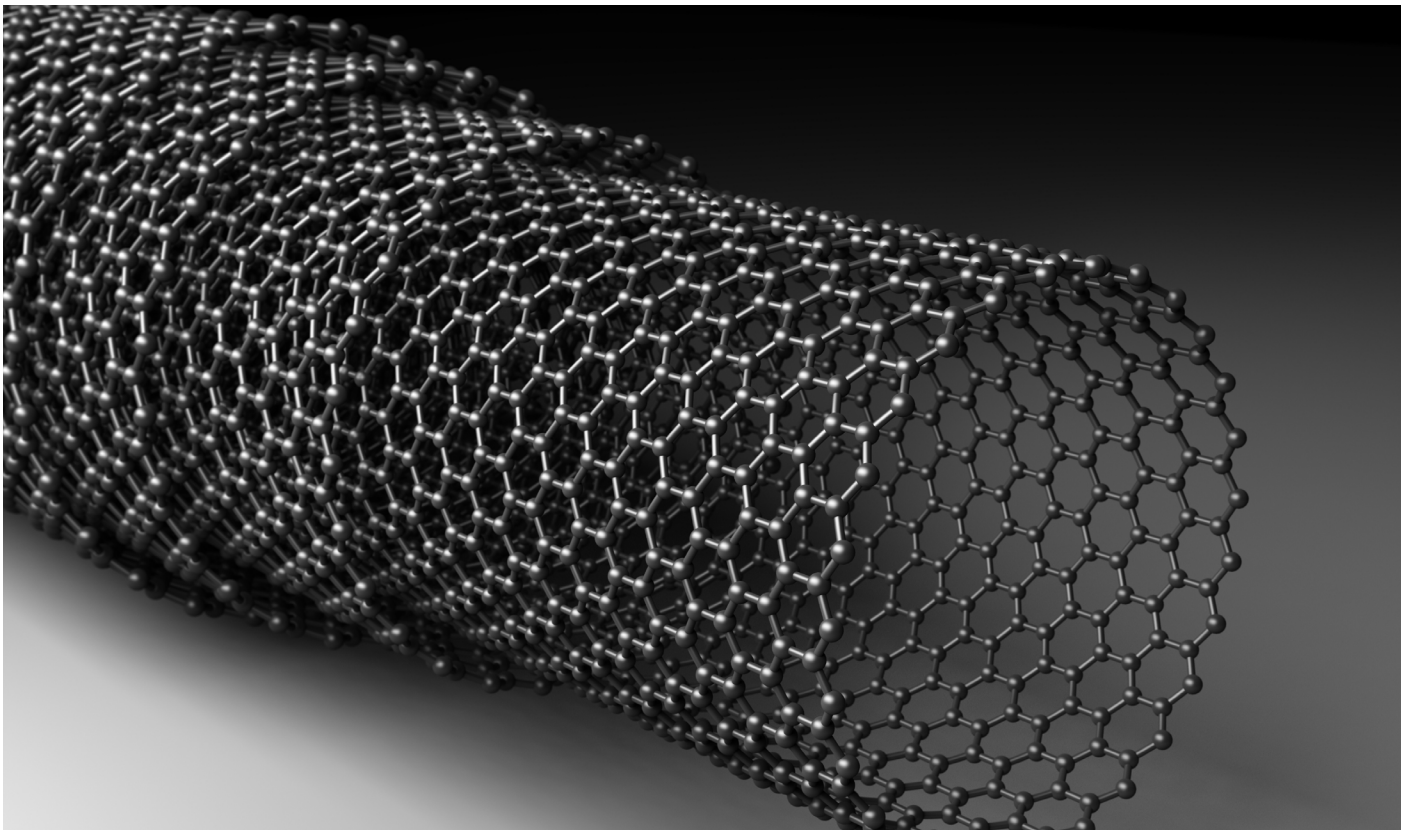

Editorial

Yet another journal?

While I am extremely honored to welcome you to this first edition of the Peer-Reviewed Proceedings of the Applied Vehicle Technology Panel, I cannot avoid imagining that the above mentioned question is gently wandering through your mind. If so, then please allow me to explain why we still consider the founding of this new journal to be a sensible and timely idea.

The Applied Vehicle Technology (AVT) Panel is one of the seven Panels within the NATO Science & Technology Organization (STO) with the mission to improve the performance, affordability and safety of vehicle, platform, propulsion and power systems operating in all environments. The focus lies on three main broad technology areas, each with their proper fields of interest: Mechanical Systems, Structures and Materials; Performance, Stability & Control and Fluid Physics; Propulsion and Power Systems. It is worthwhile mentioning that the vast NATO STO network comprises more than 5,000 scientists, engineers and research managers from governmental organizations, industry, research establishments and academia within each of the 30 NATO member states and its partner nations. They, together with their peers, are considered to be potential contributors to the present journal.

Times have changed in the world of scientific research and publishing. Researchers, now more than ever, build their careers on their numbers of indexed publications and citations. They live by their H-index, which needs to be put into perspective, but which also provides, in most scientific research domains, a worldwide accepted metric for the scientific relevance of the author. The rise of the H-index has led to a fundamental change in the way in which scientific deliverables and publications are perceived and evaluated. This evolution that has taken place over the last few decades and all of the players in the broad domain of scientific research need to adapt to it, for better or for worse. Publish or perish is now more than ever the daily tune of each and every researcher.

AGARD[1], the AVT Panel's predecessor, existed in different times when it was enough to author or co-author a Technical Report or an "AGARDograph" to be scientifically credited for the work and time invested into the research. AGARD's reputation at that time was undisputed. This has drastically changed, not because the quality of the work within the AVT Panel has decreased but because of the way in which scientific research and contributions are evaluated nowadays.

It is precisely because of the fact that the quality of the people, the researchers, their work, their papers, their contributions and presentations within the AVT Panel has not decreased that it's time for the AVT Panel to take action, adapt to the changing scientific world and capitalize on all of AVT's scientific output. This is the reason why we are convinced it is the right moment for the AVT Panel, and by extension, the NATO STO to become the publisher of its own peer-reviewed journal(s). In the first place to create the opportunity for researchers to publish their peer-reviewed papers, presented during one of the yearly organized AVT Symposia, Specialists' Meetings or Research Workshops. Naturally, it will attract young and new researchers by giving them the opportunity to publish their work in an independent NATO STO journal, which will be indexed in the different international citation databases of interest.

[1] *Advisory Group for Aerospace Research and Development*

Indexing makes the peer-reviewed papers citable and we all know that nowadays a scientific paper is most valuable when it can be cited. The existence of a dedicated but broadly scoped AVT journal, independently published by the NATO STO, is in line with this reality.

A scientific journal aiming at the publication of the AVT Panel activity proceedings under the auspices of the NATO STO and with the desire to meet the highest achievable standards in scientific research and reporting, needs an unbiased, fair, constructive, critical and expert-based peer review process. Therefore, the newly established Scientific Committee will, together with the community of peers, be the gatekeeper of the scientific and academic excellence of selected AVT Event Activities and act as the scientific and academic advisory instrument to the Panel. The Program Committee of the Event Activity, which can be a symposium, a workshop or a specialist meeting, will together with the Scientific Committee decide whether or not to publish their proceedings and undergo the peer review process.

The AVT community is a highly professional and unique mix of military, industrial, academic and governmental members and contributors, all conducting and delivering high-level research at different Technological Readiness Levels with military relevance. Therefore, we are convinced that even in a crowded world of dedicated scientific specialty journals, an important role remains for a qualitative, broadly scoped and peer-reviewed scientific journal which is relevant for all actors within the world of industrial, academic and military research on vehicle, platform, propulsion and power systems.

Prof Dr David Lecompte
Chairman
Applied Vehicle Technology Panel

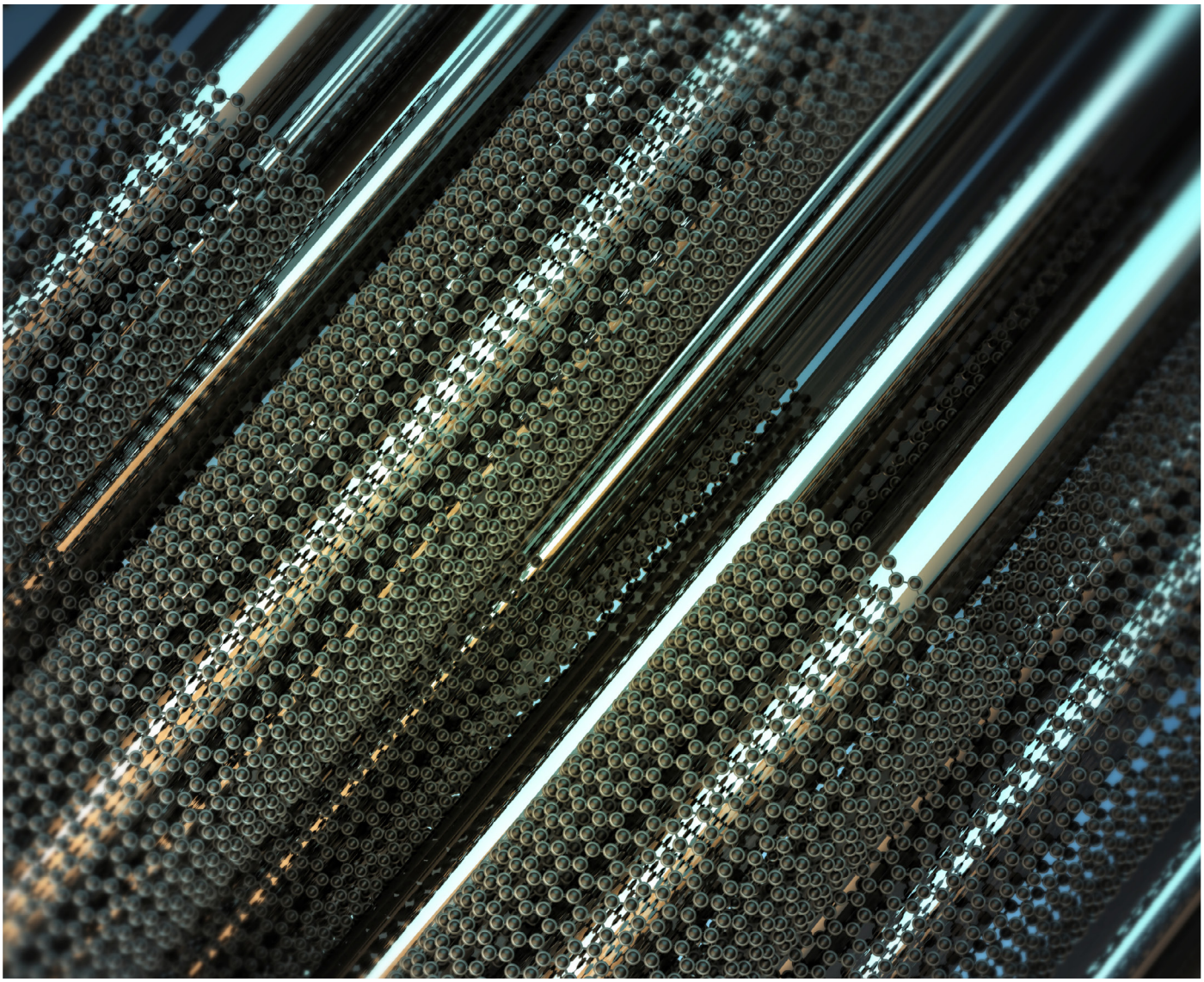

Graphene Technologies and Applications for Defence – A Research Specialists' Meeting (RSM)

Dr Steven Savage, SWE
Dr Tom Thorvaldsen, NOR

1.0 INTRODUCTION

The objective of The Journal of the Science & Technology Organization is trifold and extends beyond the traditional scope of the Organization. Firstly, the Journal will function as a medium for the dissemination of our work to the NATO STO contributing nations. Secondly, future editions of the Journal will include an outlook for the period to come and will review work the various panels have recently accomplished. Finally, but perhaps most importantly, it will serve as a peer-reviewed medium for publication of results from our Symposia, Specialists' Meetings and Workshops.

In its peer-reviewed volumes, the Journal will serve as a forum and archive for excellent conference papers and will review the work the various panels and our Programme Committees have recently accomplished. By promoting scientific excellence in topics highly relevant for defense related research and development, NATO STO supports its stakeholders to stay at the forefront of S&T.

The NATO STO AVT Panel has been the pilot to adapt the peer review process to the NATO STO environment and use the opportunity the new journal format presents to highlight a recent activity – the Research Specialists' Meeting on '*Graphene technologies and applications for defense*.' In total sixteen papers were presented during the Fall 2019 meeting in Trondheim, Norway. Of these five have been selected for publication, following peer review and based on scientific excellence and permission to publish. Hereinafter the military relevance and opportunities of novel graphene technologies are highlighted.

2.0 AVT-304: GRAPHENE TECHNOLOGIES AND APPLICATIONS FOR DEFENCE. A RESEARCH SPECIALISTS' MEETING (RSM)

Materials, and knowledge of their science and engineering applications, have facilitated human development since the Stone Age. Materials for tools, for construction, and in particular for defense, which is the focus of this, the 2nd volume of the Journal of the NATO STO are as essential today as they were then. Materials of all types, from the simple to the complex, are growing in importance as societies around the world increase in sophistication, and credible attempts are made towards colonization of other planets. The issue at hand focusses on one (class of) material with expected impact and new possibilities for current and future use, namely **graphene.**

Graphene, a two-dimensional material built up of a symmetrical hexagonal lattice of carbon atoms, is one of the most attention-grabbing material discoveries of the 21st century. For both pure and applied scientists, technologies based on the extraordinary mechanical, optical, chemical, physical and electronic properties of graphene offer much to discuss. With potential uses ranging from corrosion protection on ships to high performance rubber tires, and from multifunctional aerospace composites to energetic materials and solid propellants, there is a clear potential for a wide range of applications in defense materiel.

Exploring this potential was the objective of the Research Specialists' Meeting AVT-304 – *Graphene Technologies and Applications for Defence* held during the 44th AVT Panel Business Meeting. This issue includes selected and peer-reviewed papers from this 2-day meeting. They represent a small cross section of graphene technologies and what was presented

during AVT-304 but serve well to illustrate the diversity and the trends in research towards defense applications of graphene-based technologies.

3.0 FACTS ABOUT GRAPHENE AND OTHER 2-D MATERIALS

3.1 Graphene – The Material with Extraordinary Properties

The foundation stone for the current interest in graphene was laid when Novoselov, Geim, and co-workers published their seminal paper on the extraordinary electronic properties of graphene in 2004 [1]. For this work they were awarded the Nobel Prize in Physics only six years later. This was not however the first report about the material we now call graphene, and it is clear that the intrinsic lamellar structure of graphite oxide, a precursor used in the production of graphene today was known as long ago as 1859 [2]. A theoretical study of graphene and its electronic properties was in fact published as long ago as 1947 [3] and the term graphene was introduced by Boehm and co-workers in 1986 [4]. However, recognition of the unique combination of properties offered by graphene only became widespread during the first decade of the 21st century, since when scientific and commercial interest in this material and other materials with similar lamellar structures has grown enormously.

The electronic, optical, chemical, thermal and mechanical properties of pure graphene are now well-known. Some typical properties are given in Table 1 below.

While the individual properties of graphene are extreme compared to other materials, this is not in itself sufficient for most practical applications. It is very rare for any material to be selected for an application based on only one property. Compromises must be made, between strength, corrosion resistance, toughness, conductivity, availability, cost, etc. What makes graphene attractive for practical applications is its unique "all round" combination of several extreme properties.

The extraordinary properties of graphene arise from its atomic structure, shown schematically in Figure 1.

The graphene structure is a perfectly symmetrical 2-dimensional (2-D) arrangement of carbon atoms in a hexagonal lattice, which is only one atom thick. Each carbon-carbon bond is equal, and in pure graphene there are no defects to disturb the local atomic environment. However, pure graphene can only be produced under laboratory conditions, and for practical applications graphene will

Table 1. Brief Comparison of Graphene Properties and Other Materials.

Property	Graphene	Comparison material
Density	2.27 g/cm^3	7.75 – 8.05 g/cm^3 (steel)
Young's modulus	1034 GPa	200 GPa (steel)
Yield strength	45±7 GPa	250 MPa (steel)
Ultimate tensile strength	130 GPa	400 – 550 MPa (steel)
Failure strain	20 %	2 % (carbon fiber)
Thermal conductivity	2000 – 4000 Wm^{-1}K^{-1}	2200 – 3300 Wm^{-1}K^{-1} (diamond)
Electron mobility	40 000 cm^2 V^{-1}s^{-1}	1400 cm^2 V^{-1}s^{-1} (silicon)
Optical transparency	97.7 % @ 350 nm-2 mm	Material dependent
Permeability	Impermeable	Material dependent
Chemical stability	Stable in acid, alkali, organic solvents	Material dependent
Specific surface area	2630 m^{2}g^{-1}	100–1000 m^{2}g^{-1} (carbon nanotubes)
Bandgap	0	1.14 eV (silicon)
Magnetism	Non-magnetic	Material dependent
Melting temperature	4000°C (sublimes)	3422°C

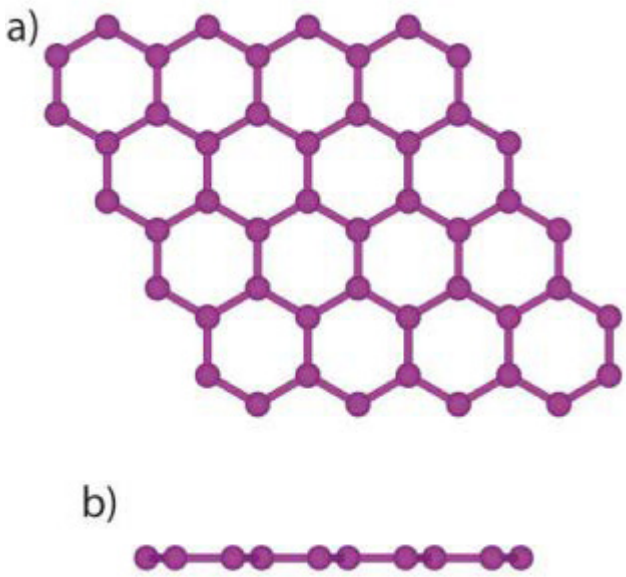

Figure 1: Illustration of a Graphene Sheet Seen from Above (a) and from the Side (b). [Copyright: L.H. Karlsson. Reprinted with permission.]

always contain imperfections and impurities, depending on the production method. Controlling the level of defects and impurities is one of the major challenges yet to be overcome, although high quality graphene can today be produced in quantities of hundreds of kilograms.

The properties of graphene can also be modified by attaching various chemical groups to the surface and edges. In this way, graphene can be made more compatible with other materials, which is especially relevant for the production and mechanical properties of graphene-polymer composites. Graphene can also be deliberately functionalized for use in chemical and biological sensors.

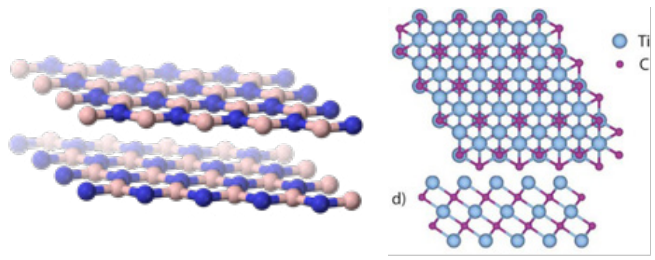

Figure 2: (Left) Illustration of Two-Dimensional Hexagonal Boron Nitride. Boron is Represented by the Blue Dots and Nitrogen by the Pink. [Copyright: Benjah-Bmm27][2] (Right) Illustration of the MXene Ti_3C_2 [Copyright: L.H. Karlsson. Reprinted with Permission].

3.2 Other Two-Dimensional (2-D) Materials

The lamellar structure of graphene is well-known, and inspired by the extreme properties being discovered, scientists began to explore other materials with similar structures. It was soon found that a large number of other two-dimensional materials with equally interesting, but different properties, exist. While these are structurally more complex than graphene, as shown in Figure 2, their different atomic compositions result in a wider variety of, in particular, electronic properties than does graphene. Today a whole new class of 2-D materials is being studied.

4.0 BACKGROUND TO THE AVT-304 RSM

4.1 Introduction/Background

Beginning from an exploratory team (AVT-ET-161 – Graphene technologies: a preliminary assessment of the military potential) back in 2016, eight nations (Bulgaria, Finland, Germany, United Kingdom, Norway, Sweden, Turkey, United States) thereafter formed a team of materials specialists in 2017 which planned and conducted the AVT-304 RSM.

Since the beginning of the 21st century enormous strides have been made in Materials Science and Engineering (MSE). Following the end of the Cold War a paradigm shift has taken place in MSE. When geopolitical tensions relaxed and concomitantly defense budgets began to shrink, cutting-edge research into materials shifted from being defense-needs driven towards meeting broader societal needs for energy efficient transport, information technology, miniaturization, mobility, environmental sustainability and healthcare. As a result, the range of materials available and knowledge of their properties is vastly greater today than at any previous time in history. Although developed for civil applications, these materials are available worldwide for defense purposes. It should be noted that the vast majority of materials are dual-use, with similar defense and civil applications.

Much defense materiel in service today was built using materials developed 50 or more years ago, before the advent of graphene,

[1] *Benjah-bmm27 grants anyone the right to use this work for any purpose, without any conditions, unless such conditions are required by law.*

additive manufacturing, electric propulsion, adaptive camouflage, high performance sensors and many of the other advanced technologies now available. As we discuss the next generation of aerospace, ground, space and marine platforms, we cannot ignore new and emerging materials currently in the "pipeline." This is not to say that existing materials have outlived their role. In many cases it is possible, and indeed likely, that existing materials, perhaps manufactured using improved methods, will continue to be important in platforms of the future. However, it is also likely that new materials, such as graphene, will give rise to new technologies and new applications. It is imperative that we evaluate and assess their strengths and weaknesses, manufacturing, availability, cost and environmental impact and their potential applications.

During the RSM, sixteen oral presentations, including two keynote lectures, and six posters were presented and displayed by scientists from nine nations (Figure 3) during this two-day meeting, which concluded with a presentation by the Technical Evaluator and a lively discussion on the way forward.

The majority of presentations were concerned with graphene technologies and their potential defense applications. However, defense

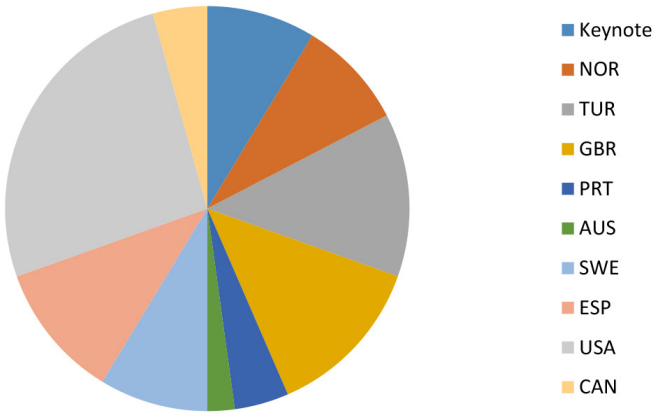

Figure 3: The National Distribution of Authors Contributing to AVT-304 RSM.

organizations are often reluctant to implement new, and unquestionably high-risk technologies, so the majority of research and development on graphene has therefore been financed by public and private investment, resulting in a growing number of civilian products.

To obtain a balanced overview and to place graphene in a broader context, a keynote presentation describing the Graphene Flagship[3] and in particular development of roadmaps was included in the RSM. A superficial roadmap of civil applications, many of which are dual-use, is given in Figure 4.

Figure 4: A Broad Roadmap Covering Civil Applications for Graphene, Many of Which Are Dual-Use. [Copyright https://graphene-flagship.eu/SiteCollecionImages/News/2018/Roadmap.png.]

[2] *Graphene Flagship,* https://graphene-flagship.eu/, *a 10-year, 1 billion euro investment in Europe.*

4.2 Applications Considered in AVT-304

The range of potential applications for graphene and related technologies is enormous. Space allows for only a few examples to be mentioned here, but the list below includes all the applications discussed during the AVT-304 RSM:

- Corrosion protection;
- Thermal management;
- Resin-transfer composites;
- Ballistic protection;
- Rocket motor insulants;
- Bearings and tribology;
- Energetic materials;
- Electro-optical, mechanical, and chemical sensors;
- Stealth technology; and
- Structural composites for aerospace.

Pure graphene, as an extremely thin 2-D layer is difficult to use alone. It is also difficult to manufacture in large quantities, although roll-to-roll production (as presented by Fisher [5]) is maturing.

Graphene shows *broadband optical transparency* and excellent *electrical conductivity*, which suggests applications as a transparent electrode in displays, for signal readout and various electro-optical sensors. Charipar et al. report in their paper [6] show how graphene can be combined with zinc oxide, a well-known optically sensitive detector material to produce a *solar-blind sensor* to detect the ultraviolet signature of a missile launch. Electronic applications, where the excellent electrical conductivity is beneficial are also possible, and a prototype broadband VIS-SWIR has recently been marketed. However, because graphene lacks a natural bandgap other 2D materials may be more suitable for some electronic applications due to their inherent bandgaps.

Graphene is extremely *impervious* even to small molecules such as gases and water vapor, suggesting applications which depend on barrier properties. It is impractical to use pure graphene in these applications, but this material can be used to enhance the properties of various types of *coatings* and *membranes*, e.g., *corrosion protection and personal protection* in gloves and clothing. There are other, less obvious, but nonetheless attractive applications, which benefit from *impermeability*. Polymers are relatively porous and easily absorb organic solvents and water, which leads to dimensional changes and changes in mechanical properties. This is a well-known problem with carbon fiber composites. Reducing the absorption rate and amount of absorbed solvent/water can lead to improved dimensional stability and reduced degradation of mechanical properties of composites in hot and humid environments.

Composites are invaluable in modern defense materiel, from structural composites in aerospace, surface vessels and ballistic protection to functional composites in rubber products, such as tires and seals, and in self-lubricating bearings. Fiber-reinforced composites, while having excellent mechanical properties in two dimensions frequently suffer from poor interlaminar fracture toughness, and poor electrical and thermal conductivity. All these parameters can be improved by the addition of small quantities of graphene flakes to the resin matrix, resulting in improved impact tolerance, reduced sensitivity to lightning strike and improved thermal conductivity. Graphene composites show important potential for aerospace applications, and they are being studied by all the major aerospace companies. Robles et al. [7] discussed the production of graphene-enhanced fiber composites by resin-transfer molding and showed that Young's modulus was improved, but at the expense of tensile strength. Okan et al. [8] showed that functionalizing graphene with oxygen functional groups was successful in improving the mechanical properties of the graphene-resin interface in fiber composites. Graphene may also be combined with bio-based fibrous composites, as presented by Abreu et al. [9], who showed interesting antibacterial properties and improved electromagnetic shielding properties of these composites. The terahertz spectrum is growing in importance in several areas of sensor technologies, and the terahertz absorption of graphene-epoxy composites was presented by van Rheenen and co-workers [10].

Thermal management is a growing problem in aerospace, where the power of electronic components is increasing while the space available for heat dissipation is decreasing. The high thermal conductivity of graphene can be useful in thermal management, as shown by Caylan et al. [11].

Ballistic protection systems are of course specific defense applications, and the mechanical properties of graphene are undoubtedly attractive to study in this application. However, strength alone is not sufficient, and the application is fraught with difficulty. A brief review by Savage [12] and preliminary studies by Gago et al. [13] suggest there is some potential, but much work remains before it can be established if there is a practical potential for graphene in ballistic protection.

4.3 Selected Papers from AVT-304

Five papers from AVT-304, each describing original research, have been selected for publication in this issue. These papers were selected on the basis of:

1. Scientific quality;
2. Clear relevance for defense; and
3. Cleared for public release.

A single-blind peer review was performed. These papers represent a small cross-section of what was presented during AVT-304, but serve well to give examples of graphene technology and trends towards defense applications. Many applications for graphene technologies are dual-use, and in these cases it is not motivated for defense organizations to invest heavily in research during their early development. It is however important to monitor their progress and evaluate their defense relevance. However, some applications are clearly defense oriented. These include a range of electro-optic sensors, ballistic protection, high performance structural materials, functional materials for warheads, and energetic materials. Papers on all these topics were presented at the RSM, and with the exception of ballistic protection, examples are included in this issue. Ballistic protection is excluded because of the complexity of the materials requirements and current lack of knowledge regarding graphene in this application.

In addition to the papers published here, two invited keynote papers were presented. The first, by Reiss [14] gave an excellent overview of the road-mapping activities of the Graphene Flagship, and the second, by Selegård [15] gave an introduction to the potential for multifunctional applications of graphene in aerospace. Although the focus of AVT-304 was on graphene technologies, a general introduction to related 2-D materials was given by Karlsson [16].

An essential aspect of the RSM was an independent evaluation of the work presented. The report by Dryfe [17] was presented at the end of the RSM and was followed by a lively discussion. In line with the applied nature of the work presented in the RSM, an analysis of graphene technologies following the DOTMLPFI methodology was also performed. This analysis is given in the appendix at the end of this introduction.

Production of graphene in sufficient quantities, of the appropriate quality and at an affordable cost is a prerequisite to any practical application, be it in batteries for energy storage, energetic materials or structural composites. Beukes et al. [18] report studies of a novel, plasma enhanced chemical vapor deposition process and the graphene flakes and coatings which can be produced by the *FORZA* process. While this is still some way from being an established production method, it is clearly an important step beyond laboratory-scale experiments. Other presenters also considered production and processing challenges, including high shear-rate methods to incorporate graphene homogeneously in a polymer matrix for structural composites and mechanical milling for self-lubricating graphene-polymer composites for wear-resistance bearings.

Polymer *composites* are used extensively in many defense applications, particularly those needing a combination of properties including high stiffness and strength, impact resistance, electrical and thermal conductivity. Polymer composites modified by the addition of graphene offer a wide range of properties, which, depending on the polymer and the

graphene addition, can be tailored for a specific application. However, incorporating graphene into a polymer is far from simple, especially on the industrial scale. Many processes which work satisfactorily on the laboratory scale are simply not suitable for industrialization. Lynch [19] describes a novel, high shear-rate melt-processing method starting from mined graphite, which requires minimum pre-processing. The process appears to be scalable, and it demonstrates its applicability for composite production using several high performance polymers. The composite produced was combined with a novel electroplated metal-foil coating. The plated graphene polymer composites showed a number of improved properties, although it is clear there is potential for further improvement through optimization of the process.

Energetic materials are essential components of many weapons systems, warheads and propellants. Depending on the application, it is necessary to tailor, and/or maximize the energy content or release rate of the material during burning or detonation. Aluminum is frequently added to energetic compositions to increase the energy content but using aluminum in its optimal form as nanopowders suffers from reduced burn rate due to the relatively thick oxide layer which forms. This reduces the energy content and the release rate. By protecting the nanopowders with graphene oxide it is possible to reduce the formation of the aluminum oxide, and simultaneously add (through the graphene oxide) additional oxygen to the composition. A number of literature reports indicate improvements obtained include burn rate, thermal stability, and energy release, combined with reduced sensitivity for electrostatic discharge, impact and shockwave. Gottfried [20] has used a novel analytical method: Laser-Induced Air Shock from Energetic Materials (LASEM) for high resolution, laboratory-scale studies of the detonation of trinitrotoluene (TNT) with additions of different sizes of aluminum powders, and with and without coatings of graphene oxide. Significantly enhanced energy release rates were observed for the aluminum nanopowders coated with graphene oxide. Although these results are promising, the need for further study of the effects of impurities was highlighted.

Continuing on the theme of warheads, Torry and Whittaker [21] propose the use of graphene to improve the performance of an inert component, that is, the *insulant* between the solid-fuel propellant and the wall of the combustion chamber in a rocket motor. Filled elastomer composites are frequently used, which can lead to problems if the propellant (or more specifically low molecular weight components such as plasticizers of the propellant) diffuse into the insulant. This leads to degradation of the propellant. Graphene is well-known to be impermeable and to provide an excellent diffusion barrier, in addition to possibly improving mechanical properties of the insulant. Tests on a graphene-modified insulant showed that diffusion of dioctyl adipate, a commonly used binder in solid propellants into the insulant, was significantly reduced. This suggests a route to extending the usable lifetime of the rocket motor. The graphene-modified insulant may also enhance the mechanical and thermal performance of the insulant. This may provide additional benefit because hot gases from burning propellant, leaking through the insulant can also degrade / severely damage the rocket motor casing and other components of the rocket motor during flight, which can lead to total failure of the missile system.

Electro-optic sensors are essential for modern information gathering. Fundamental to the sensor is the detector, where incoming information carriers in the form of photons of different wavelengths are converted to electrical signals. Ultraviolet sensors are of increasing interest because they can be used for missile launch detection, and there is an atmospheric window which can be used. The detector needs a transparent (to the photons of interest) and electrically conductive electrode. Graphene, with its broadband transparency and extraordinary electrical conductivity is an obvious candidate, which is compatible with the zinc oxide photodiode detectors. Graphene's excellent flexibility also opens for the possibility of making non-planar conformal arrays, which is not possible using conventional detector materials. The potential for ultraviolet detectors with ultrafast response times combined with high sensitivity has been explored by Charipar et al. [6].

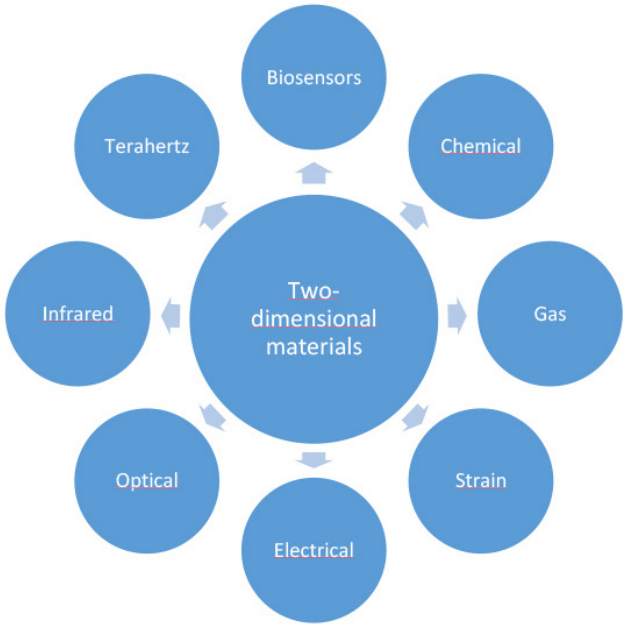

Figure 5: Various Sensors Possible Using Graphene and Other Two-Dimensional Materials. [Copyright L.H. Karlsson, 2019 and used with permission].

It was noted that while graphene alone is not an ideal photodetector, graphene/zinc oxide in combination offer high responsivity, high detectivity and fast response.

Graphene offers many other opportunities for sensor applications, which take advantage of the lightweight, large surface area, broadband absorption and chemical sensitivity with electrical readout using graphene. Karlsson [16] gave a broad overview of the sensor applications for graphene and related 2D materials, summarized in Figure 5, and Lam [22] et al. discussed the broadband applications of graphene sensors, from shortwave ultraviolet to longwave infrared. Lock [23], described a graphene-based chemical sensor to detect sulfur contamination in logistic fuel for fuel cells. This sensor has reached a TRL of 7 – 8.

5.0 SUMMARY AND THE WAY FORWARD

The field of graphene technologies is very dynamic. During the three years of the AVT-304 activity numerous new applications have been proposed. Many applications have reached higher Technology Readiness Level (TRL) and a growing number of civil products are available. It is clear that many applications are dual-use, and that at lower TRL (below about 5) most research is published in the open scientific literature. This is an immense advantage to the defense scientist since it means that much research and development does not need to be funded from defense budgets. However, it is essential that defense organizations intensify efforts to monitor and evaluate new results against defense needs, and to fund research and development in those essential applications where there are no dual-use drivers. These are typically ballistic and chemical protection, signature management, sensor technologies, weapons systems and their components including energetic materials.

It is therefore pleasing to note that the AVT Panel recently (May 2020) approved a new exploratory activity – AVT-ET-213 on The Military value of graphene technologies – to continue to evaluate graphene technologies, with a remit to focus on electro-optical sensors, propulsion, structural composites and protective coatings including signature management. This activity will continue until the Fall 2021 and will consider proposing follow-on activities in the AVT Panel.

The complete program of presentations and posters from AVT-304 is available from Science Connect. Some papers may require login.

6.0 ACKNOWLEDGEMENTS

The valuable work of materials specialists from nations which contributed to AVT-304, and in particular of the Technical Evaluator, is gratefully acknowledged. These nations are Sweden and Norway (co chairs), Bulgaria, Finland, Germany, Turkey, United Kingdom and United States. Without the excellent work of the scientists who performed peer review of the papers this issue of The Journal of the Science & Technology Organization would not have been possible.

7.0 REFERENCES

[1] Novoselov, K.S., Geim, A.K., Morozov, S.V., Jiang, D., Zhang, Y., Dubonos, S.V., Grigorieva, I.V., Firsov, A.A. Electric field effect in atomically thin carbon films. Science 306(5696):666-669, 2004.

[2] Brodie, B.C. On the atomic weight of graphite. Trans. R. Soc. 149:249-259, 1859.

[3] Wallace, P.R. The band theory of graphite. Phys. Rev. 71(9):622-634 ,1947.

[4] Boehm, H.P., Setton, R. and Stumpp, E. Nomenclature and terminology of graphite intercalation compounds. Carbon 24(2):241-245, 1986.

[5] Fisher, T.S. Roll-to-roll plasma chemical vapor deposition for scalable graphene production and electro-mechanical applications. AVT-304, October 2019.

[6] Charipar, N.A. et al. Applications of graphene as a transparent conductor. AVT-304, October 2019.

[7] Barroeta Robles, J. et al. Resin Transfer moulding processing and properties of graphene-enhanced glass fiber laminate composite. AVT-304, October 2019.

[8] Okan, B.S. et al. Design and manufacturing of high performance graphene and carbon fiber reinforced hybrid nanocomposites. AVT-304, October 2019.

[9] Abreu, I. et al. Versatile graphene-based fibrous systems for military applications. AVT-304, October 2019.

[10] van Rheenen, A.D. et al. Transmission of terahertz waves through graphene/epoxy samples – Correlation with electrical conductivity. AVT-304, October 2019.

[11] Caylan, O.R. et al. Graphene/copper heterostructures for thermal management. AVT-304, October 2019.

[12] Savage, S.J. Graphene for ballistic protection. Swedish Defence Research Agency FOI-R-4639-SE, October 2018.

[13] Gago, I. et al. Graphene-SiC Nanocomposites for new body armour systems. AVT-304, October 2019.

[14] Reiss, T. The graphene technology and innovation roadmap. AVT-304, October 2019.

[15] Selegård, L. Graphene, enabling compact and efficient aircrafts through multifunctionality. AVT-304, October 2019.

[16] Karlsson, L.H. Novel two-dimensional materials for sensor applications. AVT-304, October 2019.

[17] Dryfe, R.A.W. AVT-304 specialists' meeting on graphene technologies and applications for defense: technical evaluation report. AVT-304, October 2019.

[18] Beukes, J.A. et al. Plasma enhanced chemical vapor deposition reactor for large-scale production of high quality graphene. AVT-304, October 2019.

[19] Lynch, J. High performance, lightweight graphene enhanced polymer matrix composites for defense applications. AVT-304, October 2019.

[20] Gottfried, J.L. et al. Measuring the fast and slow energy release of laser-excited Al/GO composites. AVT-304, October 2019.

[21] Torry, S. and Whittaker, J. Graphene barrier coatings for solid rocket propellant insulants. AVT-304, October 2019.

[22] Lam, S.Y. and Pedlar, I. Graphene sensors for defense applications. AVT-304, October 2019.

[23] Lock, E. Novel graphene functionalization approach leading to ultrasensitive, robust and fast sulfur contaminants detection in aviation fuels. AVT-304, October 2019.

APPENDIX

An analysis of the potential impact of graphene on defense capabilities, using the DOTMLPFI scheme.

DOTMLPF is defined in the Joint Capabilities Integration and Development System of the U.S. DoD and used to define acquisition requirements and evaluation criteria for future defence programs. As such it is a suitable tool to analyze the potential impact of graphene technologies on future defence capabilities. NATO uses a similar tool with the addition of Interoperability, to take into account the additional requirements of a multilateral force. The U.K. MoD uses a similar tool with

the acronym TEPID-OIL. A more recent implementation of DOTMLPF also includes Policy, i.e., DOTMLPF-P. In this analysis we used the NATO implementation of the tool.

D: Doctrine

It is unlikely that the use of graphene technologies will have an immediate effect on military doctrine unless graphene enables a completely new and to date unavailable technology which could be implemented in new materiel. A new or much improved camouflage or weapon system might have an impact on doctrine.

O: Organization

It is unlikely that the use of graphene technologies will have an immediate effect on military organization, unless improvements in materiel are so profound as to affect, e.g., the numbers of personnel needed for a mission.

T: Training

It is unlikely that the use of graphene technologies will have an immediate effect on training of military personnel unless improvements in materiel are so profound that mission profiles, e.g., the use of a new and effective camouflage technology become possible.

M: Materiel

It is **highly likely** that the use of graphene technologies will affect the performance of defence materiel, in ways that are difficult to foresee. See below for a more detailed analysis.

L: Leadership

It is unlikely that the use of graphene technologies will have an immediate effect on military leadership.

P: Personnel

It is unlikely that the use of graphene technologies will have an immediate effect on military personnel.

F: Facilities

It is **highly likely** that the use of graphene technologies will have an effect on military facilities. See below for a more detailed analysis.

I: Interoperability

It is unlikely that graphene technologies will have an immediate effect on interoperability between NATO forces.

Detailed Analysis

Materiel

Implementing graphene technologies into defence materiel to improve performance and/or economy is the raison d'être for this study, and it is certain that many aspects of military materiel will be affected. Design and manufacturing must be adapted to take account of new properties and property combinations, and maintenance procedures and schedules will be affected. Repair processes will also be affected. To take one example, if graphene-based technology is used as lightning protection on airplanes the repair process after a lightning strike may be simplified. If a graphene-based sensor is used then that sensor will have properties unlike existing sensors and must be maintained in a different way. Supply chains will need to be updated as graphene technologies do not appear in existing chains, and suppliers will need to adapt. Possibly new suppliers will need to be found, and new certification procedures must be developed, e.g., if graphene-based energy storage (batteries) are implemented in materiel. This latter application seems quite likely within the near term although not in large volumes.

Facilities

To a lesser extent facilities will also be affected by the use of graphene technologies, especially repair and maintenance resources. New safety routines will need to be developed, and perhaps new or modified storage conditions will be needed. Since graphene technologies are expected to increase the robustness of materiel, it is expected that the requirements for storage facilities can be relaxed. However, for maintenance and repair it is possible that new tools may be needed.

High Performance, Lightweight Graphene Enhanced Polymer Matrix Composites for Defense Applications

Jennifer Lynch
Rutgers University, Materials Science and Engineering Department
607 Taylor Road, Piscataway, NJ 08854
UNITED STATES
Email jklynch@soe.rutgers.edu

Keywords: Composites; Exfoliation; Flakes; Graphene; High Shear; Nanometal; Properties; Scalable.

ABSTRACT

Modern defense applications require a new class of lightweight materials that offer high performance and multi functionality. Graphene-Polymer Matrix Composites (G-PMCs) are promising structural materials due to the exceptional properties of graphene and are poised to replace heavier, traditional materials in a broad array of applications. However, graphite to graphene conversion has proven costly, and most G-PMCs suffer from weak graphene-polymer interaction and an inability to incorporate high graphene concentrations. This research demonstrates a general approach to produce G-PMCs using in situ shear exfoliation of mined graphite directly within a molten polymer, thus forming a G-PMC with a uniform distribution of graphene, few-layer graphene, and multi-layer graphene, hereafter called Graphene Nanoflakes (GNFs). This method provides strong graphene matrix bonding and the possibility for high graphene concentrations, resulting in lightweight, high performance composites with multifunctional, tunable properties, including high modulus, high impact strength, electrical conductivity, thermal conductivity, and barrier resistance to small gases. Several polymers used in this work to prepare G-PMCs show an increase in tensile modulus ranging from 200 – 530 %, depending on the polymer chemistry. G-PMCs may be enhanced further with an overlay coating of nanostructured metals using electrochemical deposition to provide additional property benefits while maintaining low density. Lightweight, high performance G-PMCs prepared using this scalable, low cost method are potential solutions to structural applications for land, sea, air and space platforms; damage tolerant composite materials; lightweight, high performance ballistic protection, multifunctional coatings for corrosion and wear resistance; fibers and textiles; sensors including electro-optical and radar, and other electronic applications; sensors; energy storage; and manufacturing and scalability.

1.0 INTRODUCTION

Graphene enhanced Polymer Matrix Composites (G-PMCs) have the potential to become a disruptive technology, offering many benefits compared with traditional materials for modern defense applications. The electrical [1], [2], thermal [3], [4], and mechanical [5], [6], [7], [8] properties of graphene-based PMCs have been investigated. Most such composites have not yet realized significant mechanical property improvements, apparently due to weak graphene-polymer interaction and an inability to incorporate high weight concentrations of graphene [9]. Hence, research is underway to chemically modify graphene to enhance bonding with the polymer matrix and improve mechanical performance [10], [11], [12], [13], [14], [15]. Further, effective exfoliation of graphite using melt-processing methods was considered nearly impossible [9].

The unique melt-processing method used in this work imparts repetitive, high shear strain rates, resulting in pure shear, elongational flow and folding that enable graphite exfoliation into graphene, few-layer graphene, and multi-layer graphene (hereafter called Graphene Nanoflakes; GNFs) directly within a molten polymer, resulting in a high performance, lightweight G-PMC [16], [17], [18]. During shear

exfoliation within a molten polymer, new, pristine GNF surfaces are created, providing the opportunity for surface crystallization of the polymer and good planar adhesive bonding. Fracture of GNFs across the basal plane exposes dangling orbitals, which we suggest enables edge-covalent bonding with certain polymer matrices [19]. Thus, this method removes the need to firstly, exfoliate graphite and secondly, chemically modify the graphene prior to melt-processing. Rather, in this work, the raw material is graphite, and functionalization occurs in situ between newly created GNFs and the polymer.

Other in situ graphite exfoliation methods using melt-mixing have been presented. Expanded graphite has been exfoliated in nylon 6 using twin screw extrusion at 5, 10, and 20 wt. % [20], using twin screw extrusion up to 70 wt. % graphite [21], and using a Brabender internal mixer equipped with contrarotating blades at graphite concentrations up to 60 wt. % [22]. These methods show interesting results for graphite that must be expanded prior to exfoliation. Expanded graphite was exfoliated within an elastomer using a melt-processing method, but the method required several steps, including functionalization of the expanded graphite with maleic anhydride, ultrasonication, solvent removal prior to melt-processing in the elastomer, recovery of the functionalized graphene, and composite preparation of the functionalized graphene and elastomer using a two roll mill [23]. Graphite has been exfoliated within an elastomer using multiple passes through a three-roll mill, however, low concentrations (maximum of 5 wt. % graphite) were used [24]. Graphite Intercalated Compound (GIC) and expanded GIC have been exfoliated within polyamide to produce thermally conductive composites, however, this required pre-treatment of the graphite, and it is not clear if exfoliation created graphene from the GIC and expanded GIC within the polyamide [25]. There are other direct exfoliation methods reported, typically requiring multiple steps and lower graphite concentrations, including solution and polymerization in the presence of the exfoliated graphite or GIC [26], [27] emulsion polymerization [28], exfoliation of graphite within a solution followed by combination with the polymer [29]. A very different process reports in situ exfoliation of graphite in the solid state to form graphene/polyamide 6 nanocomposites, however, only low graphite concentrations have been used (maximum 5 wt. %) with a small increase in modulus of 29% [30].

The general method presented here requires only two components; graphite and a polymer, and requires no pre treatments. It is applicable to a wide range of thermoplastic polymers, including aerospace-grade polymers, such as Polyetheretherketonre (PEEK) and Polysulfone (PSU), to common polymers, like High Density Polyethylene (HDPE) and Polystyrene (PS), which provides great opportunity for tunable properties and broad applicability into several defense applications. This method is applicable to a wide range of concentrations of GNFs, from fractional to 50 wt. % in the polymer; however, for this work, a GNF concentration of 35 wt. % was selected, to optimize mechanical property improvements. Other properties of graphene may be exploited to impart multifunctionality to these G-PMCs. For example, optimization of electrical conductivity, thermal conductivity, wear resistance, and barrier resistance to small gases are potential areas to explore. Manufacturing G-PMCs is extremely versatile, since standard polymer processing methods may be utilized, including injection molding, extrusion, additive manufacturing, etc. Thus, mass production of complex shapes is viable for G-PMC components.

Properties of theses G-PMCs may be further enhanced by secondary processes. For example, an integrated process was used to fabricate G-PMCs with an overlay coating of nanostructured metals (Nanometal) using an electrochemical deposition process at Integran Technologies, Inc. [31], [32], [33], [34], [35], [36], [37]. Under a cooperative research project (sponsored by ONR-BAA: N00014-14-1-0046), Nanometal coated G-PMCs were investigated as a potential material for lightweight armor applications. The G-PMC was developed at Rutgers University, and the Nanometal coating was developed and applied by (subcontractor) Integran Technologies, Inc. located in Canada. Development of lightweight Nanometal coated G-PMCs was relevant to the Navy's Force Protection Thrust in that it intended to provide blast and ballistic protection for transportation

vehicles. Nanometal coated G-PMCs are lightweight and offer high flexural modulus and impact resistance.

2.0 EXPERIMENTAL METHOD

2.1 Sample Preparation

G-PMCs were prepared from mined, well-crystallized graphite (Asbury graphite mills grade 3627, 99.2% purity, average diameter 250 – 300 µm) in combination with PEEK (Solvay Specialty Polymers, Ketaspire KT 820 NT), PSU (Solvay Specialty Polymers, Udel P-1700 NT), PS (Polyone, general purpose GPPS7), and HDPE (Exxon 7960) [16]. To remove water and other volatiles prior to processing, graphite, PEEK, and PSU were placed in a furnace at 400 °C for four hours, 165 °C for six hours, and 160 °C for six hours, respectively. PS and HDPE do not require pre-drying. Dried graphite and the selected polymer were dry-blended by adding each component in a concentration of 35 wt. % graphite and 65 wt. % polymer into a small container in 50-gram batches and shaking to disperse the components evenly. Several 50-gram batches were prepared for each G PMC system to total between 1 – 3 kg and melt-processed using uniform, high shear to exfoliate graphite into GNFs directly within the molten polymer, during which homogeneous mixing of the GNFs within each matrix was achieved. Graphite concentration of 35 wt. % was selected for this work to optimize mechanical property improvements, based on previous results [19], but can be easily varied to optimize for the desired property. A high GNF concentration was selected in order to have a significant effect on mechanical properties but not too high to cause complications with processing and part fabrication. A Negri Bossi V55-200 injection molding machine was used to fabricate ASTM D638 Type I tensile specimens with dimensions 3.33 mm x 12.5 mm x 165 mm. This same melt-processing method was followed to produce pure polymer tensile specimens as a control for each G-PMC sample.

The PEEK-based G-PMC, labelled as 35G-PEEK, was selected for coating with Nanometal at Integran Technologies, Inc. using their patented electrochemical deposition process. NanovateTM N1210 NiCo alloy [38], [39] was applied to 35G-PEEK at thicknesses of approximately 75 and 182 µm. For this exploratory work, two thicknesses were selected in order to determine the effect of coating thickness on the mechanical properties

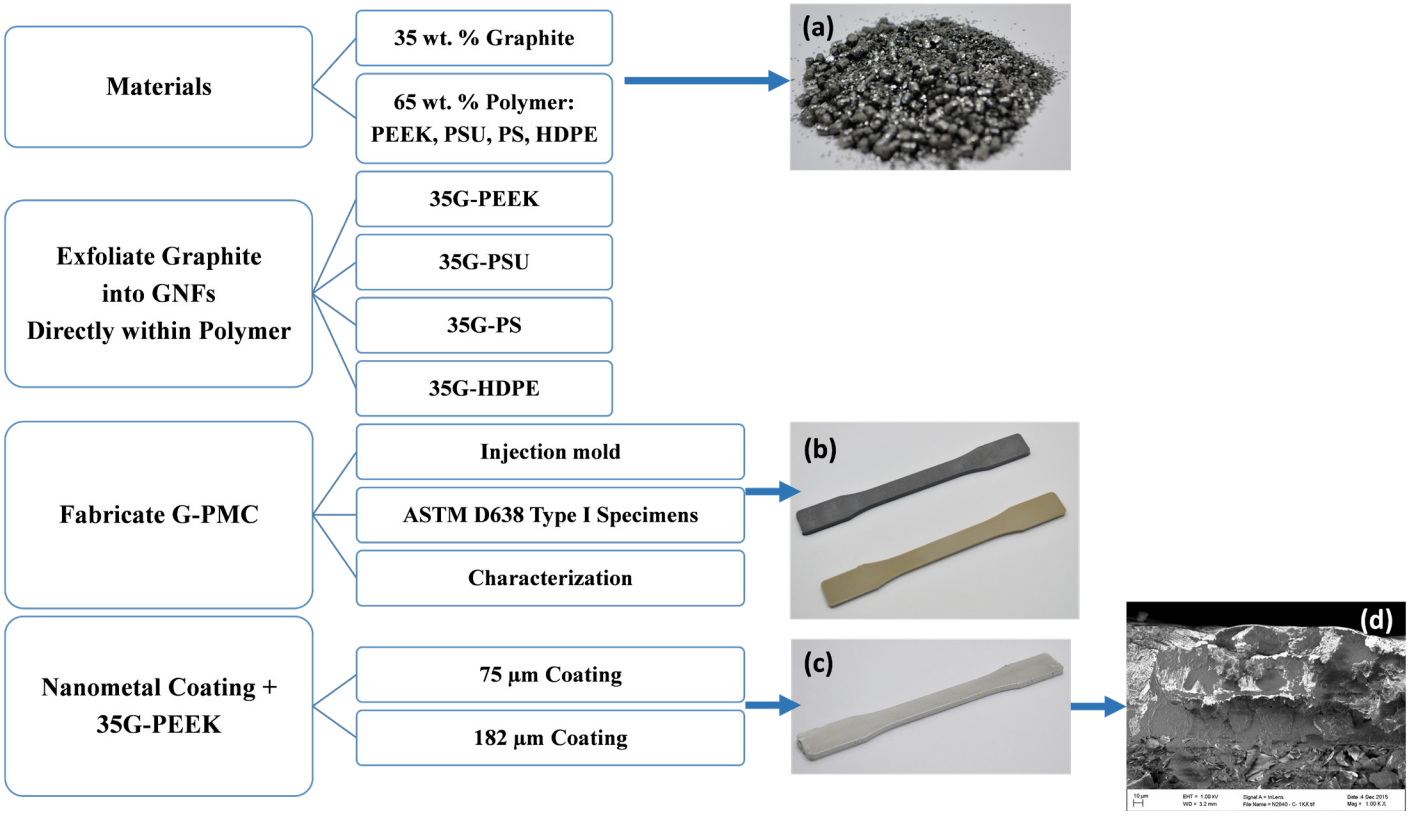

Figure 1: Experimental Method Schematic Diagram and (a) Dry-Blended Graphite and Polymer Resin, (b) Injection Molded ASTM Specimens (Black Is 35G-PEEK and Amber Is PEEK), (c) Nanometal Coated 35G-PEEK Injection Molded Specimen, and (d) SEM Image of Nanometal Coating on 35G PEEK.

and to determine the minimum thickness required to add beneficial properties. The coating thickness may be optimized for a particular application to provide sufficient property enhancements. A schematic diagram of the experimental method appears in Figure 1, showing the (a) Materials dry-blended (graphite and polymer resin pellets), (b) Injection molded specimens used for characterization (black specimen is 35G-PEEK and the amber specimen is PEEK), (c) Nanometal coated 35G-PEEK specimen, and (d) SEM image of the fracture surface of Nanometal coated 35G-PEEK.

For electrical conductivity and sensor testing, PSU was selected as the matrix for the G-PMC, based on preliminary data collected comparing different matrices. From this preliminary data, G-PSU incurred the highest electrical conductivity compared with the other matrices tested. The sample preparation is the same as previously described, except two concentrations of graphite were selected to be exfoliated within PSU, including 20 and 40 wt. %, labelled 20G-PSU and 40G-PSU. Below 20 wt. %, electrical conductivity of G-PSU was minimal, and above 40 wt. %, melt-processing became more difficult. Thus, the lower and upper limits used in this study were 20 and 40 wt. % GNFs in PSU.

2.2 Characterization

2.2.1 Morphology and Mechanical Properties

The morphology and mechanical properties of each G-PMC and the corresponding base polymer were investigated. The morphology was viewed using a field emission scanning electron microscope (Zeiss Sigma FESEM with Oxford EDS, operated at 5kV or 20 kV) to verify graphite exfoliation into a distribution of graphene, few-layer graphene, and multi-layer graphene, and to view GNF-matrix interaction. Samples were prepared by cryogenic fracture, mounted on typical aluminum studs with carbon tape, and stored in a vacuum sealed container prior to viewing on the SEM. A 5 nm gold coating was applied to HDPE and PS samples.

Tensile mechanical properties were measured for 35G-PEEK, 35G-PSU, 35G-PS, and 35G-HDPE using a MTS Q Test/25 universal testing machine with an extensometer mounted to the specimen, according to ASTM D638. Type 1 tensile specimens were tested at a cross-head speed of 5 mm/min until failure. A minimum of five specimens per sample were tested and data averaged, according to the ASTM standard. The Young's modulus in tension is reported. Tensile properties are consistent from batch to batch, as the batch size is quite large, and more than one batch has been tested for each G-PMC.

Flexural mechanical properties were measured for PEEK, 35G-PEEK, 35G-PEEK + Nanometal 75 µm, and 35G-PEEK + Nanometal 182 µm using an MTS Q Test/25 universal testing machine, according to ASTM D 790. A minimum of five specimens per sample were tested at a cross-head rate of 1.58 mm/min until 5% strain and data averaged, following the ASTM standard. Flexural properties are consistent from batch to batch, as the batch size is quite large, and more than one batch has been tested for each G-PMC.

2.2.2 Electrical Conductivity and Sensors

Electrical conductivity was determined by using a Keithley 2450 source measure unit, according to ASTM standard D4496-13. Electric current at different potentials was measured for 20G-PSU and 40G-PSU samples (5 specimens per sample were tested, according to the ASTM). Due to the potential for structural damage resulting from high current, the test was conducted up to 20 volts potential. Conductivity as a function of voltage is presented for 20G-PSU and 40G-PSU.

The sensor capability of G-PSU samples was tested by cyclically loading and unloading specimens in 3-point flexural loading using an Instron 5982 universal testing system while simultaneously monitoring current as a function of time under a potential of 10 volts using a Keithley 2450 source measure unit. Specimens (ASTM D 638 Type I) were loaded to a maximum stress of 25 N over five cycles, while remaining within the elastic region for these composites. Specimens were also loaded to 80 N over four cycles to investigate the effect of loading beyond the elastic region. Prior to the test start, specimens were preloaded to 10 N at a loading rate of 2.5 mm/sec, followed by the test loading rate

of 1 mm/min to reach 25 N and 80 N. Between loading cycles, specimens were manually unloaded, and force zeroed, which took approximately 25 seconds each time.

3.0 RESULTS AND DISCUSSION

3.1 Morphology and Mechanical Properties

Morphology images of 35G-PEEK are shown in Figure 2, and morphology images of 35 G-PSU, 35G-PS, and 35G-HDPE are shown in Figure 3. Intimate particle-matrix interaction is seen for each G-PMC. During the exfoliation process, pristine planar surfaces are created as graphene layers are sheared from graphite, which enables very good adhesive-planar bonding between GNF and polymer. Surface crystallization of the polymer in a preferred orientation growing from the pristine GNF surface is evident for PEEK in the circled region of Figure 2(b) and HDPE in Figure 3(c). PEEK and HDPE are both semi-crystalline polymers while PSU and PS are amorphous. Size reduction of the graphite particles within each G-PMC is evident in both the c-axis dimension (shearing of graphene layers from graphite into GNFs) and in the AB direction (GNF diameter). After the exfoliation process, GNFs are reduced to nano-dimensions in the c-axis direction, and the average GNF diameter is reduced ranging from 1 – 10 μm, as seen in Figure 2 and Figure 3. Further, transparent GNFs are visible in 35G PEEK, indicating few to single layer graphene, as shown in Figure 2(c). The original diameter of the graphite particles ranged between 250 – 300 μm. Thus, fracture has occurred across the AB basal plane of graphite during uniform, high shear melt-processing, allowing for covalent bonding to occur between GNF fractured edges and certain polymer chemistries (i.e., in situ functionalization).

Mechanical property measurements show a significant increase in tensile elastic modulus for each G-PMC. Tensile modulus for each polymer and its G-PMC with 35 wt. % graphite well-exfoliated into GNFs is shown in Figure 4(a). Relative to the polymer alone, tensile modulus increases by approximately 390%, 530%, 260%, and 205% for 35G-PEEK, 35G-PSU, 35G-PS, and 35G-HDPE, respectively. The modulus increase is dependent on

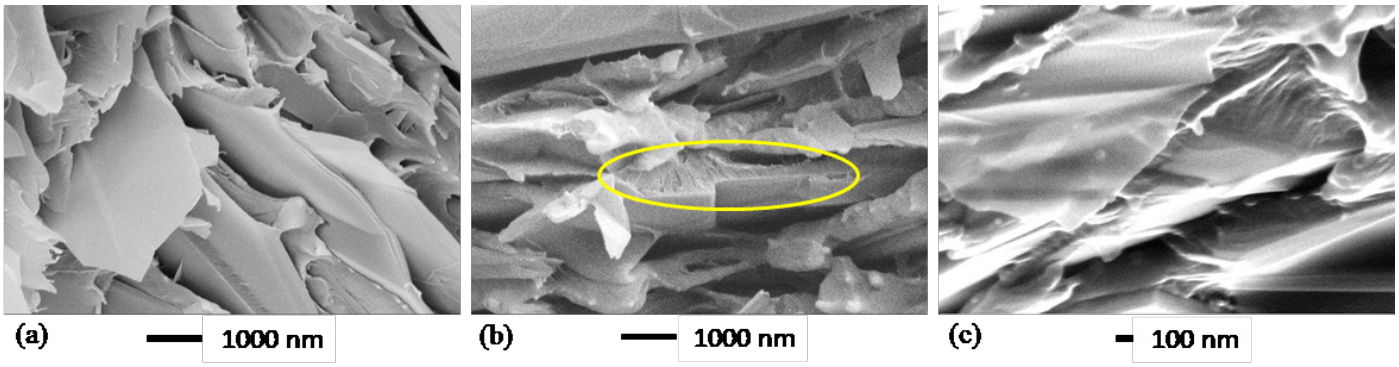

Figure 2: SEM Micrographs of 35 G-PEEK at Different Positions and Length Scale.

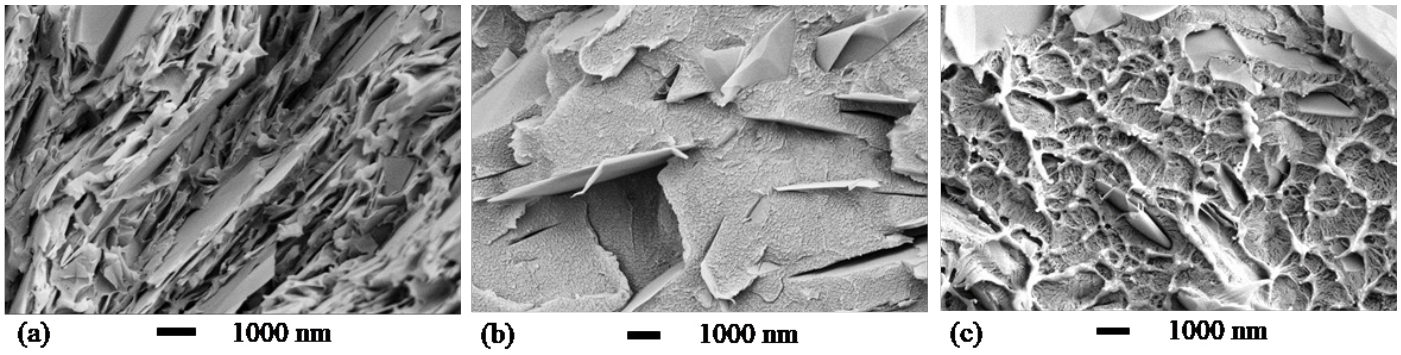

Figure 3: SEM Micrographs of (a) 35G-PSU, (b) 35G-PS, and (c) 35G-HDPE.

GNF-matrix interaction, which may be due to mechanical and/or chemical bonding, with stronger GNF matrix interaction resulting in better mechanical properties. Certain polymer chemistries allow for edge covalent bonding (chemical bonding) to occur between GNF edges and the matrix, providing stronger GNF-matrix interaction and better mechanical properties. For example, a polymer with a double bond to a side group in its structural repeat unit has the potential to convert to a single bond and leave an open location for chemical bonding with a GNF. For 35G-HDPE, there is no double bond in the HDPE repeat unit but mechanical interactions between GNFs and HDPE occur that cause a 205% increase in modulus, which is likely due to surface crystallinity of HDPE on GNF surfaces. For 35G-PEEK, there is a higher percentage increase in modulus than for 35G-HDPE, which is likely due to PEEK having a double bond to an oxygen in its repeat unit that allows for edge-covalent bonding between GNFs and PEEK, as well as surface crystallinity of PEEK on GNF surfaces [19]. Additionally, the modulus of 35G-PEEK is 20 GPa, which is equivalent to 30 wt. % carbon fiber reinforced PEEK.

Tensile stress at yield increases for each G-PMC relative to the polymer alone, as shown in Figure 4(b). The linear line between the stress value for the polymer alone and its G-PMC is not a trend line but simply connects the two data points for better visibility. The increase is not as significant as for the modulus. Thus, the strong GNF-matrix interactions significantly affect modulus but not tensile stress at yield, which may be due to a competing phenomenon. During in situ exfoliation, larger graphite particles are exfoliated into GNFs within each polymer and undergo size reduction in the c-axis direction (thickness) and in the AB direction (diameter), resulting in a distribution of the number of graphene layers within each GNF. The presence of a thicker GNF particle may act as a stress concentration, causing a reduction in strength. With a better degree of exfoliation, the size reduction of the GNF particles becomes more uniform, which will allow the strong GNF matrix interaction to affect the strength values more significantly [19]. Furthermore, from the polymer perspective, experiments in molding are necessary to increase strength further (i.e., optimizing mold temperature), and with more efficient exfoliation, as the process is improved, polymer degradation will decrease.

The flexural modulus of PEEK, 35G-PEEK, 35G-PEEK with Nanometal coating of 75 microns, and 35G-PEEK with Nanometal coating of 182 μm is 3.8 GPa, 17 GPa, 30 GPa, and 43 GPa, respectively Figure 5. The modulus of aluminum is approximately 69 GPa but has approximately 2.5 times greater density than the polymer. Additionally, the Nanometal coating on 35G-PEEK enhances strain to fracture, as seen in the flexural stress-strain curves in Figure 6. For 35G-PEEK with Nanometal coating of 182 μm, the Nanometal coating is able to withstand high loads and does not fracture prior to 5% strain

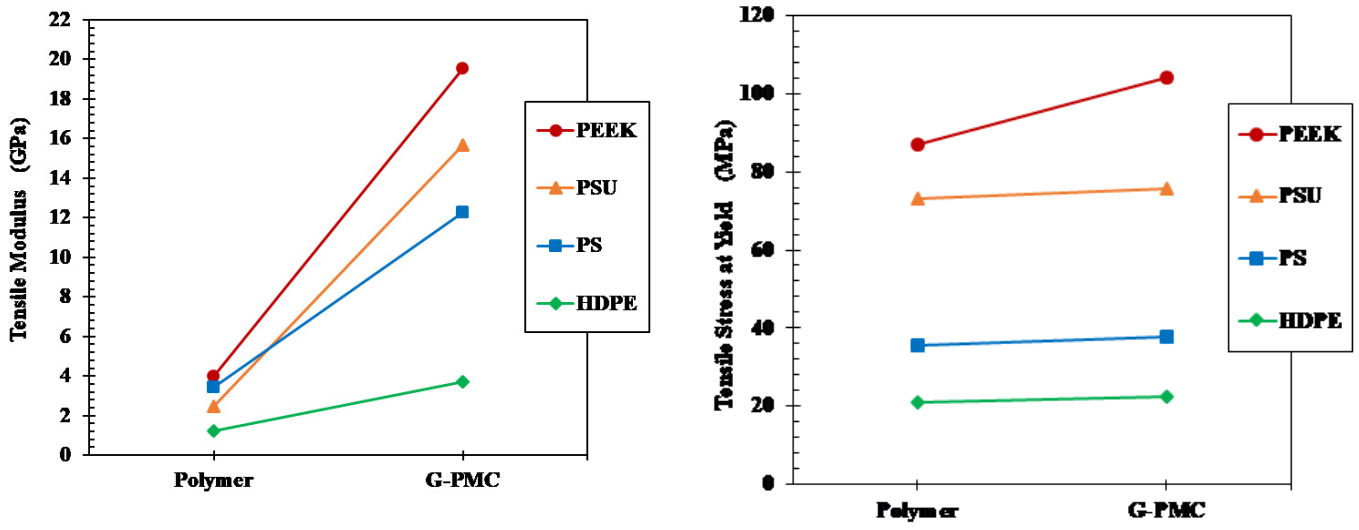

Figure 4: Tensile Properties of 35 wt. % GNF Enhanced G-PMCs and Each Polymer (a) Modulus and (b) Stress at Yield. Lines are for improved visibility only.

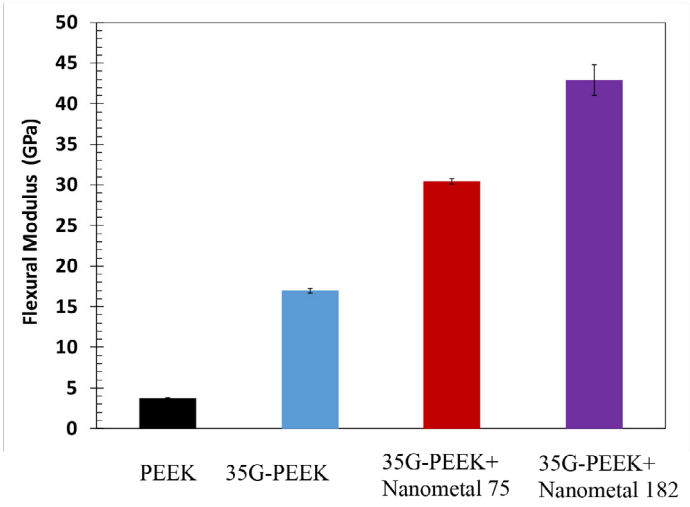

Figure 5: Flexural Modulus of PEEK, 35G-PEEK, 35G-PEEK with 75 µm Nanometal Coating, and 35G-PEEK with 182 mm Nanometal Coating.

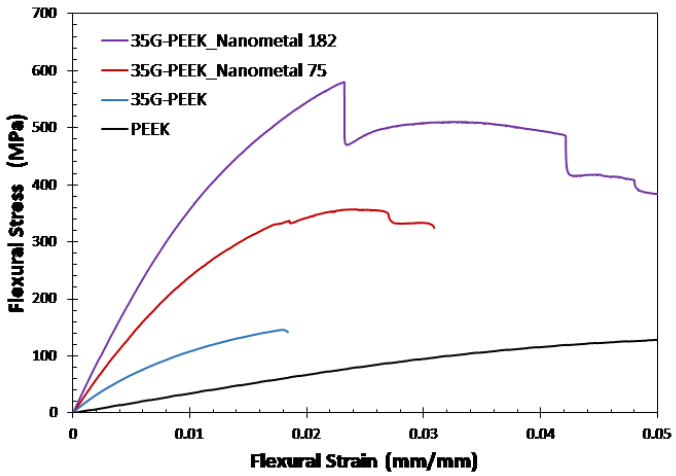

Figure 6: Flexural Stress-Strain Curves for PEEK, 35G-PEEK, 35G-PEEK with Nanometal Coating 75 mm, and 35G-PEEK with Nanometal Coating 182 mm.

(test termination). Izod impact resistance of un-notched specimens for 35G-PEEK and 35G-PEEK with Nanometal coating (approximately 100 µm thickness) is 1,783 J/m and 4,700 J/m, respectively. These results suggest intimate particle-matrix interaction, as well as strong G-PMC-Nanometal coating interaction.

3.2 Electrical Properties and Sensors

Electrical conductivity as a function of voltage for 20G-PSU and 40G-PSU appears in Figure 7. With an increase in GNF concentration from 20 to 40 wt. % in PSU, electrical conductivity increases by an order of magnitude. The morphology of 40G-PSU allows for more efficient electrical conductivity, as the distance between GNFs decreases with increasing GNF concentration. The easy tunability of these G-PMCs allows for optimization of functional properties, for example electrical conductivity, while simultaneously offering structural integrity.

Cyclic loading of 40G-PSU and the corresponding current versus time curves are shown in Figure 8, when loaded to 25 N (a), (b) and 80 N (c), (d). The current increases while under load and decreases as the load is removed, indicating that 40G-PSU is a good candidate for sensor applications. When loaded to 25 N, the stresses remain within the elastic region for the material.

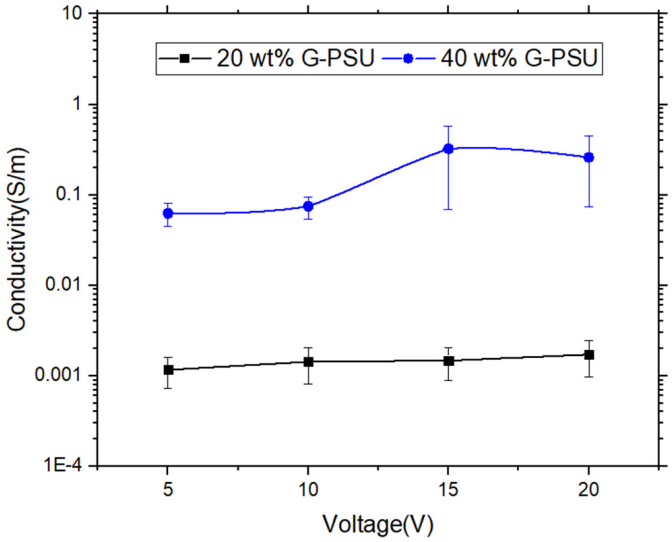

Figure 7: Electrical Conductivity as a Function of Voltage for 20G-PSU (Black) and 40G-PSU (Blue).

Loading to 80 N exceeds the material's yield stress, however, the current response is still good. Comparing (a) and (c), the current response is slightly different due to the difference in maximum loading in that the current does not decrease fully after each loading for the sample loaded to 80 N in (c). Cyclically loading 40G-PSU to 80 N is above the material's yield stress and likely caused plastic deformation. In application, loading should be kept within the elastic region to avoid plastic deformation. Interestingly, the mechanical response improves from the first to last loading cycle, as seen in both (b) and (d).

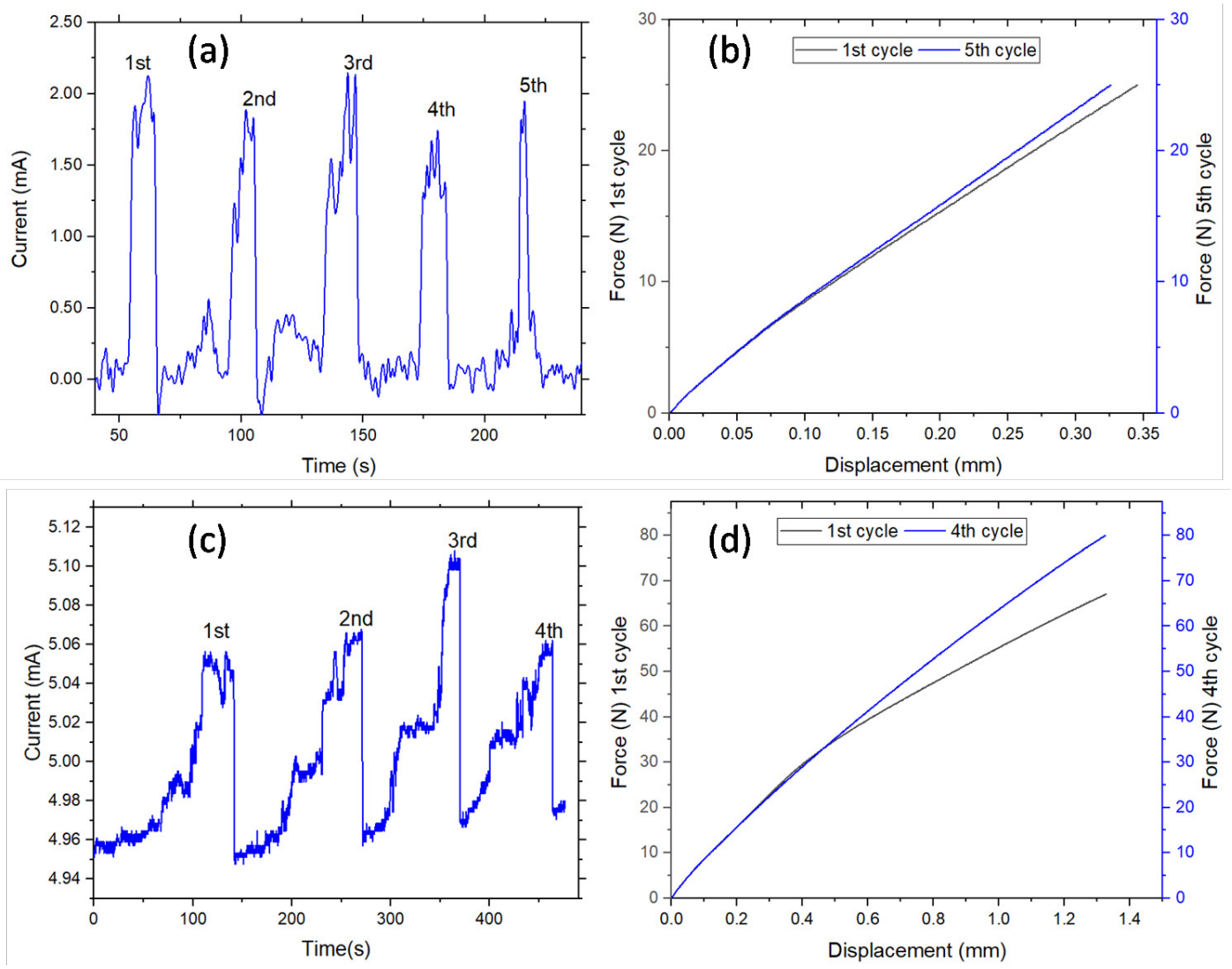

Figure 8: Sensor Characterization of 40G-PSU Showing Current as a Function of Time and Corresponding Force Versus Displacement During Cyclic Loading to 25 N (a), (b) and 80 N (c), (d).

4.0 CONCLUSION

The general approach presented in this work will enable fabrication of a new class of high performance, lightweight G-PMCs with tunable, multifunctional properties. The high shear melt-processing method offers simple, versatile manufacturing; low raw materials costs; and the opportunity to enhance properties of the G PMC with further treatment like Nanometal coatings. These materials will allow entry into a broad array of defense applications to meet current and future needs. Compared to existing solutions, materials substitution using G-PMCs offers cost and weight savings in a particular application. By reducing vehicle weight by 30%, operational energy cost savings arise since fuel consumption will be lowered, longer service lifetime is possible since these materials are corrosion resistant, and manufacturing costs will be reduced. Improved logistics capabilities through increased range, increased payload (more ammunition per vehicle) and improved protection to the warfighter can be achieved. Some potential applications include: lightweight vehicular armor that serves as the structural component while providing ballistic protection, lightweight personnel armor that would allow reduced combat load weight and increased ammunition per soldier, lightweight UAVs that offer higher payloads and longer loitering times, lightweight munitions, lightweight tactical bridges, and sensors.

Key advantages of this in situ graphite exfoliation process to fabricate G-PMCs are that any thermoplastic polymer may be used. Very high concentrations of graphite may be added to the polymer, which are subsequently converted into GNFs; new, pristine surfaces and edges are created on exfoliated GNFs and these bond well with

the surrounding molten polymer. Significant modulus enhancement occurs and GNFs impart electrical and thermal conductivity [40] and barrier resistance to small gases [41]. G-PMC properties are multifunctional and easily tunable; and manufacturing using standard polymer processing methods may be used, including extrusion, injection molding, and additive manufacturing.

5.0 ACKNOWLEDGEMENTS

This work was sponsored by ONR-BAA: N00014-14-1-0046 and ONR-BAA: N00014-17-1-2712. Secondary funding was provided by the AMIPP Center at Rutgers University. Other inventors of the G-PMC technology include Thomas Nosker and Bernard Kear. Rutgers University students involved with the project include Arya Tewatia, Meredith Taghon, and Jamie Wooding. Electrical conductivity research was funded by TLC Products, Inc. and performed by Ali Ashraf at Rutgers University.

6.0 REFERENCES

[1] Stankovich, S, Dikin, D.A, Dommett, G.H.B., Kohlhaas, K.M., Zimney, E.J., Stach, E.A., et al. Graphene-based composite materials. *Nature*, 442:282-286, 2006.

[2] Zhang, H.-B., Zheng, W.-G., Yan, Q., Yang, Y., Wang, J.-W., Lu, Z.-H., et al. Electrically conductive polyethylene terephthalate/graphene nanocomposites prepared by melt compounding. *Polymer,* 51:1191-1196, 2010.

[3] Shiu, S.-C., Tsai, J.-L. Characterizing thermal and mechanical properties of graphene/epoxy nanocomposites. *Composites Part B: Engineering*, 56:691-697, 2014.

[4] Hwang, Y., Kim, M., Kim, J. Improvement of the mechanical properties and thermal conductivity of poly(ether-ether-ketone) with the addition of graphene oxide-carbon nanotube hybrid fillers. *Composites Part A*, 55:195-202, 2013.

[5] Rafiee, M.A., Rafiee, J., Wang, Z., Song, H., Yu, Z., Koratkar, N. Enhanced mechanical properties of nanocomposites at low graphene content. *ACS Nano*, 3:3884-3890, 2009.

[6] Potts, J.R., Dreyer, D.R., Bielawski, C.W., Ruoff, R.S. Graphene-based polymer nanocomposites. *Polymer*, 52:5-25, 2011.

[7] Potts, J.R., Lee, S.H., Alam, T.M., An, J., Stoller, M.D., Piner, R.D. et al. Thermomechanical properties of chemically modified graphene/poly(methyl methacrylate) composites made by in situ polymerization. *Carbon,* 49:2615-2623, 2011.

[8] Song, P., Cao, Z., Cai, Y., Zhao, L., Fang, Z., Fu, S. Fabrication of exfoliated graphene-based polypropylene nanocomposites with enhanced mechanical and thermal properties. *Polymer,* 52:4001-4010, 2011.

[9] Wakabayashi, K., Pierre, C., Dikin, D.A., Ruoff, R.S., Ramanathan, T., Brinson, L.C. et al. Polymer–graphite nanocomposites: Effective dispersion and major property enhancement via solid-state shear pulverization. *Macromolecules,* 41:1905-1908, 2008.

[10] Gong, L., Yin, B., Li, L., Yang, M. Nylon-6/graphene composites modified through polymeric modification of graphene. *Composites Part B: Engineering,* 73:49-56, 2015.

[11] Wang, J., Xu, C., Hu, H., Wan, L., Chen, R., Zheng, H. et al. Synthesis, mechanical, and barrier properties of LDPE/graphene nanocomposites using vinyl triethoxysilane as a coupling agent. *Journal of Nanoparticle Research*, 13:869-878, 2011.

[12] Ha, H.W., Choudhury, A., Kamal, T., Kim, D., Park, S. Effect of chemical modification of graphene on mechanical, electrical, and thermal properties of polyimide/graphene nanocomposites. *ACS Applied Materials & Interfaces,* 4:4623-4630, 2012.

[13] Satti, A., Larpent, P., Gun'Ko, Y. Improvement of mechanical properties of graphene oxide/poly(allylamine) composites by chemical crosslinking. *Carbon*, 48:3376-3381, 2010.

[14] Wang, Y., Yang, C., Mai, Y., Zhang, Y. Effect of non-covalent functionalisation on thermal and mechanical properties of graphene-polymer nanocomposites. *Carbon*, 102:311-318, 2016.

[15] Nadiv, R., Shtein, M., Buzaglo, M., Peretz-Damari, S., Kovalchuk, A., Wang, T. et al. Graphene nanoribbon – Polymer composites: The critical role of edge functionalization. *Carbon,* 99:444-450, 2016.

[16] Lynch-Branzoi, J.K., Nosker, T.J., Kear, B.K. Tewatia, A., Taghon, M., Wooding, J. Lightweight, high performance polymer composites for modern engineering applications. Advanced Materials: TechConnect Briefs, 1:192-195, 2018.

[17] Nosker, T.J., Lynch, J.K., Kear, B., Hendrix, J., Chiu, G. In situ exfoliation method to fabricate a graphene-reinforced polymer matrix. *Composite,* US 20160083552, 2016.

[18] Nosker, T.J., Lynch, J.K., Hendrix, J., Kear, B.H., Chiu, G., Tse, S. In situ exfoliation method to fabricate a graphene-reinforced polymer matrix. *Composite*, US 9,896,565, 2018.

[19] Lynch-Branzoi, J.K., Ashraf, A., Tewatia, A., Taghon, M., Wooding, J., Hendrix, J. et al. Shear exfoliation of graphite into graphene nanoflakes directly within polyetheretherketone and a spectroscopic study of this high modulus, lightweight nanocomposite. *Composites Part B: Engineering*, 2020 ;188:107842, 2020.

[20] Chen, Y., Zou, H., Liang, M. Non-isothermal crystallization study of in-situ exfoliated graphite filled nylon 6 composites. *Journal of Polymer Research*, 21, 2014.

[21] Zhou, S., Lei, Y., Zou, H., Liang, M. High thermally conducting composites obtained via in situ exfoliation process of expandable graphite filled polyamide 6. *Polymer Composites*, 34:1816-1823, 2013.

[22] Zhou, S., Yu, L., Song, X., Chang, J., Zou, H., Liang, M. Preparation of highly thermally conducting polyamide 6/graphite composites via low-temperature in situ expansion. *J Appl Polymer Sci,* 131, 2014.

[23] Feng, Z., Zuo, H., Hu, J., Yu, B., Ning, N., Tian, M. et al. In situ exfoliation of graphite into graphene nanosheets in elastomer composites based on diels-alder reaction during melt blending. *Industrial and Engineering Chemistry Research*, 58:13182-13189, 2019.

[24] Li, Y., Zhang, H., Crespo, M., Porwal, H., Picot, O., Santagiuliana, G. et al. In situ exfoliation of graphene in epoxy resins: A facile strategy to efficient and large scale graphene nanocomposites. *ACS Applied Materials and Interfaces*, 8: 24112-24122, 2016.

[25] Kim, S.R., Poostforush, M., Kim, J.H., Lee, S.G. Thermal diffusivity of in-situ exfoliated graphite intercalated compound/polyamide and graphite/polyamide composites. *Express Polymer Letters*, 6:476-484, 2012.

[26] Lee, J.W., Lee, J.U., Jo, J.W., Bae, S., Kim, K.T., Jo, W.H. In-situ preparation of graphene/poly(styrenesulfonic acid-graft-polyaniline) nanocomposite via direct exfoliation of graphite for supercapacitor application. *Carbon*, 105:191-198, 2016.

[27] Polakova, L., Sedlakova, Z., Ecorchard, P., Pavlova, E., Peter, J., Paruzel, B. et al. Poly(meth) acrylate nanocomposite membranes containing in situ exfoliated graphene platelets: Synthesis, characterization and gas barrier properties. *European Polymer Journal,* 94:431-445, 2017.

[28] Hassan, M., Reddy, K.R., Haque, E., Minett, A.I., Gomes, V.G. High-yield aqueous phase exfoliation of graphene for facile nanocomposite synthesis via emulsion polymerization. *J Colloid Interface Sci*, 410:43-51, 2013.

[29] Tsai, M., Tseng, I., Huang, Y., Yu, H., Chang, P. Transparent polyimide film with improved water and oxygen barrier property by in-situ exfoliating graphite. *Advanced Engineering Materials,* 18:582-590, 2016.

[30] Wei, P., Cui, S., Bai, S. In situ exfoliation of graphite in solid phase for fabrication of graphene/polyamide-6 composites. *Composites Science and Technology*, 153:151-159, 2017.

[31] Emrich, R. Nanometal/polymer hybrid material makes lighter, stronger snowboard bindings. *Advanced Materials and Processes,* 169:50-51, 2011.

[32] Erb, U., Palumbo, G., Jeong, D., Kim, S., Aust, K.T. Grain size effects in nanocrystalline electrodeposits. Processing and Properties of Structural Nanomaterials: Proceedings of Symposia (held at Materials Science and Technology 2003 Meeting), November 9, 2003 – November 12, Minerals, Metals and Materials Society, 2003.

[33] Gonzalez, P. Electroplate alternatives to hard chrome: Nanocrystalline metals and alloys. National Association for Surface Finishing Annual Conference and Trade Show 2010. SUR/FIN 2010, June 14, 2010 – June 17, National Association for Surface Finishing, 2010.

[34] Heard, R., Erb, U., Palumbo, G. Exploiting hall-petch strengthening for sustainability. 2008 Materials Science and Technology Conference. MS and T'08, October 5, 2008 – October 9, American Ceramic Society, 2009.

[35] Lindsay, J.H. Canadian company is engineering innovative materials for the future of metal finishing. *Plating and Surface Finishing*, 91:7-9, 2004.

[36] Palumbo, G., Gonzalez, F., Tomantschger, K., Erb, U., Aust, K.T. Nanotechnology opportunities for electroplating industries. *Plating and Surface Finishing*, 90:36-45, 2003.

[37] Nagarajan, N., Kowpak, T., Tomantschger, K., Gonzalez, F., Neacsu, M., Ronis, T. et al. NanoMetal polymer hybrids oberflachen technik journal. *Jahrbuch Oberflachentechnik*, 67, 2011.

[38] Integran Technologies. Nanovate, https://www.integran.com/what-is-nanovate-technology, 2020.

[39] Integran Technologies. Ultralightweight Parts with Nanovate Plating on Plastics, 4, 2016.

[40] Ashraf, A., Jani, N., Farmer, F., Lynch-Branzoi, J.K. Non-destructive investigation of dispersion, bonding, and thermal properties of emerging polymer nanocomposites using close-up lens assisted infrared thermography. *MRS Advances*, 1-8, 2020.

[41] Lynch-Branzoi, J., Nosker, T., Kear, B., Chang, C. Use of Graphene-polymer composites to improve barrier resistance of polymers to liquid and gas permeants. US WO/2019/143662, 2019.

Graphene Barrier Coatings for Solid Rocket Propellant Insulants

Simon Torry, Jack Whittaker
QinetiQ Fort Halstead
Sevenoaks, Kent, TN14 7BP
UNITED KINGDOM
Email satorry@qinetiq.com

Keywords: Barrier; Composite; Defence; Diffusion; Graphene; Insulant; Propellant; Plasticiser.

ABSTRACT

Most in-service missiles have solid propellant rocket motors, the major component being the energetic propellant cast in an insulant-lined combustion chamber. The insulant is typically a solid-filled polymer that is thermally sacrificed during motor combustion. The reactivity of some propellant ingredients with typical rubber formulation components can limit insulant formulation. The aim of this programme was to formulate effective barrier coatings suitable for application between the insulant and propellant that, if successful, could increase the range of materials that could be safely used in insulants and thereby improve their performance. A number of graphene and functionalised graphenes were investigated as to their suitability in binder systems that are known to be compatible (non-reactive) with composite and double base propellants.

Although described as graphene and graphene oxide, some off-the-shelf materials were found to consist of thick flakes (assessed by optical and scanning electron microscopy) that proved difficult to exfoliate by both ultrasound and acoustic mixing. The graphene samples were unable to form stable colloids in typical graphene "solvents" (as measured using visible spectroscopy). Even materials that did form stable solutions were found, using an optical microscope, to consist of thick particles as opposed to single or multilayer graphene sheets (with less than ten layers). An alkylamine functionalised graphene oxide dispersion was found to contain sheets of material that were flexible and transparent suggesting this material had stable graphene-like dimensions.

The alkylamine functionalised graphene oxide was added to two families of binders – single component binders crosslinked at 120°C and two component binders crosslinked at 95°C. Traditional "drying" agents, such as zinc caprylate, were found to be not beneficial for creating an even graphene coating on glass microscope slides. Insulant samples (silica / carbon fibre filled Polyvinylchloride/Nitrile (PVC/NBR) or Ethylene-co-Propylene Diene Monomer (EPDM) rubber) coated on one side with test barrier coating were soaked in bis-(2-ethyl hexyl)adipate (DOA) / polybutadiene solutions at 50°C, over five days, to test barrier efficacy. Samples were cross-sectioned using a microtome and the extent of diffusion of the DOA plasticiser into the insulant was measured using an infrared microscope. Samples coated (one to three coats) with the one component binders at a binder to graphene additive ratio of 1:1 were ineffective barriers.

The two component binder systems, at ratios of functionalised graphene to binder of 1:3 or 1:4, were found to be effective barrier coats to DOA diffusion. Eight barrier coats, totalling approximately 0.015 mm thick, were found to decrease the amount of DOA at the insulant surface by more than 95%.

1.0 INTRODUCTION

Graphene and the family of functionalised graphenes, have potential to being beneficial in energetic materials and other materials such as adhesives and insulants used in rocket motors, by exploiting graphene's' chemistry,

topology and electrical properties. In the case of energetic composites, there is a potential for graphene to:

- Improve ballistic performance by catalysing and controlling how a propellant burns;
- Improve thermal conductivity lowering thermal hazard effects of energetic materials;
- Improve mechanical properties of explosives and propellants;
- Decrease sensitivity to electrostatic hazards;
- Stabilise energetic molecules in host structures;
- Decrease sensitiveness to mechanical impact; and
- Control migration of energetic molecules via barrier properties.

Energetic materials are often used in weapon sub-systems, for example solid rocket motors. Undesirable interactions can occur during their service life. This can be a particular problem when low molecular weight species migrate from their original position potentially causing degradation of adjacent components, decrease liner-propellant bond strength and cause potential system failure. This could be mitigated if there were an effective barrier between components. A number of barrier coatings based on high aspect ratio nanocomposites such as vermiculite in latex [1], polymer/layered silicates [2], multi-walled carbon nanotubes, modified layered-silicates, polyhedral oligomeric silsesquioxanes [3], nano-metal oxides, nano glass flakes, nano-nitrides [4] have been developed and can decrease gas permeability 20 to 30 fold [1]. For energetic applications, it is desirable to use fillers with little reactivity towards nitrate esters and other energetic moieties, hence in this work, carbon based materials were considered as fillers in a barrier formulation. Carbon is commonly used as an additive in energetic materials (as a ballistic modifier and in low friction coatings). Although carbon black has been used in barrier applications, Christopher et al. [5] found that graphene fillers outperformed carbon black in corrosion barrier applications. Similarly, Yang et al. [6] found that plate-like fillers were superior to carbon black in nitrile butyl rubber barrier applications. Due to its high aspect ratio and high electron density in its aryl ring structure, graphene has a reputation of being a good barrier towards even small atoms such as helium [7], [8]. The permeability towards gases and other molecules depends on the defects in the graphene, how the graphene sheets assemble into macrostructures and how well the graphene is dispersed and orientated. It is thought that multilayer graphene sheets should impede diffusion by increasing the tortuosity and diffusant pathlength. Some workers have found that addition of graphene to polymers induces the polymer to crystallise thereby decreasing the more permeable amorphous content [9].

The aim of this work was to investigate the use of graphene as a barrier to prevent or impede the diffusion of DOA plasticiser into a rocket motor insulant. Self-assembling of the graphene into flat sheets would effectively increase the diffusion pathway of the plasticiser (as per Figure 1) and hence limit plasticiser migration.

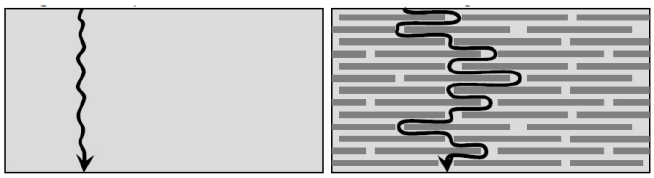

Figure 1: Diffusion Through Self-Assembled Graphene Sheets. Normal diffusion (left), impeded diffusion through graphene (right).

2.0 EXPERIMENTAL

2.1 Binders

Binders (Hydroxy Terminated Polybutadiene (HTPB), Cray Valley; polyvinyl butyral, Sigma-Aldrich; polyvinylformal, Sigma-Aldrich; polycaprolactone, Perstorp) were dried before use in a vacuum, overnight at 60°C. Crosslinker species (isophorone diisocyanate IPDI, Sigma-Aldrich; Isocyanate N3600, Bayer; epoxy, Momentive) were used as received. Insulants were proprietary formulations based on Ethylene co Propylene Diene Monomer (EPDM) and Polyvinylchloride/Nitrile (PVC/NBR).

Table 1: Graphene Sources.

Sample	Source
Elicarb Materials Grade Graphene Powder	Thomas Swan, County Durham
Graphene oxide	Sigma-Aldrich, 763713-1G
Graphene oxide, alkylamine functionalised 2 mg per cm^3 in toluene	Sigma-Aldrich, 809055-50ML
Graphene oxide powder, 15 – 20 layers, 4 – 10% edge-oxidised (Aldrich)	Sigma-Aldrich, 796034-1G
10 mg/mL, graphene dispersion in N-Methyl-2-Pyrrolidone (NMP)	Sigma-Aldrich, 803839-5ML
Graphene ink C2131121D3	Gwent Group

2.2 Graphene Samples

The five graphene and graphene oxide samples, used in this programme, are summarised in Table 1. Three samples were solid powders, whilst the alkylamine functionalised graphene oxide, and graphene dispersion were supplied in solvent.

Within a week of receipt, the graphene in NMP solvent settled out of solution – application of low power ultrasound did not disperse the graphene into a stable colloid. There appeared to be no visible change in the alkylamine functionalised graphene oxide dispersion in toluene over a period of at least three months. Throughout the programme, it remained as a stable, pale brown dispersion slightly more viscous than pure toluene. Most exfoliation work was performed on the Elicarb graphene. For comparison, other graphene samples were investigated.

2.3 Spectroscopy

Fourier Transform Infrared (FTIR) measurements were performed using a Nicolet iS50 spectrometer fitted with an inbuilt diamond Attenuated Total Reflection (ATR) detector. Infrared mapping experiments were performed using a Nicolet iN10 FTIR microscope in transmission mode (ultrafast mode, 150 x 20 µm step size and 150 x 20 µm aperture) at a spectral resolution of 16 cm^{-1}. Raman spectroscopy was collected using an iS50 Raman Module with a 1064 nm laser (variable power up to 0.5 W) with a 50 µm spot size.

Visible spectroscopy was performed using matched 10 mm silica cuvettes in a Perkin Elmer Lambda 20 spectrometer. An absorption measurement was performed every ten seconds over a period of ten hours.

Nuclear Magnetic Resonance (NMR) measurements were performed using a Bruker Avance 400 spectrometer (proton frequency 400 MHz) fitted with a 5 mm quattro nucleus probe. Samples were dissolved in deuterated Dimethyl Formamide (DMF) and proton spectra measured at 25°C.

2.4 Microscopy

Microscopy was performed using a Zeiss AxioImager A1m microscope in transmitted or reflected light modes (2.5 to 50 times magnification). Image analysis was conducted using the AutoMeasure Plus module in the microscope's Zeiss AxioVision 4.6 software.

Scanning Electron Microscopy (SEM) was carried out using a Hitachi S-3500N Electron Microscope and an Oxford instruments X-Max50 EDX with Aztec software. Samples were mounted onto stubs coated with conductive adhesive tape.

2.5 Graphene Dispersion

Two methods of exfoliation were attempted in this work:

- Acoustic mixing; and
- Ultrasound bath.

Acoustic mixing was performed using a Resodyn LabRAM acoustic mixer fitted with a bespoke polycarbonate vial holder. Samples were mixed in disposable 10 ml glass vials fitted with PTFE faced screw tops. The mixer's power input and mixing time were varied in an attempt to improve exfoliation and dispersion.

Attempts were made to disperse graphene samples in solvents (1 mg per cm^3) in an ultrasound bath (200 to 400 W), at room temperature for up to two hours.

2.6 Plasticiser Diffusion in Insulant

The alkylamine functionalised graphene oxide was provided as 2 mg/cm^3 in toluene. The dispersion was further diluted with the binder system in THF (dried over 4A molecular sieve). Rocket motor insulant plaques (6 mm x 12 mm x 19 mm) were coated on one side with the barrier coating solution as per Figure 2. Solution was dripped onto the surface using a pipette (typically 3 drops per 2.2 cm^2 surface). The solvent was allowed to evaporate, and a further three drops were applied to the surface. The surface was then allowed to cure at temperature for a known amount of time. If required, the sample was recoated.

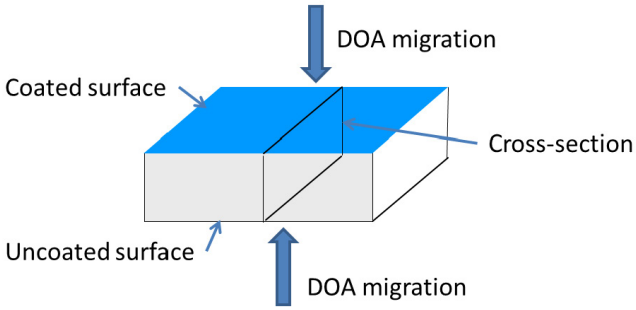

Figure 2: Insulant Plaque Configuration.

The barrier efficacy was assessed by soaking the coated insulant plaque in a polymer/plasticiser solution (46% bis-(2-ethylhexyl) adipate (DOA), 53% HTPB, 1% antioxidant) for up to five days at 50°C. After ageing, the samples were patted dry using tissue paper. The centre portion of the plaque was cut out and sectioned to a thickness of 25 and 30 µm using a Bright cryogenic microtome at -36°C using a tungsten carbide knife set at an angle of 23°. The insulant centre slice was mounted between sodium chloride plates.

Infrared microscopy was used to assess the relative DOA concentration by measuring the carbonyl peak area at 1739 cm^{-1} through the plaque cross-section.

3.0 RESULTS

3.1 Graphene Characterisation

Attempts were made to characterise the graphenes using diamond ATR infrared and Raman spectroscopy. Additionally, optical and SEM microscopy was performed on the samples.

The ATR IR spectra of the solid graphenes / graphene oxides were mostly featureless. The Elicarb and graphene oxide 1 – 20 sheets were broad band IR absorber. The graphene oxide was in the form of thick, large (~1 to 5 mm^2) sheets. Its IR spectrum exhibited OH stretches, and carboxylic acid signals. Broad signals around 1500 to 1000 cm^{-1} are thought to be in part due to polyaromatic species.

IR measurements of alkylamine functionalised graphene in toluene (Figure 3) indicated that toluene was still in the sample after 1.75 hours drying (as indicated by the peaks at 1494, 752 and 693 cm^{-1}). The IR suggested that as well as alkyl species (2922, 2855, 1465 cm^{-1}), carboxylates (1740 to 1600 cm^{-1}) and polyaromatic species (1450 – 895 cm^{-1}) are present. These signals are also observed in the Sigma-Aldrich graphene oxide.

Attempts were made to measure the Raman spectra of the graphene samples using a near infrared (1064 nm) laser.

The laser power was altered from 0.05 to 0.5 W, and the number of scans was increased in attempt to measure a structural spectrum. The Elicarb sample did not exhibit the normal graphene signals using 1064 nm excitation. The spectra generally consisted of a broadband emission peak at 3400 cm^{-1} and other minor peaks. The graphene sample spectra were similar to carbon black signals.

Measurements were also performed on the same material using a 532 cm^{-1} laser [10]. The Raman spectrum consisted of 2D, g and D peaks (Figure 4). The ratio of the 2D/g peak

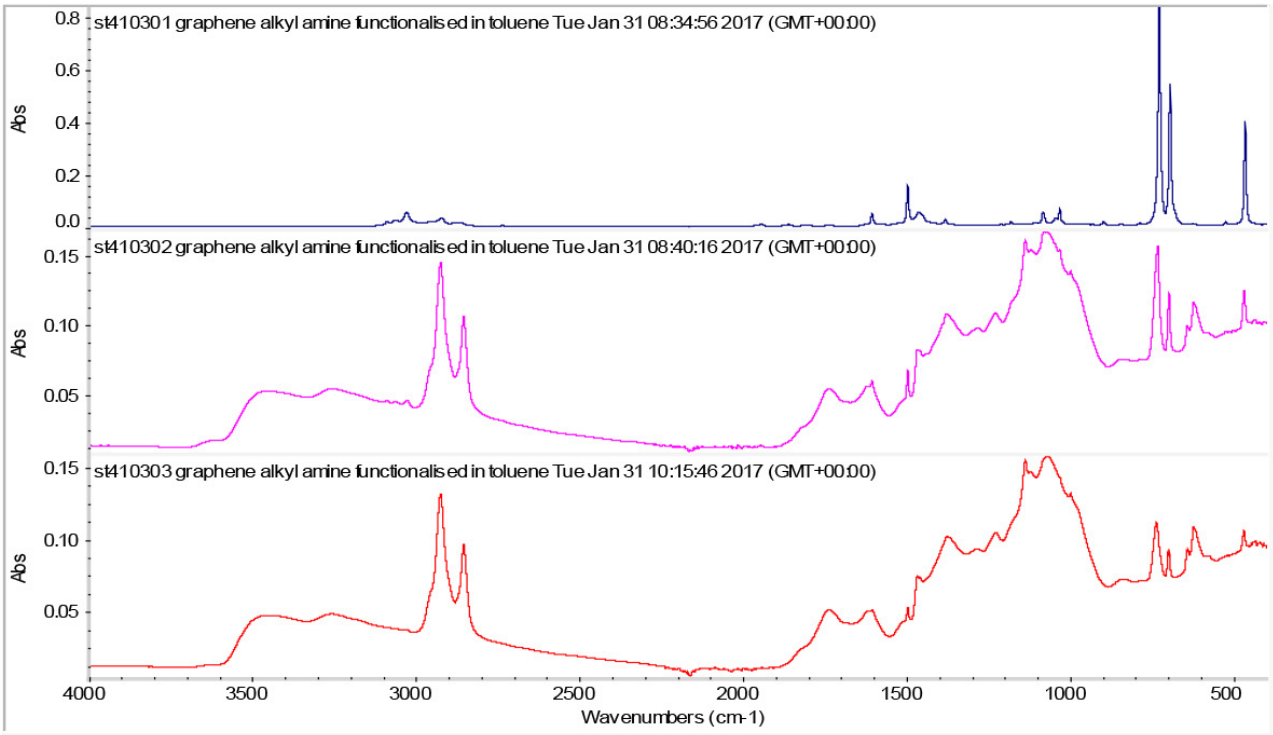

Figure 3: ATR IR of Alkylamine Functionalised Graphene Oxide. Top as received, middle dried for five minutes, bottom dried for 1.75 hours.

areas indicated that the material consists of graphene structures (D/G ratio of 0.087). According to the manufacturers, Elicarb graphene materials grade should have a D/G ratio of typically 0.07 to 0.1 and consist of a "few layers" graphene platelets of 5 µm lateral size.

The Raman spectrum of alkylamine functionalised graphene oxide consisted of broad humps at 3500, 1800 to 1000 and 900 to 100 cm^{-1}. These are probably associated with OH and carboxylic acid groups decorating the graphene surface.

Unless careful surface preparation is performed on slides with optimised refractive indices, single layer graphene sheets are nominally invisible to optical microscopy measurements [11], [12], [13]. As no surface preparation was performed on the optical slides used in this work, the observation of visible flakes was used as evidence for multilayer graphene/graphite. The Elicarb graphene powder consisted of agglomerates and flakes (Figure 4). The graphene oxide consisted of large flakes (several mm^2) with smooth surfaces. The graphene oxide 15 – 20 layers consisted of very small particles and loose agglomerates.

Upon drying, the graphene dispersed in NMP consisted of visible flakes whilst the as received alkylamine functionalised graphene

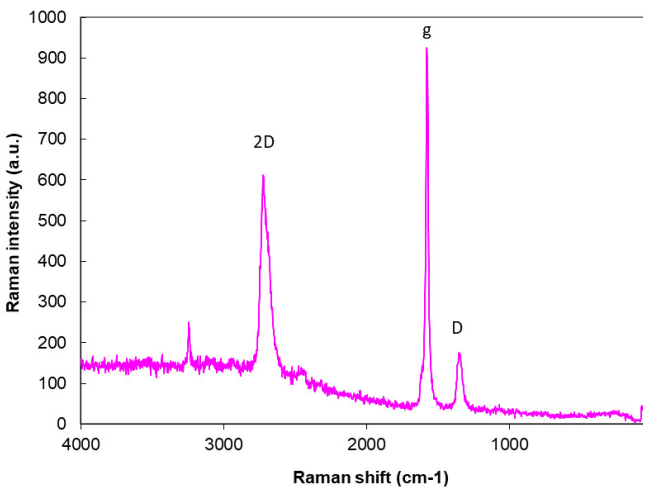

Figure 4: Raman of Elicarb Graphene.

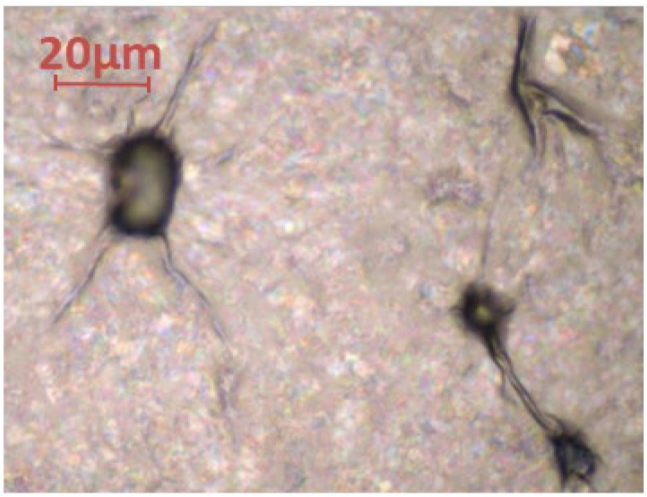

Figure 5: Optical Micrograph of Amine Functionalised Graphene Oxide.

oxide was nominally invisible under the microscope. Folds around particles and other unfocused features (Figure 5) were observed. Some thicker flakes were observed – they exhibited interference bands which suggest that some of the flakes have thicknesses of the order of 100 to 400 nm.

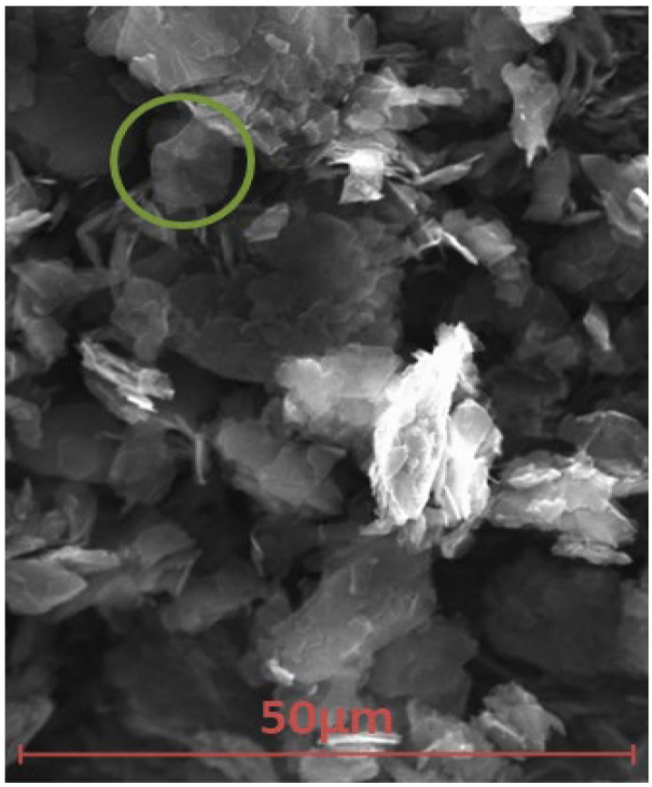

Figure 6: SEM Micrograph of Elicarb.

The samples were subjected to SEM and EDX measurements to assess morphology and carbon to oxygen ratio. The solid Thomas Swan Elicarb graphene appeared to be a free-flowing fine powder. The graphene was built up to a thickness which would prevent the electron beam interacting with the mounting tab. At a low magnification, the graphene was found to be agglomerated. At higher magnifications, using the SE detector, small sections of graphene, appearing to be semi-transparent to the electron beam due to the thin layers of atoms (e.g., Figure 6, highlighted by green circle).

EDX analysis indicated 96.8% carbon with 3.0% oxygen and copper and sodium impurities at 0.1% each. Graphene dispersion behaviour is thought, in part, to be a function of the C/O ratio.

Graphene oxide and graphene oxide (15 – 20 layers) contained 4.9% and 14.8% oxygen, respectively. Graphene from NMP and functionalised graphene oxide could not be deposited in a thick enough layer to measure the oxygen content reliably. As in optical observations, SEM microscopy of amine functionalised graphene oxide did not observe individual sheets but did observe folds and creases of material around occluded particles.

3.2 Graphene Exfoliation and Deposition

The process of exfoliating solid graphene/graphite into graphene sheets requires the use of solvents that interact well with the graphene surface. Traditionally, solvents such as DMF, NMP, and isopropanol have been used to form stable graphene dispersions. Such solvents interact with the graphene surface in such a way as to prevent the graphene sheets reassembling into graphite. These solvents tend to have high boiling points or functional groups that are potentially reactive with typical binder systems. In this work, solubility parameters have been used to assess potential, non-reactive, solvents that interact well with graphene forming a stable solution and that could also flash off after coating a surface (causing graphene deposition). According to the Hansen solubility parameter method [14], solvents such as cyclohexanone, THF, NMP and 1,3-dioxalane are expected to interact well with graphene (Table 2).

Low "R" numbers (calculated as per Equation 1) indicate good interaction between the solvent and graphene. Solvents such as water, ethanol and methanol are expected to act as bad dispersion solvents. The degree of solvent interaction will depend on the nature of the graphene. If the graphene is oxidised then the Hansen parameters will be different, and the family of dispersion solvents will also change. It is noted that although graphene is poorly dispersed in water, graphene oxides are well dispersed in water. Most of the exfoliation work was carried out using Elicarb Materials Grade Graphene Powder. As the stable dispersion mass level per unit volume of solvent was unknown, all solutions were prepared at a concentration of 1 mg per cm^3 of solvent.

Table 2: Solubility Parameters [16].

Material/Solvent	Boiling Point (°C)	Δ∂d /MPa0.5	Δ∂p /MPa0.5	Δ∂h /MPa0.5	R
Graphene [17]	-	**18**	**9.3**	**7.7**	-
Cyclohexanone	155.6	17.8	8.4	5.1	2.78
Methylene chloride	39.6	17	7.3	7.1	2.89
NMP	202	18	12.3	7.2	3.04
1,3-Dioxolane	75	18.1	6.6	9.3	3.14
Acetone	56	15.5	10.4	7	5.16
N,N-Dimethyl acetamide	165	16.8	11.5	10.2	4.10
Tetrahydrofuran	66	16.8	5.7	8	4.34
Methyl propyl ketone	101	16	7.6	4.7	4.78
Acetonitrile	81	16	12.8	6.8	5.39
Methyl acetate	57.1	15.5	7.2	7.6	5.42

$$R = \sqrt{4(\Delta\partial_d)^2 + (\Delta\partial_p)^2 + (\Delta\partial_h)^2}$$

Equation 1

In this work, two methods of exfoliation were studied:

1. Acoustic mixing (medium shear mixing technique); and
2. Ultrasound (200 to 400 W).

The rate of graphene falling out of solution for some samples was assessed by following the change in absorption at 660 nm using a visible light spectrometer [15]. Sample solutions were deposited onto microscope slides to assess whether the processing had exfoliated the sample to "invisible" graphene sheets. It was assumed that if the graphene were fully exfoliated then the broken down aggregates would form graphene sheets that would be invisible under an optical microscope. Only thick layers would be observed.

Where Δ∂d, Δ∂p, Δ∂h, are the difference between the graphene and solvent dispersion (∂d), polar (∂p), and hydrogen bonding (∂h) solubility parameters.

Although high mixer input powers and extended mixing times were employed, acoustic mixing processing could only break down the Elicarb aggregates to visible sheet-like particles. These particles shimmered in solvent when shaken. This suggested the acoustic mixing could not exfoliate Elicarb to graphene sheets.

Ultrasound was also used in an attempt to exfoliate Elicarb and other graphenes to form stable colloids. In this work, UV-Vis spectroscopy was used to see how stable the graphene colloid was. Samples of graphene exfoliated by acoustic mixing or ultrasound were left in a UV-Vis cuvette overnight. For most samples, the graphene precipitated out of the solution within 1.5 hours (Figure 7) to concentrations between 0.025 to 0.075 mg per cm^3.

Most of the Elicarb samples were unstable in THF or DMF (processed using ultrasound or acoustic mixer). Addition of polymer (Butvar) and surfactants (Zn caprylate, Zn neodecanoate) appeared to stabilise the Elicarb sample to some extent (taking from 340 to 480 minutes to reach 0.1 mg per cm^3). The graphene oxide (15 to 20 layers) appeared to be stable for at least ten hours post ultrasound processing. Similar solutions left on the bench appeared to be visibly stable for more than eight weeks. Graphene oxide (15 to 20 layers) processed using acoustic mixing was less stable than the equivalent ultrasound processed material. Graphene solutions were deposited onto

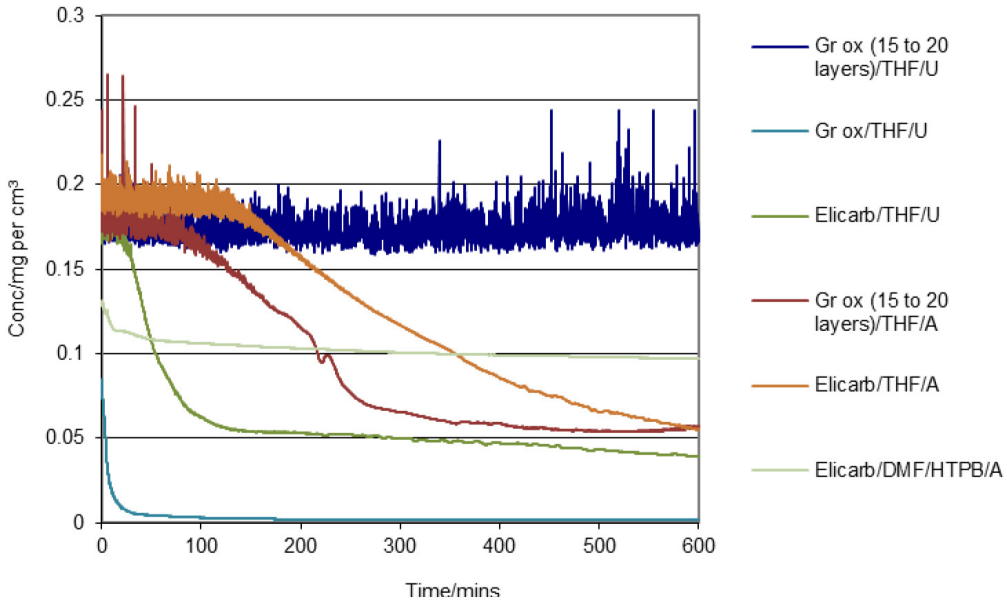

Figure 7: UV Assessment of Some Graphene/Graphene Oxide Stability in Solvents and Additives. A = acoustic mixing exfoliation, U = ultrasound exfoliation.

glass microscope slides to assess whether the exfoliation process and the use of additives facilitated the exfoliation and even deposition of graphene over the slide surface. Zirconium (IV) 2-ethylhexanoate, zinc neodecanoate, zinc caprylate and zinc stearate surfactant additives with and without polybutadiene or Butvar did not facilitate the even distribution of graphene layers on the slide.

Higher ultrasound powers and alternative shear mixing techniques may be more suitable for exfoliating the graphene powders. However, in this work the only material that evenly coated the slide was alkylamine functionalised graphene oxide (surfactants did not improve the coating ability of the graphene oxide).

3.3 Curing Reactions With/Without Graphene

Alkylamine functionalised graphene oxide fulfilled the criteria of fully coating a rough surface (observation of folds around surface particles). Hence alkylamine functionalised graphene oxide was used in barrier coating formulations. Two types of binder systems were considered for coating formulations: 1) high temperature crosslinking one component systems; and 2) low temperature crosslinking two component systems. The high temperature processes, although nominally poorly controlled, are simple reaction processes.

These were originally considered as good binder candidates as it was thought that extraneous reactions were less likely to occur. The two component crosslinking reactions in this work (epoxy ring opening and isocyanate reactions) are sensitive to moisture. This is especially an issue using dilute solutions/ solvents that have to be employed when handling graphene dispersions. Graphenes are only stable in dispersions at low concentrations. Care was taken to ensure solvents were dry for use. Excess curative (typically 10%) was used in case solutions were contaminated with water. None of the crosslinking processes have been optimised with respect to curing ratio, additives, temperature, etc. These are scoping reactions to see if the binder systems facilitate the coating of graphene onto uneven rubber surfaces.

The effect of alkylamine functionalised graphene oxide on the curatives and crosslinking processes were assessed by mixing amine functionalised graphene oxide with the binder system, casting the sample onto a silicon plate, measuring the IR spectrum, heating the sample at a known temperature and time, and measuring the change in the IR spectrum. As the graphene has a large surface area and is decorated with a number of unknown functionalities, there is potential for the graphene to interfere with the binder crosslinking process.

Eight binder systems were investigated at elevated temperatures (95 to 120°C):

1. Polybutadiene oxidisation;
2. Isocyanate oligomerisation and reaction with ambient moisture;
3. Epoxy ring opening by moisture and catalysts;
4. Polyvinyl butyral transacetalisation;
5. Polyvinyl formal transacetalisation;
6. Hydroxyl Terminated Polybutadiene (HTPB) / isocyanate urethane formation;
7. Polycaprolactone / isocyanate urethane formation; and
8. Epoxy/butanediol/catalyst ring opening.

There was qualitative evidence that the alkylamine functionalised graphene oxide did not affect polybutadiene oxidation. The functionalised graphene oxide may have impeded isophorone diisocyanate oligomerisation and may have reacted with isocyanate Desmodur N3600 (hexamethylene diisocyanate isocyanurate). It was difficult to observe transacetalisation in polyvinyl formal and polyvinyl butyral and the effect of amine functionalised graphene oxide. It proved difficult to observe epoxy ring opening and any effect of the graphene oxide. Isocyanate N3600 and IPDI readily reacted with HTPB or polycaprolactone in the presence of alkylamine functionalised graphene.

3.4 Coated Insulants and Diffusion

Assuming the diffusion processes are Fickian in nature and that DOA is mutually soluble in all the materials, then the diffusion profile could be modelled by:

- Coated surface. DOA diffusing from solution to the barrier coating surface (diffusion coefficient Ds). DOA diffusing through a thin layer of barrier coating into the polymer plaque (diffusion coefficient Db). DOA diffusing into the polymer plaque (diffusion coefficient Dp).
- Uncoated surface. DOA diffusing from solution to the polymer plaque surface (diffusion coefficient Ds). DOA diffusing into the polymer plaque (diffusion coefficient Dp).
- Initial conc. = 1 in solution, Initial conc. = 0 in barrier and plaque. Rate at which DOA leaves solution = rate at which it enters interfaces. DOA solution $Ds = 1 \cdot e^{-5}\ cm^2\ s^{-1}$. Barrier coating at 10 mm; 0.05 mm thick, $Db = 5 \cdot e^{-11}\ cm^2\ s^{-1}$. Plaque at 10.05 mm to 16.05 mm, $Dp = 1 \cdot e^{-8}\ cm^2\ s^{-1}$.

Figure 8 illustrates a predicted DOA diffusion profile, calculated using the PDE functionality in MATLAB, of a plaque with a good barrier coating on one surface (right side of plaque cross-section) and no coating on the right hand plaque surface. The initial DOA concentration profile (orange line) is predicted to evolve an unsymmetrical profile in the presence of an effective barrier coating.

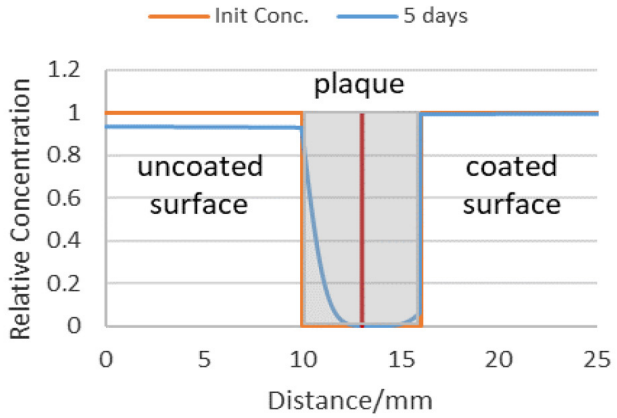

Figure 8: Theoretical Profile of DOA Diffusing into Coated (Right) and Uncoated (Left) Plaque Surfaces. Grey area = plaque cross-section.

The predicted plaque DOA profile compares well with the measured profile of a insulant coated with a good barrier. Typical IR maps of plaques with a poor barrier coat and a good barrier coat for EPDM insulants are illustrated in Figure 9. The bottom contour map in Figure 9 indicates the DOA readily migrates through the uncoated surface, but plasticiser migration (right hand side) is impeded through the coated surface.

Microtome slices can be of uneven thickness and therefore alter the apparent peak intensity of the DOA. Variation in carbonyl content due to sample thickness was avoided by calculating the ratio of the DOA carbonyl peak height at 1739 cm^{-1} against a polymer/insulant peak that was independent of DOA spectral features (peak height at 3323 cm^{-1}). Six DOA profiles

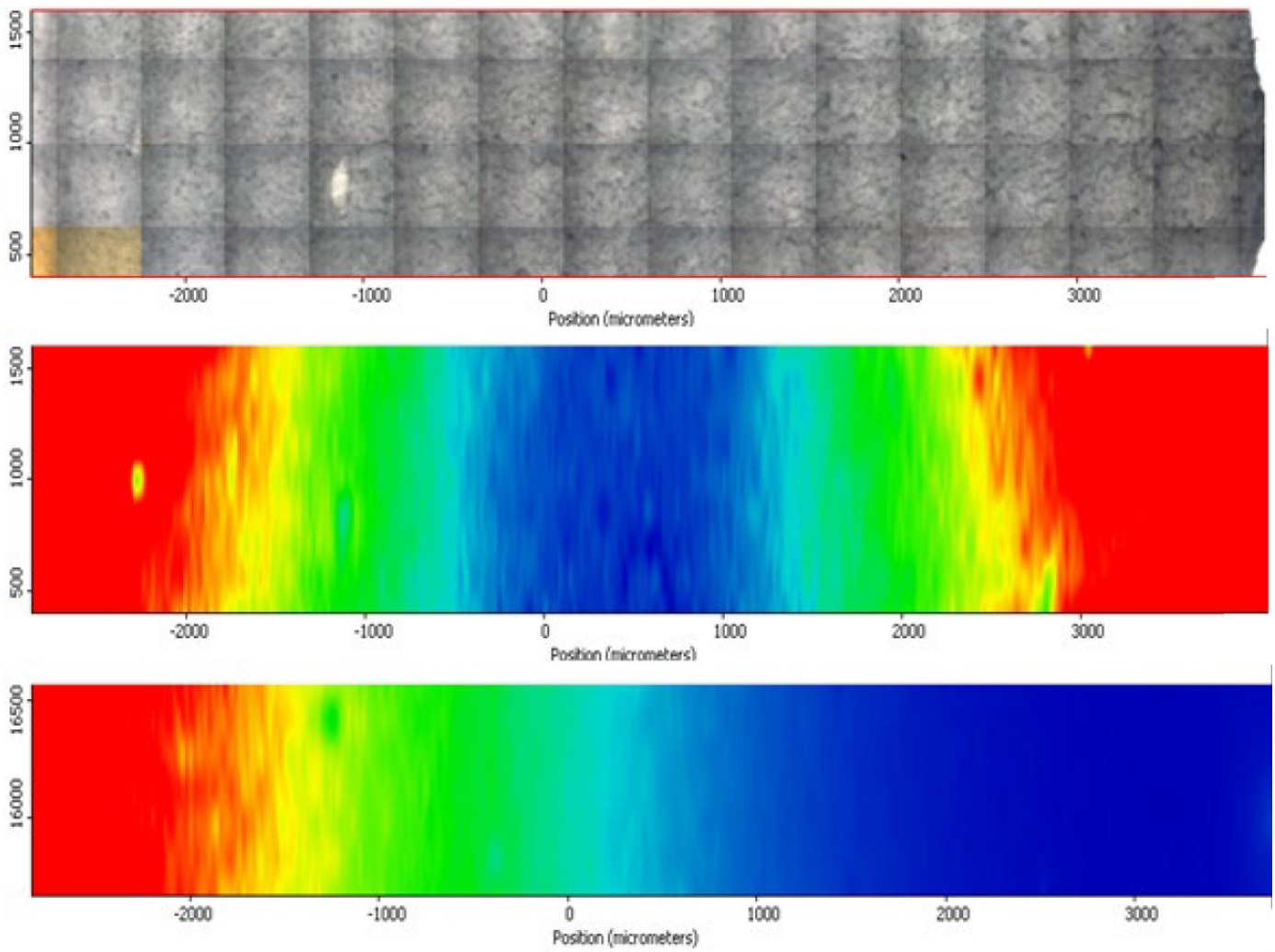

Figure 9: DOA Distribution, Barrier Coating Right Hand Side – Composite Optical Micrograph (Top), IR Map of Poor Barrier Coating (Middle), IR Map of Good Barrier Coating (Bottom). Hot colours (red, orange, yellow) = high concentration of DOA. Cold colours (green, cyan, blue) = low concentration of DOA.

(Figure 10) overlay each other reasonably well. The profiles are relatively "noisy" as each spectrum samples a volume that contains areas of impermeable fibre.

The ratio of the DOA peak concentration at the uncoated surface relative to the coated surface was used as a metric for barrier efficacy (DOA surface ratio). Additionally, in the case of DOA absorbed in PVC/NBR insulant, the centre baseline value subtracted from both edge values before calculating the DOA surface ratio.

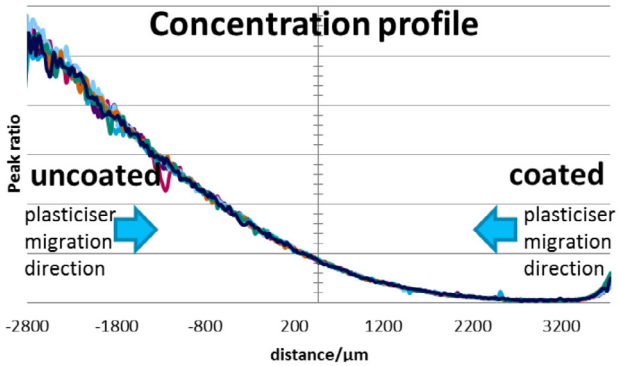

Figure 10: Profile Plot of DOA Distribution in 8x Coated EPDM.

None of the single component binder systems exhibited good barrier properties (1:1 binder to graphene composition). Even samples with three coats exhibited poor barrier coating efficacy – the lowest DOA surface ratio was 0.81.

Two component binder systems with higher binder content performed much better as barrier coatings. In the absence of graphene, the binder systems did not appear to impede DOA diffusion to any significant extent into the insulants. Hence the presence of graphene was critical to the barrier efficacy of the tested coatings. The barrier efficacy depended on the number of applied coats (Figure 11). Eight barrier coats in on EPDM insulant decreased the DOA surface ratio to below 0.05. That is to

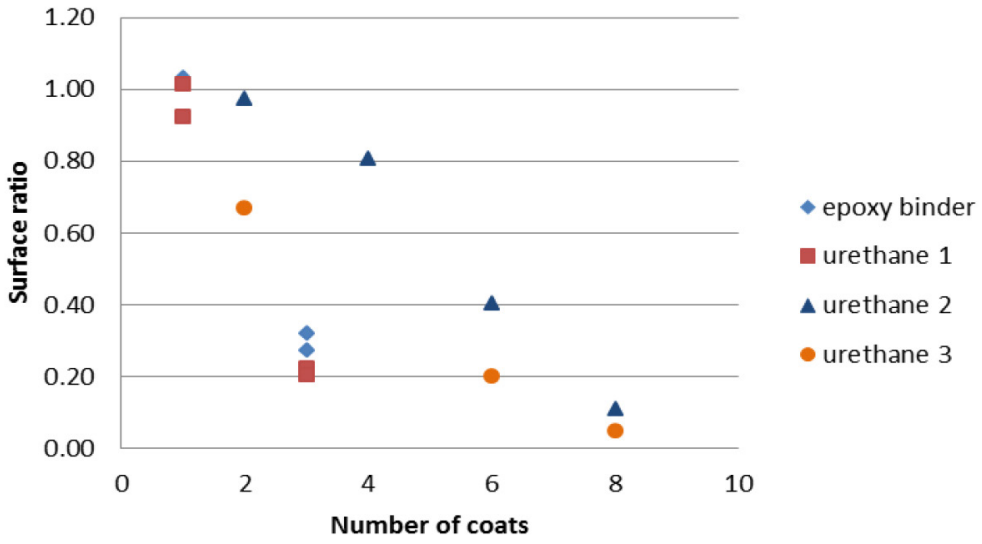

Figure 9: DOA Distribution, Barrier Coating Right Hand Side – Composite Optical Micrograph (Top), IR Map of Poor Barrier Coating (Middle), IR Map of Good Barrier Coating (Bottom). Hot colours (red, orange, yellow) = high concentration of DOA. Cold colours (green, cyan, blue) = low concentration of DOA.

say the permeability has decreased by at least 95%. A plaque with eight coats is thought to have approximately 1.3 mg of binder/graphene per cm^2 surface. Assuming the density of the binder/graphene is 0.9 g per cm^3, this would mean the barrier coating is approximately 0.015 mm thick.

4.0 SUMMARY AND CONCLUSIONS

The aim of this programme was to investigate and formulate effective barrier coatings suitable for application between the insulant and propellant that, if successful, could increase the range of materials that could be safely used in insulants and thereby improve their performance.

A number of graphene and functionalised graphenes were investigated as to their suitability in binder systems that were known to be compatible (non-reactive) with composite and double base propellants. It proved difficult to exfoliate by both ultrasound and acoustic mixing (high shear) some graphene materials. The graphene samples were unable to form stable colloids in typical graphene "solvents". Even materials that did form stable solutions were found, using an optical microscope, to consist of thick particles as opposed to single or multilayer graphene sheets (with less than ten layers). Although the graphene and graphene oxides used in this work exhibited characteristics that are associated with graphenes, most materials proved not to be suitable as a coating component. An alkylamine functionalised graphene oxide (2 mg per cm^3 in toluene) was found to contain sheets of material that were flexible and transparent suggesting this material had stable graphene-like dimensions.

The alkylamine functionalised graphene oxide was added to two families of binders – single component binders crosslinked at 120°C and two component binders crosslinked at 95°C. Traditional surfactant agents such as zinc caprylate were found not to be beneficial for creating an even graphene coating on glass microscope slides. Insulant samples (PVC/NBR or EPDM rubbers) coated on one side with test barrier coating were soaked in dioctyl adipate/polybutadiene solutions at 50°C to test barrier efficacy. Samples coated (one to three coats) with the one component binders at a binder to graphene additive ratio of 1:1 were ineffective barriers.

The two component binder systems, at ratios of alkylamine functionalised graphene to binder of 1:3 or 1:4, were found to be effective barrier coats to DOA diffusion. Eight barrier coats, totalling approximately 0.015 mm thick, were found to decrease the amount of DOA at the insulant surface by more than 95%.

For future work, the binder formulations should be optimised with respect curing ratio, additives, and cure temperature. Better

control of surface coverage, both homogeneity and applied mass, should be investigated. The binder to graphene ratio and graphene concentration should be optimised. Other bespoke functionalised graphenes should be synthesised and investigated in an attempt to increase the concentration of stable functionalised graphene dispersion. Application methodologies, such as spraying, should be investigated.

5.0 REFERENCES

[1] Takahashi, S., Goldberg, H.A., Feeney, C.A., Karim, D.P., Farrell, M., O'Leary, K., Paul, D.R. Gas barrier properties of butyl rubber/vermiculite nanocomposite coatings. *Polymer,* 47:3083-3093, 2006.

[2] Yeh, J.-M., Chang, K.-C. Polymer/layered silicate nanocomposite anticorrosive coatings. *Journal of Industrial and Engineering Chemistry*, 14:275-291, 2008.

[3] Joshi, M., Adak, B., Butola, B.S. Polyurethane nanocomposite based gas barrier films, membranes and coatings: A review on synthesis, characterization and potential applications. *Progress in Materials Science,* 97:230-282, 2018.

[4] Pourhashem, S., Saba, F., Duan, J., Rashidi, A., Guan, F., Nezhad, E.G., Hou, B. Polymer/inorganic nanocomposite coatings with superior corrosion protection performance: A review. Journal of Industrial and Engineering Chemistry, 2020, doi: https://doi.org/10.1016/j.jiec.2020.04.029.

[5] Christopher, G., Anbu Kulandainathan, M., Harichandran, G. Comparative study of effect of corrosion on mild steel with waterborne polyurethane dispersion containing graphene oxide versus carbon black nanocomposites. *Progress in Organic Coatings*, 89:199-211, 2015.

[6] Yang, X., Schneider, L.K.A., Giese, U., Schuster, R.H. Characterization of permeability of elastomers Part II, 63(11):496-505, 2010.

[7] Nine, M.J., Cole, M.A., Tran, D.N.H., Losic, D. Graphene: A multipurpose material for protective coatings. *J. Mater. Chem. A*, 3:12580-12602, 2015.

[8] Cui, Y., Kundalwal, S.I., Kumar, S. Gas barrier performance of graphene/polymer nanocomposites. *Carbon*, 98:313-333, 2016.

[9] Al-Jabareen, A., Al-Bustami, H., Harel, H., Marom, G. Improving the oxygen barrier properties of polyethylene terephthalate by graphite nanoplatelets. *Journal of Applied Polymer Science,* 128(3):1534-1539, 2013.

[10] Baker, C., West, R. email communication. *QinetiQ*, 21/10/2016, 0937, 2016.

[11] Zan, R., Ramasse, Q.M., Jalil, R., Bangert, U. Atomic structure of graphene and h-BN layers and their interactions with metals, nanotechnology and nanomaterials. In Advances in Graphene Science, IntechOpen Ltd, Mahmood Aliofkhazraei (Ed.), ISBN 978-953-51-1182-5, July 31, 2013.

[12] Lee, W., Oh, Y., Lee, K.E., Lee, J.U. Contrast enhancement for quantitative image analysis of graphene oxide using optical microscopy for Si-based field effect transistors. *Materials Science in Semiconductor Processing,* 39:521-529, 2015.

[13] Blake, P., Hill, E.W., Castro Neto, A.H., Novoselov, K.S., Jiang, D., Yang, R., Booth, T.J., Geim, A.K. Making graphene visible. *Applied Physics Letters,* 91:063124, 2007.

[14] Hansen, C.M. Hansen Solubility Parameters: A User's Handbook. CRC Press, Inc., Boca Raton FL, 1999. Second edition 2007. ISBN: 9780849372483.

[15] Wajid, A.S., Das, S., Irin, F., Tanvir Ahmed, H.S., Shelburne, J.L., Parviz, D., Fullerton, R.J., Jankowski, A.F., Hedden, R.C., Green, M.J. Polymer-stabilized graphene dispersions at high concentrations in organic solvents for composite production. *Carbon*, 50:526-534, 2012.

[16] Grulke, E.A. Solubility parameter values, polymer handbook, Wiley, J. Brandrup (Ed.), E.H. Immergut, 3rd edition, 1989.

[17] Esaú Del Rio-Castillo, A., Merino, C., Díez-Barra, E., Vázquez, E. Selective suspension of single layer graphene mechano-chemically exfoliated from carbon nanofibers. *Nano Research*, 7:963-972, 2014.

Measuring the Fast and Slow Energy Release of Laser-Excited Aluminum / Graphene Oxide Composites

Jennifer L. Gottfried, Chi-Chin Wu
CCDC Army Research Laboratory
Weapons and Materials Research Directorate
Aberdeen Proving Ground, MD 21005
UNITED STATES
Email jennifer.l.gottfried.civ@mail.mil

Xiaolin Zheng
Stanford University
Department of Mechanical Engineering
Stanford, CA 94305
UNITED STATES

Keywords: Aluminized; Defense; Energetic; Explosive; Graphene Oxide; Measurement.

ABSTRACT

Graphene Oxide (GO) has been used to facilitate the oxidation of micron- and nano-sized aluminum (Al) particles on both the microsecond- and millisecond-timescales relevant to detonation chemistry and combustion performance, respectively. A laboratory-scale technique based on the pulsed laser excitation of milligram quantities of material was used to evaluate the energy release from the Al/GO composites. High-speed video images of the reacting materials and time-resolved emission spectra provided further insight into the differences in chemistry between the samples. Transmission Electron Microscopy (TEM) was used to characterize the structures and spatial distribution of elemental species for the Al/GO composite samples. Micron-Al/GO and nano-Al/GO demonstrated enhanced energy release on both the fast and slow timescales compared to pure micron-Al and nano-Al. Mixtures of the Al/GO composites (20 wt %) with the military explosive Trinitrotoluene (TNT) suggest that unlike conventional aluminized explosives, Al/GO composites have the potential to increase the detonation performance as well as providing enhanced blast effects.

1.0 INTRODUCTION

Because of its high specific energy (31 kJ/g) and widespread availability, micron-sized aluminum (micron-Al) powders have been extensively used in energetics applications, primarily for blast enhancement on extended timescales (i.e., following the formation of detonation products). A key goal in energetic materials research is to accelerate the reaction of metals during an explosion so that the detonation performance of the explosive is enhanced. In addition to reacting too slowly to influence the detonation performance, micron-Al particles often suffer from incomplete combustion. Nano-sized Al (nano-Al) particles have the potential to react faster due to the increased specific surface area and kinetics-based (rather than diffusion-limited) reaction times, but suffer from issues such as the formation of a native oxide layer (alumina; Al_2O_3), which delays the reaction of the Al core and contributes significantly to the total mass of nano-Al particles, and strong agglomeration of the particles resulting in incomplete combustion.

Various approaches to improving the combustion efficiency and oxidation rate of Al have been investigated by our group and many others, including replacing the oxide layer with a more energetically favorable passivation layer [1], [2], [3], ball-milling the Al with faster-reacting metal species [4], formulation with energetic binders [5], and manipulation of the particle morphology [6], [7]. Because the oxidation of Al in an energetic formulation on a microsecond-timescale results in the Al scavenging oxygen (O) from the detonating explosive and reducing the detonation velocity [8], [9], enhancement of the detonation properties of an aluminized explosive requires additional oxidizing species in the formulation to maintain the optimal oxygen balance for the detonating explosive.

Graphene Oxide (GO) is typically synthesized by reacting graphite powders with strong oxidizing agents such as sulfuric acid ($H2SO_4$) and potassium permanganate ($KMnO_4$); the resulting GO sheets consisting of ordered nanoscale sp2 carbon domains, highly disordered oxidized sp3 domains, and carbon vacancy defects are functionalized with various carboxylic acid, phenol, hydroxyl, and epoxide groups [10]. While GO is an important precursor for the large-scale synthesis of graphene, GO has many interesting and unique properties as well [11], [12]. GO can be viewed as either molecules (along the ~1 nm nanometer-thick edge) or particles (along the active surface/basal plane, up to hundreds of micrometers).

Of particular interest for this work is the energetic nature of GO, which has been shown to undergo disproportionation reactions at 200 °C (~30% mass loss and ~1.3 kJ/g heat release under both air and argon [13]), resulting in the formation of reduced-GO, heat, and gases [14], [15]. GO contaminated with alkali salts from the chemical synthesis process is highly flammable in air, producing additional heat and gas due to carbon combustion reactions at 500°C (~40% mass loss and ~8.9 kJ/g heat release). GO has been demonstrated as an effective catalyst for various reactions [16], [17], [18], [19], [20], [21], [22]. Table 1 gives an overview of some of the energetic applications of GO that have been explored.

Table 1: Example Energetic Applications of GO.

Reference	Sample/Formulation	Description of results
Brodie [23]	GO	First report of the thermal instability of GO.
Croft [24]	GO	Also noted the thermal instability of GO upon heating.
Boehm and Scholz [25]	GO	Reported combustion of GO upon heating.
Jimenez [26]	GO	Measured the thermal decomposition of GO.
Sabourin et al. [27]	Nitromethane/GO	GO catalyzed nitromethane combustion, leading to lower ignition temperatures and increased burning rates.
Kim et al. [28]	GO	Observed spontaneous ignition of GO contaminated with potassium (K) in air.
Krishnan et al. [10]	GO	Demonstrated that the thermal instability of GO is due to the presence of alkali impurities such as K or sodium (Na).
Li et al. [29]	Cyclotetramethylene tetranitramine (HMX)/GO	GO decreased the impact and friction sensitivity of HMX and increased the thermal stability.
Zhang et al. [30]	Nitrocellulose (NC)/GO	GO added to enhance the optical ignition with a Nd:YAG laser and increase the burning rate of NC; also increased the thermal stability.
Zhang et al. [31]	Nitromethane/GO	Molecular dynamics simulations showing the mechanisms for catalytic decomposition of hot nitromethane by GO.
Liu et al. [32]	Hexanitrohexaaza-isowurtzitane (HNIW or CL-20)/GO	GO found to have no significant effect on the thermal properties of CL20.
Yu et al. [33]	CL-20/binder/GO	GO was found to slightly decrease the impact and friction sensitivity of the CL-20/binder, lower the decomposition temperature, increase the heat of decomposition, and decrease the critical explosion temperature during slow cook-off tests.
Qiu et al. [34]	GO	Observed explosive decomposition of GO samples in inert gas during thermal reduction, leading to laboratory equipment damage; 0.04 wt% K lowers the onset temperature for GO reduction and increases the probability for explosive reduction; increasing the sample mass enables the internal build-up of heat and gas, leading to thermal runaway in quantities as small as a few milligrams.
Thiruvengadathan et al. [35]	BiO_3/Al/GO	GO used to direct the self-assembly of Al and Bi_2O_3 nanoparticles, resulting in nearly double the energy release.
Thiruvengadathan et al. [36]	BiO_3/Al/GO	GO used to direct the self-assembly of Al and Bi_2O_3 nanoparticles, resulting in enhanced pressure generation, pressurization rate, burning rate, and specific impulse.

Chen et al. [37]	Metal nanoparticles / reducedGO films	Developed process to uniformly distribute reactive metal nanoparticles in a reduced-GO film; demonstrated energetic properties of nano-Al embedded in reduced-GO, which served as a barrier to oxidation and agglomeration for the Al.
Qiu et al. [38]	GO	Concluded that the explosive thermal decomposition of GO is a function of mass; for higher masses, the reaction rates exceed heat losses to the surrounding environment, leading to thermal runaway.
Memon et al. [39]	GO / Ammonium Perchlorate (AP) / Hydroxyl-Terminated Polybutadiene (HTPB)	Used recrystallization / fast crash method to create AP/GO composite, which resulted in increased propellant burning rates at high pressures.
Wang et al. [40]	HMX/Viton/GO	GO desensitized HMX: improved thermal stability, lower impact and shock wave sensitivities.
Yan et al. [41]	GO/energetic materials	Review of GO (and other functionalized carbon nanomaterials) in energetic compositions, with emphasis on Chinese literature.
Yan et al. [42]	Al@Fe_2O_3/GO	Fe_2O_3 deposited on GO/Al substrates via atomic layer deposition results in reduction of GO and formation of energetic composites with increased energy release and reduced electrostatic discharge sensitivity.
Yan et al. [43]	rGO@Fe_2O_3/AP	Reduced GO decorated with Fe_2O_3 nanoparticles was used to catalyze the decomposition of AP.
Tao et al. [44]	Al/CuO/GO	GO quantum dots (<100 nm in lateral dimensions) used as building blocks to assemble metastable intermolecular composites of Al and CuO, resulting in increased energy release and specific heat.
Wang et al. [45]	TKX-50/GO	GO changed the morphology of TKX-50, decreased the impact and friction sensitivities, and did not affect the thermal stability.
An et al. [46]	GO/Triaminoguanidine (TAG)/AP	Transition metal complexes of TAG nitrate with GO as a dopant were used to catalyze the decomposition of AP.
Jiang et al. [13]	micron-Al/GO	Micron-Al wrapped in GO to increase the optical ignition of Al with a Xe flash tube, also increased combustion efficiency.
Lyu et al. [47]	GO-doped PVDF/CuO/Al	Electrospinning the GO-doped nanocomposites improved the heat of reaction, density, and anti-oxidation capability compared to mechanical mixing, while GO improved the reaction efficiency of PVDF/CuO/Al.
Chen et al. [48]	GO/TAG	Transition metal complexes of TAG nitrate with GO as a dopant were used to investigate the mechanisms for GO stabilization of energetic materials.
Lakhe et al. [49]	GO	Demonstrated that GO can explosively decompose at normal drying temperatures with pressure generation rates >1000s psig/min, with surface area determining the critical mass necessary for decomposition.
Zhang et al. [50]	GO/TAG	Studied decomposition of GO/TAG via Reactive Force-Field (ReaxFF) with experimental validation; GO decreases the decomposition temperature of TAG.
Chen et al. [51]	GO/TAG/AP	Transition metal complexes of TAG nitrate with GO were used to study the decomposition of AP; the photon transfer between O and O_2 determines the catalytic decomposition pathways, depending on the reactive center.
Cheng et al. [52]	Functionalized-GO/AP	The effect of surface functional groups on metal-free GO energetic performance, thermal stability, and catalytic properties with respect to AP was investigated.
Hanafi et al. [53]	Functionalized-GO/AP or RDX	Highly energetic coordination polymers were synthesized by cross-linking functionalized GO; these polymers had a strong catalytic effect on the decomposition of AP and stabilized RDX.
Huang et al. [54]	GO/CL-20	GO used to improve the thermal stability and decrease the mechanical sensitivity of CL-20 composites.
Qi et al. [55]	GO/energetic materials	Investigated the compatibility of various GO-related systems with energetic materials such as AP, RDX, and HMX.
Jiang et al. [56]	micron-Al/GO/ Fluorinated Graphene (FG)	GO facilitates the dissociation of FG, and FG accelerates the disproportionation and oxidation of GO; together, they greatly accelerate Al combustion.

The enhancement of the ignition and combustion properties of micron-Al particles with as little as 3 wt % GO was recently demonstrated [13]. In addition to enabling micron-sized Al to be ignited by an optical Xenon (Xe) flash, the GO also promoted the more efficient combustion of Al in air on the millisecond-timescale. Analysis of the combustion reactions, post-combustion products, and reactive molecular dynamics simulations confirmed that the addition of GO promotes the oxidation of micron-Al particles via additional heat release (from exothermic disproportionation and oxidation reactions), catalytic effects (by providing active sites for stabilization of free radicals), and gas generation (CO_2, H_2O, etc.). The goal of this work was to determine if the exothermic disproportionation of GO and reactions of the resulting gaseous products could be used to facilitate the oxidation of micron-Al and/or nano-Al on the microsecond-timescale in order to improve the detonation performance of military explosives.

A laser-based technique developed at the Combat Capabilities Development Command's (CCDC) Army Research Laboratory (ARL) for evaluating the energetic performance of milligram quantities of material was used to measure the energy release of Al/GO composites on both the fast (i.e., detonation-relevant) and slow (i.e., propellant/blast-related) timescales. The Laser-Induced Air Shock From Energetic Materials (LASEM) technique uses a high energy, nanosecond-pulsed laser to ablate, atomize and excite a residue material, forming a laser-induced plasma with temperatures exceeding 10,000 K [57]. The heating rate and microsecond-timescale conditions in the laser-induced plasma are very similar to those during detonation initiation and within the chemical reaction zone behind a detonation front during an explosion, respectively. Just as reactions behind the detonation front drive a shock wave through the bulk material, the high-temperature reactions in the laser induced plasma increase the velocity of the laser-induced shock wave that expands into the air above the sample; thus, the more energetic the material is on the microsecond-timescale, the faster the resulting laser induced shock velocity [58]. On the millisecond-timescale, the intensity and duration of combustion (or deflagration) reactions indicate the potential of the material for propellant-based applications [59]. The LASEM method for estimating detonation performance has been demonstrated for conventional military explosives [58], novel energetic materials [60], military explosives with added Al or boron [9], and novel metal additives [1], [2], [3], [61]. For both conventional [58] and aluminized [9] military explosives, the laser-induced shock velocities from LASEM can be directly correlated to the detonation velocity from large-scale detonation testing. Here, we compare the energy release rates for micron-Al/GO and nano-Al/GO powders and estimate the detonation performance of TNT mixtures with 20% added Al/GO.

2.0 EXPERIMENTAL

2.1 Synthesis of Al/GO Composites

Al/GO composites (80/20 wt %) were prepared by mechanical mixing, also known as ultrasonic mixing. The Al particles were either an average 3.9 µm or 70 nm in diameter. The Al was sonicated in a 1:1 dimethylformamide and isopropyl alcohol solution (10 mg/mL) for 15 min. The GO powder (0.55 – 1.2 nm thick, 0.5 – 3 µm diameter) was sonicated in dimethylformamide (1 mg/mL) for 2 hours. The two suspensions were then mixed and sonicated for 1 hour, filtered, heated at 100 °C for 1 hour to vaporize the solvent residue, and dried in a vacuum desiccator overnight [13].

2.2 Sample Imaging and Elemental Map Acquisition

Transmission Electron Microscope (TEM) specimens were prepared via a standard nanoparticle suspension technique by dispersing a small quantity of Al/GO in acetonitrile and sonicating until a colloidal solution was formed. A few drops of the Al/GO-containing solution were then added onto the holey carbon film-supported TEM grid (Ted Pella; 300 mesh) and air dried. The samples were studied using a JEOL 2100FX microscope operated at a 200 kV acceleration voltage (JEOL USA, Inc.). The samples were imaged under Bright Field (BF) image conditions with a Gatan Digital Micrograph and an Orius digital camera (Gatan, Inc.). The

chemical analyses were performed by acquiring elemental X-ray maps of the nano-Al/GO derived from spectrum images acquired using the TEAM Analysis software (EDAX, Inc.) in the Scanning Transmission Electron Microscopy (STEM) mode.

2.3 LASEM Measurements

The LASEM technique has been described in detail previously [57], [58], and the configuration for this work is shown in Figure 1. Briefly, a 6-ns pulsed laser (1064 nm, 850 mJ) was focused below the sample surface. The laser ablates, atomizes, ionizes, and excites the sample – resulting in the generation of a laser-induced plasma. The heating rate and plasma conditions (temperature, pressure, electron density, etc.) are very similar to those occurring during the initiation and within the propagating chemical reaction zone of detonating energetic materials, respectively. The high-temperature reactions in the laser-induced plasma are monitored using time resolved, gated emission spectroscopy with an echelle / Intensified Charge Coupled Device (ICCD) spectrometer (200 – 1000 nm, 0.02-nm resolution). The formation of the laser-induced plasma generates a laser-induced shock wave, which expands into the air above the sample. A high-speed color camera records the expansion of the shock wave via schlieren imaging [62] at 84,000 frames-per-second (1 µs shutter). Exothermic chemical reactions occurring in the plasma during the expansion of the shock wave through the plasma region (<10 µs) increase the plasma temperature and accelerate the shock wave (which rapidly decays to the speed of sound in air following cessation of the laser pulse). The characteristic laser-induced shock wave for the sample under the given experimental conditions is determined by the y-intercept of a 5th order polynomial fit of the shock wave velocity versus time.

Particles ejected off the sample surface by the laser-induced shock wave can start combusting as they pass through the region of air heated by the plasma and the passage of the shock wave. These self-sustained combustion reactions, which occur on the millisecond-timescale, are monitored with a second time-resolved emission spectrometer (230 – 900 nm, 0.25-nm resolution) and photodiodes that are

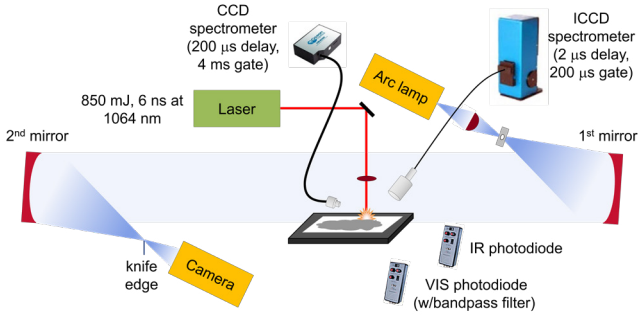

Figure 1: Experimental Schematic for the Laser Ablation and Excitation of Al/GO Composites Using LASEM. The emission from the laser-induced plasma and subsequent combustion reactions was detected with spectrometers gated to the appropriate time regime and time-resolved emission integrated over the Visible (VIS) and Infrared (IR) wavelengths was recorded with photodiodes. The laser-induced shock wave was recorded with a high-speed camera using schlieren imaging.

integrated over the infrared (900 – 1700 nm) or visible (300 – 1050 nm) emission regions. A bandpass filter at 486 nm was added to the visible photodiode to monitor the AlO emission during the combustion reactions.

In addition to the Al/GO composites prepared for this work, LASEM data on the 70 nm Al precursor for the nano-Al/GO composites was obtained; previous data on a micron-Al sample [9] and a commercial GO was used. The military explosive Trinitrotoluene (TNT) was obtained from colleagues at ARL and hand-mixed with the Al additives (20% by weight) for comparison to the tritonal formulation of TNT with 20% micron-Al previously studied [4]. All samples were prepared by spreading a thin layer of material on double-sided tape affixed to a glass microscope slide (~100 µg/mm^2). While the laser-induced shock velocities are independent of the material thickness (since excess material is ejected off the sample slide out of the laser-material interaction region), the extent and duration of the millisecond-timescale combustion reactions depends strongly on the residue thickness [2] – thus the sample thicknesses were kept as consistent as possible between samples and between different sample slides.

3.0 RESULTS

3.1 TEM Analyses

For the micron-Al/GO composite, the morphology and structural features of the

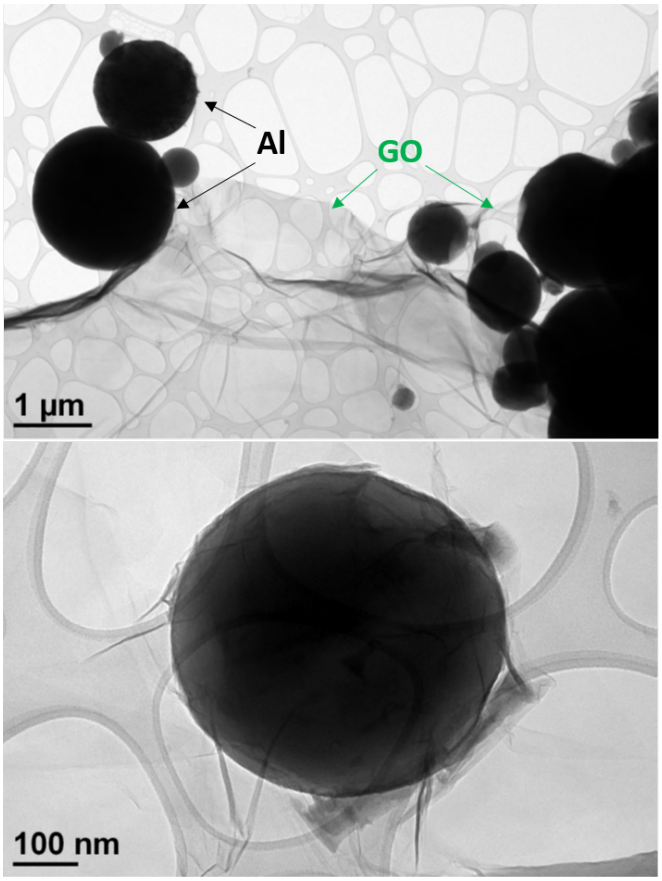

Figure 2: TEM Images of Micron-Al/GO Showing Inconsistent Particle Wrapping with the GO. Recorded with a high-speed camera using schlieren imaging.

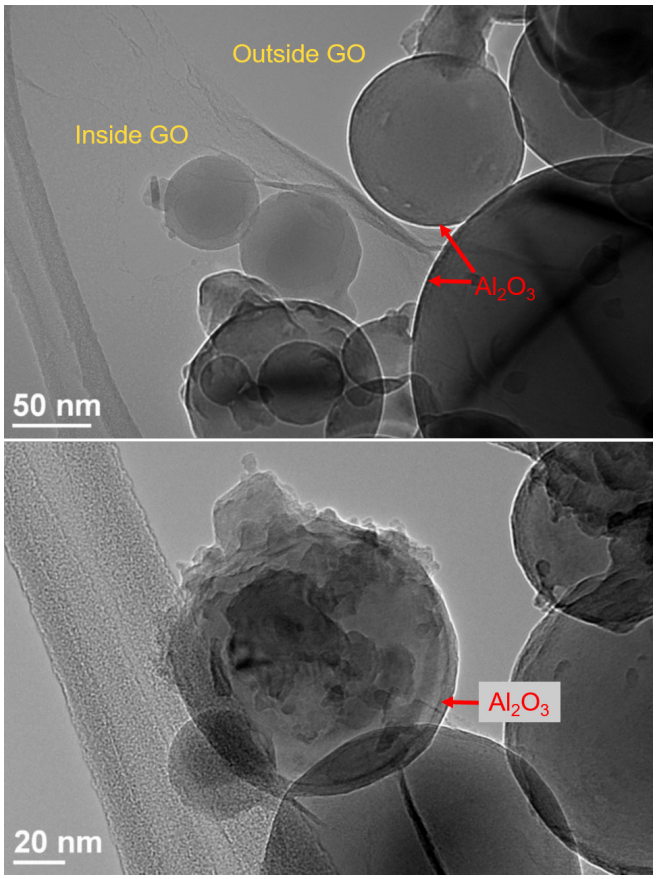

Figure 3: TEM Images of Nano-Al/GO Showing the Wrapping of the GO Sheets Around The Nano-Al, the Presence of the Al_2O_3 Shell, and the Contamination Present on Some of the Al Particle Surfaces.

micron-Al particles cannot be fully revealed in TEM because of the relatively large particle diameters, which make the sample opaque to electrons; a typical thickness for an electron-transparent specimen is usually less than 100 nm. Scanning Electron Microscope (SEM) images of the micron-Al/GO composites were previously published [13]. After surveying many different regions with TEM, we found that GO wrapping was not successful for most micron-Al particles. As shown in Figure 2, complete wrapping of the micron-Al/GO was only achieved for smaller Al particles, e.g., the approximately 500 nm Al particle shown in the bottom of Figure 2. This can be attributed to direct spatial blocking effects due to the relatively large particle sizes. The difficulty in GO wrapping was also exacerbated due to the presence of agglomerated micron-Al, as shown in the top right of Figure 2.

On the other hand, detailed structural features were revealed in TEM for the nano-Al/GO particles because they were much more electron beam transparent. The amorphous Al_2O_3 shell surrounding the crystalline Al core was clearly visible with different contrasts in the TEM images (Figure 3). The nano-Al/GO particles had better surface coverage of the nano-Al by the GO. The white rings in the images shown in Figure 3 indicate an under focus condition, which was chosen to show the strong contrast of the crystalline Al core. Surface contamination on the nano-Al/GO particles resulting in "Christmas ornament"-like particles was also observed sporadically. The source of the observed impurities in nano-Al/GO composites is not yet clear. However, the contaminants may have been introduced during the sonication process used for the sample preparation.

In order to further characterize the wrapping of the nano-Al particles with the GO and the origin of the observed structural features, elemental maps of the nano-Al/GO sample were obtained via STEM Mode in TEM (Figure 4). These elemental maps show the presence of nitrogen (N), which is seemingly concentrated near the particle-particle

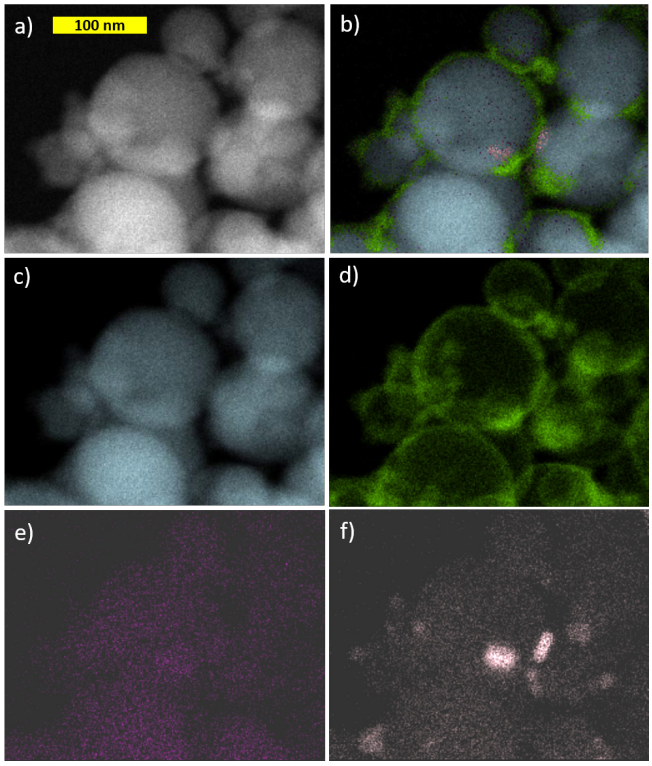

Figure 4: (a) TEM Image and (b) the Corresponding Elemental Map Obtained Using STEM Showing the Spatial Distributions of (c) Aluminum, (d) Oxygen, (e) Carbon, and (f) Nitrogen in Nano-Al/GO.

interfaces and O on the surface of the nano-Al particles (from the native Al_2O_3 layer and/or the GO). Nitrogen can be introduced into the nano-Al particles during the commercial synthesis process. While a longer collection time was needed to obtain a stronger carbon (C) signal, the C (from GO and/or surface functional groups) appears well-dispersed throughout the nano-Al particles.

3.2 Emission Spectra

Time-resolved emission spectra from the laser-induced plasma of excited Al/GO composites provide information about the elemental composition of the ablated material, a technique known as Laser-Induced Breakdown Spectroscopy (LIBS) [63]. The LASEM setup

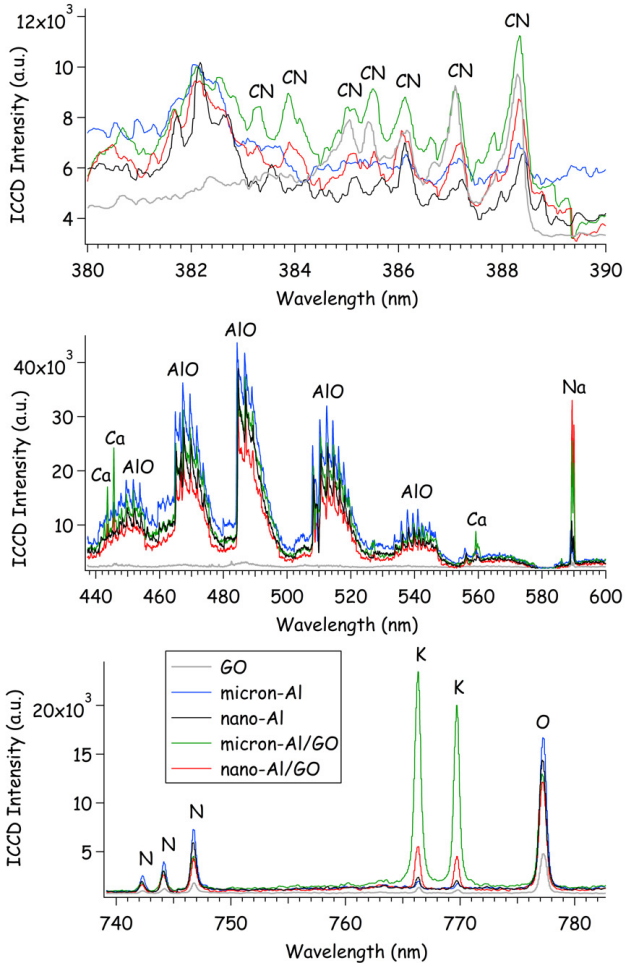

Figure 5: Emission Spectra integrated over the first 200 µs of the Laser-induced Plasma Lifetime (following a 2 µs delay to avoid the Broadband Continuum Emission).

incorporates LIBS as part of the diagnostic information collected. Previous work by Serrano et al. demonstrated the characterization and discrimination of graphite, graphene, and GO samples with LIBS [64]. Selected regions of the emission spectra of the GO, Al, and Al/GO samples are shown in Figure 5. Carbon emission is present in all the spectra, including Al; C in the Al spectra is a result of organic surface functional groups and/or organic impurities. The molecular Cyano (CN) radical emission, formed primarily from the recombination of C and N atoms in the plasma

Table 2: Emission Intensity Ratios (with 95% Confidence Intervals) from the Spectra of GO, Al, and Al/GO Composites.

Sample	O/N	H/C	CN/C	Al/O	AlO/Al	Na/C	K/C
GO	4.4 ± 1.0	2.5 ± 0.5	4.8 ± 2.0	--	--	0.82 ± 0.37	0.35 ± 0.29
micron-Al	2.5 ± 0.2	7.1 ± 1.6	1.9 ± 0.8	1.3 ± 0.2	1.0 ± 0.1	5.9 ± 2.7	0.63 ± 0.38
nano-Al	2.7 ± 0.3	5.3 ± 1.2	2.3 ± 0.5	1.4 ± 0.1	1.1 ± 0.3	6.7 ± 3.5	0.65 ± 0.99
micron-Al/GO	6.0 ± 0.2	3.4 ± 0.9	4.8 ± 1.0	0.58 ± 0.06	4.9 ± 1.0	14 ± 4	14 ± 3
nano-Al/GO	5.4 ± 1.0	10 ± 4	9.6 ± 3.6	0.87 ± 0.14	2.7 ± 0.5	55 ± 28	8.2 ± 4.2

(including N from air), is significantly stronger for the GO-containing samples. In the previous study [64], C_2 emission was not observed in the GO spectra (over a much shorter gate, 0.5 µs) – here, we have observed only very weak C_2 emission in the GO spectra over the 200 µs gate (near 516 nm). Depletion of C_2 radicals through competitive reactions with O in the plasma has been shown to reduce or eliminate C_2 emission from carbon-containing molecules [65]. While the presence of Al may promote the formation of C_2 (by preferentially reacting with the available O and reducing the formation of CO and CO_2), unfortunately any C_2 emission in the Al/GO composites is obscured by the strong aluminum monoxide (AlO) emission. All sample spectra also contain significant hydrogen (H) emission (not shown). The presence of hydrogen gas during the reduction of GO has been shown to result in violent reactions with –OH groups on GO surface [66], inducing thermal decomposition. Thus, increasing the hydrogen concentration in the composite material could potentially lead to GO decomposition reactions even faster. Hydrogen bonds also serve as bridges between adjacent nanosheets within the GO lattice [67].

While most of the O and N emission is due to entrainment of air into the laser-induced plasma, the O/N ratio (using background-corrected emission intensities) is higher for the GO-containing samples (Table 2) – which may serve as an indication of the extent of oxidation of the GO compared to other graphene-related samples. Higher O/C content has also been shown to increase the decomposition rate of GO [68], although in this case the C in the Al samples contributes significantly to this ratio. The AlO emission is only present in the Al-containing samples and indicates the extent of aluminum oxidation on the microsecond-timescale. The Al/O and AlO/Al ratios indicate that the Al/GO composites have less unoxidized Al in the first 200 µs of the reactions compared to pure Al particles.

In addition to the emission from the primary elemental species (C, Al, O), emission from impurities was also observed. The Al/GO composites contain higher concentrations of the alkali [lithium (Li), sodium (Na), and potassium (K)] and alkaline earth [magnesium (Mg), calcium (Ca), and strontium (Sr)] metals.

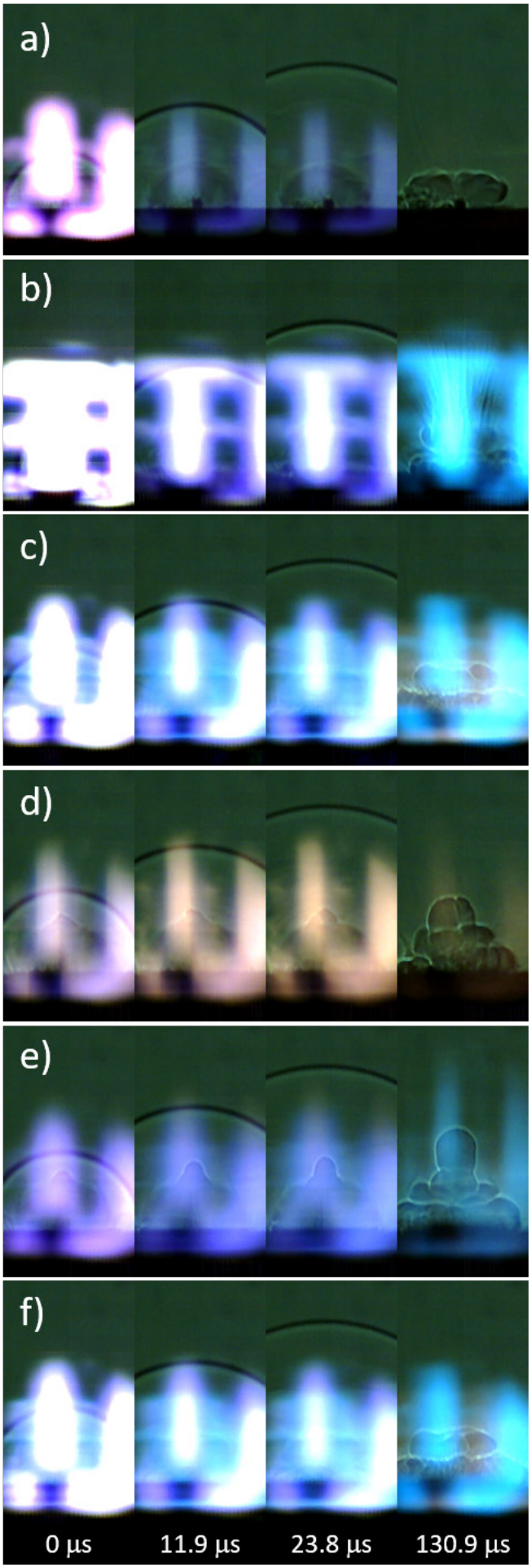

Figure 6: Snapshots from the High-Speed Video of Laser-Excited (a) Blank Tape, (b) Micron-Al, (c) Nano-Al, (d) GO, (e) Micron-Al/GO, and (f) Nano-Al/GO.

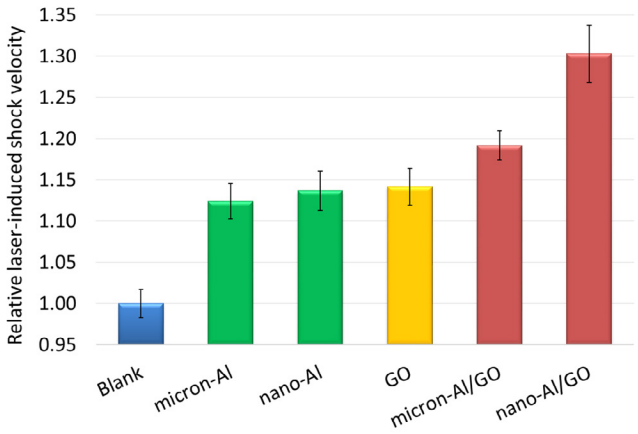

Figure 7: Relative Laser-Induced Shock Velocities for the Blank Tape Substrate, Micron-Al, Nano-Al, GO, and the Micron-Al/GO and Nano Al/GO Composites.

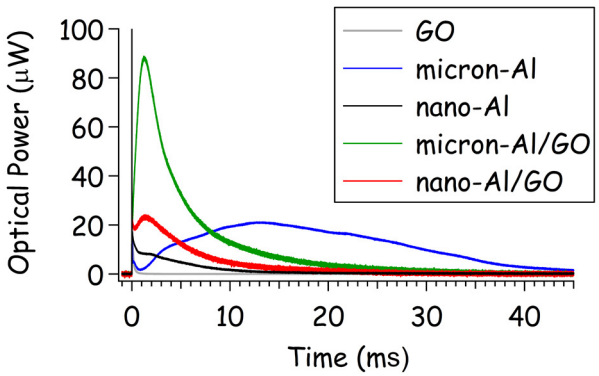

Figure 8: Emission from the Laser-Induced Plasma (1st Sharp Spike Near Time Zero) and the Subsequent Combustion Reactions of the GO, Al, and Al/GO Particles Ejected Into the Air Above the Sample Surface.

It is important to note that the pure GO and Al samples were similar, but not identical, to the materials used to make the Al/GO composites – so the impurities in the Al/GO composites could have originated from the starting components and were not necessarily introduced during the synthesis process. Because each laser shot samples only tens of micrograms of material, the concentration of these impurities (e.g., K) can vary significantly from shot-to-shot. Since alkali impurities are known to catalyze the decomposition of GO and increase flammability [10], the relative quantities of these impurities could potentially be used to evaluate the safety of GO-containing composites. For this application, where the heat released from the exothermic reactions of GO facilitates the oxidation of Al, the presence of the alkali salt contaminants may actually increase the efficiency of this process since they promote the further combustion of the reduced-GO products – thus enhancing the total energy release from GO.

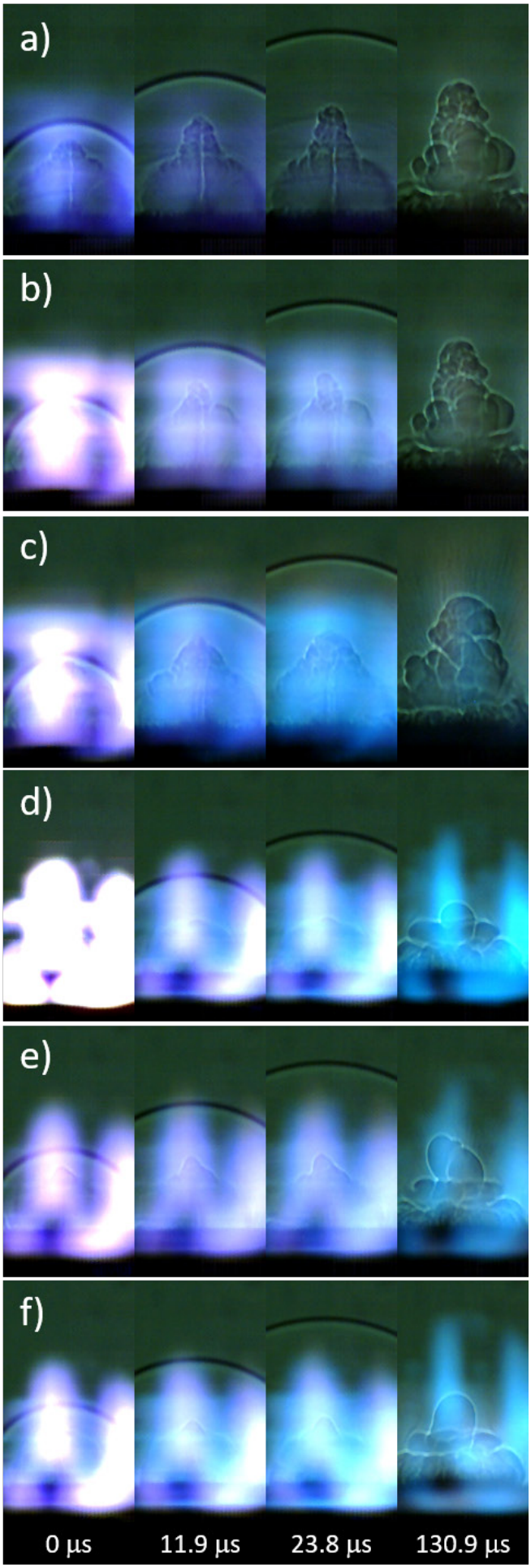

Figure 9: Snapshots from the High-Speed Video of Laser-Excited (a) TNT, (b) TNT+Al_2O_3, (c) TNT+micron-Al, (d) TNT+nano-Al, (e) TNT+micron-Al/GO, and (f) TNT+nano-Al/GO.

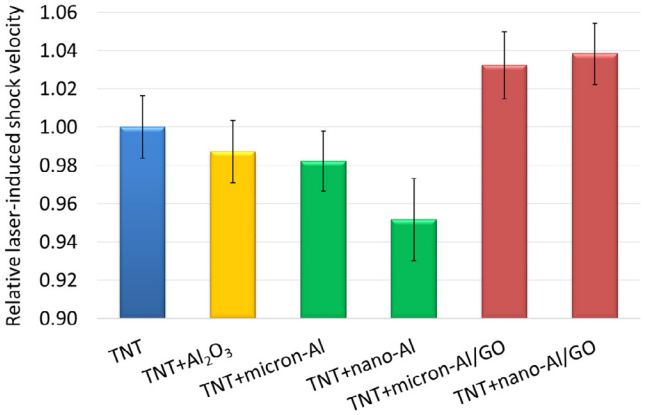

Figure 10: Relative Laser-Induced Shock Velocities for Pure TNT, TNT+Al_2O_3, TNT+micron-Al, TNT+nano-Al, TNT+micron-Al/GO, and TNT+nano-Al/GO.

3.3 Laser-Induced Shock Waves

Snapshots from the high-speed video of the laser excitation of the blank tape, micron-Al, nano-Al, GO, micron Al/GO, and nano-Al/GO are shown in Figure 6. All images have been cropped (from the top) and the brightness enhanced (+40%) to increase the contrast of the shock wave and background. In general, inert materials produce significantly more visible plasma emission [57]. Blue emission from AlO is visible in the images from Al-containing samples, purple CN emission appears in the GO-containing samples – as does the orange-ish Na emission from combustion of the GO at later times. The ejection of burning Al particles is visible in the micron-Al image at 130.9 µs (Figure 6(b), appearing as dark streaks). Significant differences in the plume expansion can be observed for the samples at later times, as shown in the last frame used to measure the shock position (130.9 µs, shock wave position cropped out-of-frame). Understanding the observed differences in plume expansion would require modelling the hydrodynamic

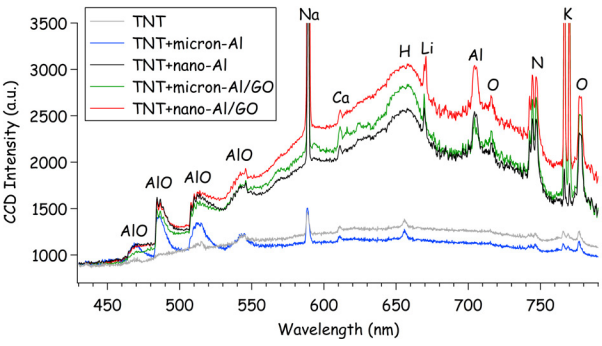

Figure 12: Emission Spectra for TNT, TNT+Al, and TNT+Al/GO Samples Integrated Over the First 4 ms of the Combustion Reactions Following the Laser-Induced Plasma.

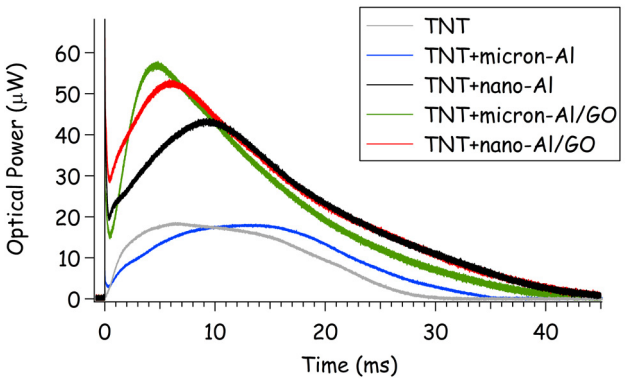

Figure 11: Emission from the Laser-Induced Plasma (1st Sharp Spike Near Time Zero) and the Subsequent Combustion Reactions of TNT, TNT+Al, and TNT+Al/GO Particles Ejected Into the Air Above the Sample Surface.

effects resulting from the high-temperature chemical reactions, which is beyond the scope of this study.

3.4 Energy Release Rates

The microsecond-timescale energy release rates (<10 µs), as measured by the laser-induced shock velocities, are shown in Figure 7. The energy release from micron-Al, nano-Al, and GO was exothermic compared to the inert blank tape substrate. Enhanced microsecond-timescale energy release was observed for the Al/GO composites compare to the pure Al samples. The energy release from nano-Al/GO was significantly higher than that of micron-Al/GO, as a result of the higher specific surface area of the nano-Al and/or more intimate contact between the Al and GO.

In contrast, the nano-Al/GO had less millisecond-timescale energy release than micron-Al/GO, as measured by the combustion emission (Figure 8). There are two contributions to this behavior:

1. Because the oxide layer comprises a more significant fraction of the mass of the nano-Al, it has a lower active Al content and thus less overall energy to release; and
2. Because the nano-Al reacts earlier, most of the Al had reacted by the time the combustion reactions occur.

Both Al/GO composites combust significantly faster and more strongly than their pure Al counterparts.

3.5 TNT+Al/GO Composites

In order to investigate the effect of the enhanced microsecond timescale reactions of the Al/GO composites on the detonation performance of TNT, mixtures of 20% by weight additive were prepared and tested. Images from the high-speed videos of laser-excited TNT, TNT+Al2O3, TNT+micron-Al, TNT+nano-Al, TNT+micron-Al/GO, and TNT+nano-Al/GO are shown in Figure 9. The characteristic laser-induced shock velocities for the samples are shown in Figure 10. While the addition of the inert Al2O3 reduces the laser-induced shock velocity of TNT (and thus the estimated detonation velocity), the micron-Al and nano-Al further reduce the estimated detonation velocity of TNT since the oxidation of the Al that reacts on the microsecond-timescale scavenges the O from the detonation products [8], [9]. Since the nano-Al is more reactive on the microsecond-timescale due to its larger specific surface area, this effect is more extreme than for the micron-Al. On the other hand, both the micron-Al/GO and nano Al/GO increase the estimated detonation velocity of TNT, suggesting that they contribute to the exothermic energy release without scavenging O from the detonation products – likely as a result of the O available due to the disproportionation reactions of GO. Interestingly, no significant difference in the laser-induced shock velocities between TNT+micron-Al/GO and TNT+nano Al/GO was observed, perhaps suggesting that the increased reactivity of the nano-Al is not sufficiently balanced by the presence of additional oxidizing agents from the GO.

In addition to the predicted increase in detonation performance by the Al/GO composites compared to Al, the increase in millisecond-timescale combustion observed for the composites (Figure 11) suggest that significantly enhanced blast effects may also be possible. The time to peak combustion is also faster for the Al/GO composites than Al. Unlike the emission spectra from the high-temperature laser-induced plasma (Figure 5), the combustion emission spectra are dominated by emission from molecular species and blackbody radiation from the burning particles (Figure 12). The Na and K emission from the TNT+Al/GO composites nearly saturate the spectrometer at ~12,000 counts each (off-scale).

4.0 CONCLUSIONS

By wrapping micron-Al and nano-Al in GO via sonication, enhanced energy release on both the microsecond and millisecond-timescales has been demonstrated. We speculate that the heat released from the exothermic disproportionation reactions of GO during rapid heating facilitate the oxidation of Al. Furthermore, the gases also released (e.g., CO, CO_2) reduce the agglomeration of product species that could have otherwise inhibited efficient combustion. According to the TEM analyses, efficient GO wrapping was achieved for nano-Al particles but not for the majority of the micron-Al particles – resulting in considerably different energy release rates between these two composites. The nano-Al/GO had significantly enhanced microsecond-timescale energy release. Further studies are needed to quantify the effect of alkali impurities on the catalytic effect of GO and improve the wrapping efficiency, especially for micron-Al particles. An improved methodology for preparing transmission transparent micron-Al/GO TEM specimens is also necessary to study their detailed structural and chemical properties, most likely involving tedious sample preparation to sandwich the particles in epoxy, followed by Focused Ion Beam (FIB) milling and lift out. Mixtures of TNT with 20% Al/GO showed enhanced microsecond- and millisecond-timescale energy release compared to TNT+Al mixtures. Increased microsecond-timescale energy release is expected to result in increased detonation performance, i.e., higher detonation velocities (shattering ability) and/or Gurney velocities (metal-pushing ability), while increased millisecond-timescale energy release is expected to result in increased blast effects (late-time impulse). Optimization of the formulation to achieve a better oxygen balance and improve performance is necessary. The predicted performance enhancements must then be confirmed with large-scale detonation testing.

5.0 REFERENCES

[1] Davari, S.A., Gottfried, J.L., Liu, C., Ribeiro, E.L., Duscher, G., Mukherjee, D. Graphitic-coated Al nanoparticles manufactured as superior energetic materials via laser ablation synthesis in organic solvents. Appl. Surf. Sci., 473:156-163, 2019.

[2] Gottfried, J.L., Smith, D.K., Wu, C.-C., Pantoya, M.L. Improving the explosive performance of aluminum nanoparticles with Aluminum Iodate Hexahydrate (AIH). Scientific Reports, 8: 8036, 2018.

[3] Miller, K.K., Gottfried, J.L., Walck, S.D., Pantoya, M.L., Wu, C.-C. Plasma surface treatment of aluminum nanoparticles for energetic material applications. Combust. Flame, 206:211-213, 2019.

[4] Wainwright, E.R., Dean, S.W., Lakshman, S.V., Weihs, T.P., Gottfried, J.L. Evaluating compositional effects on the laser-induced combustion and shock velocities of Al/Zr-based composite fuels. Combust. Flame, 213:357-368, 2019.

[5] Anderson, P.E., Cook, P., Davis, A., Mychajlonka, K. The effect of binder systems on early aluminum reaction in detonations. Propellants Explos. Pyrotech., 38:486-494, 2013.

[6] Yarrington, C.D., Son, S.F., Foley, T.J., Obrey, S.J., Pacheco, A.N. Nano aluminum energetics: The effect of synthesis method on morphology and combustion performance. Propellants Explos. Pyrotech., 36:551-557, 2011.

[7] Zha, M., Lv, X., Ma, Z., Zhang, L., Zhao, F., Xu, S., Xu, H. Effect of particle size on reactivity and combustion characteristics of aluminum nanoparticles. Combust. Sci. Technol., 187:1036-1043, 2015.

[8] Gottfried, J.L. Laser-induced plasma chemistry of the explosive RDX with various metallic nanoparticles. Appl. Opt., 51:B13-B21, 2012.

[9] Gottfried, J.L., Bukowski, E.J. Laser-shocked energetic materials with metal additives: evaluation of chemistry and detonation performance. Appl. Opt., 56:B47-B57, 2017.

[10] Krishnan, D., Kim, F., Luo, J., Cruz-Silva, R., Cote, L.J., Jang, H.D., Huang, J. Energetic graphene oxide: Challenges and opportunities. Nano Today, 7:137-152, 2012.

[11] Zhu, Y., Murali, S., Cai, W., Li, X., Suk, J.W., Potts, J.R., Ruoff, R.S. Graphene and graphene oxide: Synthesis, properties, and applications. Adv. Mater., 22:3906-3924, 2010.

[12] Singh, R.K., Kumar, R., Singh, D.P. Graphene oxide: Strategies for synthesis, reduction and frontier applications, RSC Advances, 6:64993-65011, 2016.

[13] Jiang, Y., Deng, S., Hong, S., Zhao, J., Huang, S., Wu, C.-C., Gottfried, J.L., Nomura, K.-i., Li, Y., Tiwari, S.C., Kalia, R.K., Vashishta, P., Nakano, A., Zheng, X. Energetic performance of optically activated aluminum/graphene oxide composites. ACS Nano, 12:11366-11375, 2018.

[14] Dreyer, D.R., Park, S., Bielawski, C.W., Ruoff, R.S. The chemistry of graphene oxide. Chemical Society Reviews, 39:228-240, 2010.

[15] Gao, W. The Chemistry of Graphene Oxide, in: W. Gao (Ed.) Graphene Oxide: Reduction Recipes, Spectroscopy, and Applications. Springer International Publishing, Cham, 2015, pp. 61-95, 2015.

[16] Pyun, J. Graphene oxide as catalyst: application of carbon materials beyond nanotechnology. Angew. Chem. Int. Ed., 50:46-48, 2011.

[17] Dreyer, D.R., Todd, A.D., Bielawski, C.W. Harnessing the chemistry of graphene oxide. Chem. Soc. Rev., 43:5288-5301, 2014.

[18] Adeel, M., Bilal, M., Rasheed, T., Sharma, A., Iqbal, H.M.N. Graphene and graphene oxide: Functionalization and nano-bio-catalytic system for enzyme immobilization and biotechnological perspective. Int. J. Bio. Macromol., 120:1430-1440, 2018.

[19] Singh, S.B., Hussain, C.M. Nano-graphene as groundbreaking miracle material: Catalytic and commercial perspectives. ChemistrySelect, 3:9533-9544, 2018.

[20] Ahmad, H., Fan, M., Hui, D. Graphene oxide incorporated functional materials: A review. Composites Part B, 145:270-280, 2018.

[21] Campisciano, V., Gruttadauria, M., Giacalone, F. Modified nanocarbons for catalysis. ChemCatChem, 11:90-133, 2019.

[22] Xiangjun, P., Xianyun, X., Fujiang, H., Qian, L., Liangxian, L. Graphene oxide and its derivatives: Their synthesis and use in organic synthesis. Current Org. Chem., 23:188-204, 2019.

[23] Brodie, XIII, B.C. On the atomic weight of graphite. Philos. Trans. R. Soc. Lond., 149:249-259, 1859.

[24] Croft, R.C. Lamellar compounds of graphite. Quarterly Reviews, Chem. Soc., 14:1-45, 1960.

[25] Boehm, H.P., Scholz, W. Der "Verpuffungspunkt" des graphitoxids. Zeitschrift für anorganische und allgemeine Chemie, 335:74-79, 1965.

[26] Jimenez, P.S.V. Thermal decomposition of graphite oxidation products DSC studies of internal combustion of graphite oxide. Mater. Res. Bull., 22:601-608, 1987.

[27] Sabourin, J.L., Dabbs, D.M., Yetter, R.A., Dryer, F.L., Aksay, I.A. Functionalized graphene sheet colloids for enhanced fuel/propellant combustion. ACS Nano, 3:3945-3954, 2009.

[28] Kim, F., Luo, J., Cruz-Silva, R., Cote, L.J., Sohn, K., Huang, J. Self-propagating domino-like reactions in oxidized graphite. Adv. Funct. Mater., 20:2867-2873, 2010.

[29] Li, R., Wang, J., Shen, J.P., Hua, C., Yang, G.C. Preparation and characterization of insensitive HMX/graphene oxide composites. Propellants Explos., Pyrotech., 38:798-804, 2013.

[30] Zhang, X., Hikal, W.M., Zhang, Y., Bhattacharia, S.K., Li, L., Panditrao, S., Wang, S., Weeks, B.L. Direct laser initiation and improved thermal stability of nitrocellulose/graphene oxide nanocomposites. Appl. Phys. Lett., 102:141905, 2013.

[31] Zhang, C., Wen, Y., Xue, X. Self-Enhanced Catalytic Activities of functionalized graphene sheets in the combustion of nitromethane: Molecular Dynamic simulations by molecular reactive force field. ACS Appl. Mater. & Interfaces, 6:12235-12244, 2014.

[32] Liu, J., Ren, H., Jiao, Q.-J., Yu, L. The influence of GO/RGO on the thermal decomposition of HNIW. Integrated Ferroelectrics, 152:127-136, 2014.

[33] Yu, L., Ren, H., Guo, X.-y., Jiang, X.-b., Jiao, Q.-j. A novel e-HNIW-based insensitive high explosive incorporated with reduced graphene oxide. J. Thermal Anal. Calorim., 117:1187-1199, 2014.

[34] Qiu, Y., Guo, F., Hurt, R., Külaots, I. Explosive thermal reduction of graphene oxide-based materials: Mechanism and safety implications. Carbon, 72:215-223, 2014.

[35] Thiruvengadathan, R., Chung, S.W., Basuray, S., Balasubramanian, B., Staley, C.S., Gangopadhyay, K., Gangopadhyay, S. A versatile self-assembly approach toward high performance nanoenergetic composite using functionalized graphene. Langmuir, 30:6556-6564, 2014.

[36] Thiruvengadathan, R., Staley, C., Geeson, J.M., Chung, S., Raymond, K.E., Gangopadhyay, K., Gangopadhyay, S. Enhanced combustion characteristics of bismuth trioxide-aluminum nanocomposites prepared through graphene oxide directed self-assembly. Propellants Explos. Pyrotech., 40:729-734, 2015.

[37] Chen, Y.N., Egan, G.C., Wan, J.Y., Zhu, S.Z., Jacob, R.J., Zhou, W.B., Dai, J.Q., Wang, Y.B., Danner, V.A., Yao, Y.G., Fu, K., Wang, Y.B., Bao, W.Z., Li, T., Zachariah, M.R., Hu, L.B. Ultra-fast self-assembly and stabilization of reactive nanoparticles in reduced graphene oxide films. Nat. Commun., 7:12332, 2016.

[38] Qiu, Y., Collin, F., Hurt, R.H., Külaots, I. Thermochemistry and kinetics of graphite oxide exothermic decomposition for safety in large-scale storage and processing. Carbon, 96:20-28, 2016.

[39] Memon, N.K., McBain, A.W., Son, S.F. Graphene oxide/ammonium perchlorate composite material for use in solid propellants. J. Propul. Power, 32:682-686, 2016.

[40] Wang, J., Ye, B., An, C., Wu, B., Li, H., Wei, Y. Preparation and properties of surface-coated hmx with viton and graphene oxide. J. Energ. Mat., 34:235-245, 2016.

[41] Yan, Q.-L., Gozin, M., Zhao, F.-Q., Cohen, A., Pang, S.-P. Highly energetic compositions based on functionalized carbon nanomaterials. Nanoscale, 8:4799-4851, 2016.

[42] Yan, N., Qin, L., Hao, H., Hui, L., Zhao, F., Feng, H. Iron oxide/aluminum/graphene energetic nanocomposites synthesized by atomic layer deposition: Enhanced energy release and reduced electrostatic ignition hazard, Appl. Surf. Sci., 408:51-59, 2017.

[43] Yan, N., Qin, L., Li, J., Zhao, F., Feng, H. Atomic layer deposition of iron oxide on reduced graphene oxide and its catalytic activity in the thermal decomposition of ammonium perchlorate. Appl. Surf. Sci., 451:155-161, 2018.

[44] Tao, Y., Zhang, J., Yang, Y., Wu, H., Hu, L., Dong, X., Lu, J., Guo, S. Metastable intermolecular composites of Al and CuO nanoparticles assembled with graphene quantum dots. RSC Advances, 7:1718-1723, 2017.

[45] Wang, J., Chen, S., Yao, Q., Jin, S., Zhao, S., Yu, Z., Li, J., Shu, Q. Preparation, characterization, thermal evaluation and sensitivities of TKX-50/GO composite. Propellants Explos. Pyrotech., 42:1-8, 2017.

[46] An, T., He, W., Chen, S.-W., Zuo, B.-L., Qi, X.-F., Zhao, F.-Q., Luo, Y., Yan, Q.-L. Thermal behavior and thermolysis mechanisms of ammonium perchlorate under the effects of graphene oxide-doped complexes of triaminoguanidine. J. Phys. Chem. C, 122:26956-26964, 2018.

[47] Lyu, J.-Y., Chen, S., He, W., Zhang, X.-X., Tang, D.-y., Liu, P.-J., Yan, Q.-L. Fabrication of high-performance graphene oxide doped PVDF/CuO/Al nanocomposites via electrospinning. Chem. Eng. J., 368:129-137, 2019.

[48] Chen, S., He, W., Luo, C.-J., An, T., Chen, J., Yang, Y., Liu, P.-J., Yan, Q.-L. Thermal behavior of graphene oxide and its stabilization effects on transition metal complexes of triaminoguanidine. J. Hazard. Mater., 368:404-411, 2019.

[49] Lakhe, P., Kulhanek, D.L., Sun, W., Zhang, B., Green, M.J., Mannan, M.S. Calorimetry of explosive thermal decomposition of graphite oxide. J. Hazard. Mater., 366:275-281, 2019.

[50] Zhang, C., Fu, X., Yan, Q., Li, J., Fan, X., Zhang, G. Study on the thermal decomposition mechanism of graphene oxide functionalized with triaminoguanidine (GO-TAG) by molecular reactive dynamics and experiments. RSC Advances, 9:33268-33281, 2019.

[51] Chen, S., An, T., Gao, Y., Lyu, J.-Y., Tang, D.-Y., Zhang, X.-X., Zhao, F., Yan, Q.-L. Gaseous products evolution analyses for catalytic decomposition of AP by graphene-based additives, Nanomaterials, 9:801, 2019.

[52] Cheng, J., Yan, J., Wang, L., Zhang, R., Liu, Z., Wang, R., Li, Z. Functionalization graphene oxide with energetic groups as a new family of metal-free and energetic burning rate catalysts and desensitizers for ammonium perchlorate. J. Thermal Anal. Calorim., 140:2111-2122, 2020.

[53] Hanafi, S., Trache, D., He, W., Xie, W.-X., Mezroua, A., Yan, Q.-L. Thermostable energetic coordination polymers based on functionalized go and their catalytic effects on the decomposition of AP and RDX. J. Phys. Chem. C, 124:5182-5195, 2020.

[54] Huang, B., Xue, Z., Chen, S., Chen, J., Li, X., Xu, K., Yan, Q.-L. Stabilization of e-CL-20 crystals by a minor interfacial doping of polydopamine-coated graphene oxide. Appl. Surf. Sci., 510:145454, 2020.

[55] Qi, X., Chen, S., Liu, X., Yan, N., Jin, B., Liu, P., Yan, Q.-L. Comparative study on compatibility of graphene-based catalysts with energetic ingredients by using DSC and VST methods. J. Thermal Anal. Calorim., in press (2020) https://doi.org/10.1007/s10973-020-09646-3, 2020.

[56] Jiang, Y., Deng, S., Hong, S., Tiwari, S., Chen, H., Nomura, K.-i., Kalia, R.K., Nakano, A., Vashishta, P., Zachariah, M.R., Zheng, X. Synergistically chemical and thermal coupling between graphene oxide and graphene fluoride for enhancing aluminum combustion. ACS Appl. Mater. & Interfaces, 12:7451-7458, 2020.

[57] Gottfried, J.L. Influence of exothermic chemical reactions on laser-induced shock waves. Phys. Chem. Chem. Phys., 16:21452-21466, 2014.

[58] Gottfried, J.L. Laboratory-scale method for estimating explosive performance from laser-induced shock waves. Propellants Explos. Pyrotech., 40:674–681, 2015.

[59] Collins, E.S., Gottfried, J.L. Laser-induced deflagration for the characterization of energetic materials. Propellants Explos. Pyrotech., 42:592-602, 2017.

[60] Gottfried, J.L., Klapötke, T.M., Witkowski, T.G. Estimated detonation velocities for TKX-50, MAD-X1, BDNAPM, BTNPM, TKX-55 and DAAF using the laser-induced air shock from energetic materials technique. Propellants Explos. Pyrotech., 42:353-359, 2017.

[61] Gottfried, J.L., Dean, S.W., Collins, E.S., Wu, C.-C. Estimating the relative energy content of reactive materials using nanosecond-pulsed laser ablation. MRS Adv., 3:875-886, 2018.

[62] Settles, G.S. Schlieren and Shadowgraph Techniques. Springer-Verlag, New York, 2001.

[63] Cremers, D.A., Radziemski, L.J. Handbook of Laser-Induced Breakdown Spectroscopy, 2nd ed. John Wiley & Sons, Ltd., Singapore, 2013.

[64] Serrano, J., Cabalín, L.M., Moros, J., Laserna, J.J. Potential of laser-induced breakdown spectroscopy for discrimination of nano-sized carbon materials. Insights on the optical characterization of graphene, Spectrochim. Acta, Part B, 97:105-112, 2014.

[65] De Lucia Jr., F.C., Gottfried, J.L. Characterization of a series of nitrogen-rich molecules using laser-induced breakdown spectroscopy. Propellants Explos. Pyrotech., 35:268-277, 2010.

[66] Shen, B., Lu, D., Zhai, W., Zheng, W. Synthesis of graphene by low-temperature exfoliation and reduction of graphite oxide under ambient atmosphere. J. Mater. Chem. C, 1:50-53, 2013.

[67] Medhekar, N.V., Ramasubramaniam, A., Ruoff, R.S., Shenoy, V.B. Hydrogen bond networks in graphene oxide composite paper: Structure and mechanical properties. ACS Nano, 4:2300-2306, 2010.

[68] Jin, M., Jeong, H.-K., Kim, T.-H., So, K.P., Cui, Y., Yu, W.J., Ra, E.J., Lee, Y.H. Synthesis and systematic characterization of functionalized graphene sheets generated by thermal exfoliation at low temperature. J. Phys. D, 43:275402, 2010.

Plasma Enhanced Chemical Vapor Deposition Reactor for Large Scale Production of High-Quality Graphene

Jon Are Beukes, Anh Hoang Dam and Kaja Skålnes Knudsen
CealTech AS, Røynebergsletta 32,
4033 Stavanger
NORWAY
Email beukes@cealtech.com

Keywords: Batteries; Coatings; Composites; CVD; Elastomers; Flakes; Graphene; Production; Properties; Scalable.

ABSTRACT

Combining graphene with bulk materials holds great promise for advancing and developing both civilian and defense technologies.

Here, we present a large scale Plasma Enhanced Chemical Vapor Deposition, PECVD, reactor system, FORZA, that has been developed exclusively for the production of high-quality graphene flakes and coatings. The reactor system is the largest known system of its kind, and can coat large surfaces, up to 86 cm width and 390 cm length, with vertically oriented graphene. FORZA is capable of large-area graphene coating directly on materials and devices and the graphene may be harvested continuously as a powder.

FORZA graphene has been incorporated into various materials and products. It has been used to improve electric conductivity of polymers (epoxy). Further, it has been used to enhance mechanical properties of polymer material (poly lactic acid), fiber reinforced polymer composite (glass fiber/ polyester) and elastomers. FORZA graphene has been used to improve ballistic performance of polymer composite material (glass fiber / polyvinyl ester) for vehicles and body armor. In addition, it is possible to coat surfaces directly with FORZA graphene on various materials (such as knife edges, carbon fiber, aluminum and copper foils) for multiple property enhancements. Graphene's possibilities for boosting battery charging performances has also been demonstrated.

1.0 INTRODUCTION

Although the potential of graphene has been highlighted in numerous laboratory studies, there are still challenges in producing graphene with sufficient quality and scale necessary for industrial applications. The FORZA system is used both as a research reactor for determining optimum parameters for new specialized coating machines, as well as serving as a graphene machine for large scale production. Commercial and defense applications of graphene-based materials are numerous. As an example, these materials may be used as anti-corrosion and anti-icing coatings for helicopter rotor blades [1], [2], [3]. As an additive, flake graphene imparts high strength-to-weight ratio and can contribute enhanced mechanical, thermal, and electrical properties to polymers even at very low concentrations. As a continuous thin film or coating, graphene can be applied to a wide range of materials, providing a flexible, transparent, electrically conductive, corrosion-resistant, gas-impenetrable, and atomically thin diffusion barrier. Moreover, graphene-based materials are believed to provide high strength-to-weight ballistic solutions for vehicles and body armor. There are also significant possibilities for the enhancement of battery energy density and charge rate performance with the use of graphene.

Current methods for producing flake graphene are based on top-down exfoliation of graphite by either mechanical or chemical means [4]. Techniques, such as the Scotch-tape method [5] or shear-force mixing, can produce high-quality graphene flakes with little contamination, but are limited to small production volumes. Chemical exfoliation and chemical synthesis can produce higher volumes of graphene than mechanical exfoliation, but the process is harsh and results in substantial damage and undesirable effects on the graphene itself including defects, oxide functionalities, substitutional nitrogen, and residual metallic contaminants. Chemical waste is also an issue with chemical exfoliation [6].

High-quality graphene films can be produced by Chemical Vapor Deposition (CVD) [7]. CVD of graphene is a bottom-up process whereby gaseous hydrocarbons are converted to crystalline graphene via high temperatures and catalytic substrates. Although thermal CVD can produce high-quality graphene films, the trade-offs include the need for high temperatures, ~1000°C, slow growth times, and a limited number of substrates on which is can be applied. Plasma Enhanced CVD (PECVD) is a variant of thermal CVD wherein reactive growth species are generated within a plasma environment rather than with high temperatures [8]. The advantages of PECVD include lower growth temperature, faster deposition, improved film quality, and the ability to deposit multilayer films. The high growth rates of PECVD allow graphene to be grown perpendicularly (see Figure 1) to the substrate as opposed to regular CVD processing that only deposits parallel layers. This makes it possible to grow substantially more graphene per growth area, which can easily be harvested to be used as flakes. However, a challenge with PECVD has been scaling the process to industrially relevant size.

The reactor system, FORZA, is based on a scalable microwave plasma technology platform. The system can transform carbon containing gases and hydrogen and continuously deposit vertical 3D graphene areas of up to 6.7 m^2. Large-area graphene deposition has been demonstrated on a variety of substrates, including stainless steel, Inconel, aluminum, quartz, and copper, as well as more complicated structures, including metal mesh, carbon fiber cloth, and particles. Deposition can occur below 400°C, which allows for coating of temperature sensitive materials and electronic devices. As will be shown, characterization of FORZA flake graphene with Scanning Electron Microscopy (SEM), Transmission Electron Microscopy (TEM), and Raman spectroscopy maps reveal excellent uniformity and high crystallinity. Properties of the graphene can further be controlled by changing the growth conditions by varying the growth time, gas compositions, input energy, pressure, and temperatures.

In this paper, we briefly describe the FORZA machine and address ways of using graphene for improving various material properties for practical applications.

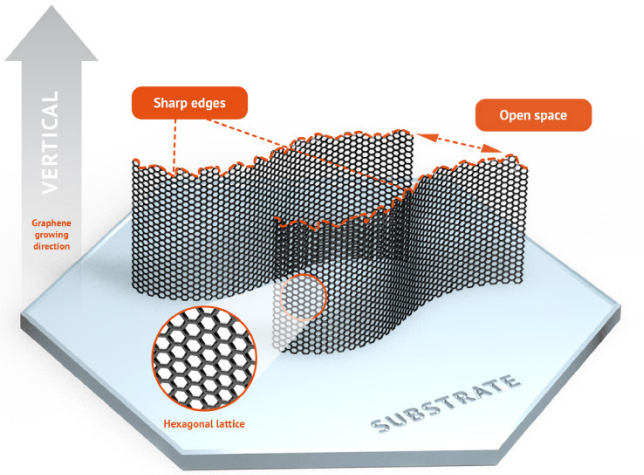

Figure 1: 3D Graphene is Growing Perpendicularly from a Substrate.

2.0 METHODOLOGY

2.1 High Volume Production of Graphene

The FORZA machine (see Figure 2) was constructed as a factor 6700 scale-up of the environment from a patented laboratory device set-up with a 1 cm^2 growth area [9]. The corresponding growth areas in the FORZA machine consists of two 3.9 meter long metal bands where graphene can be perpendicularly deposited either by dynamically moving the belts, or by stepwise-static mode (see Figure 3). In this way it is possible to grow perpendicular graphene with different base length for the graphene sheets, which depending on residence time in the plasma zones, has been observed from a few hundred nm up to 30 µm thickness.

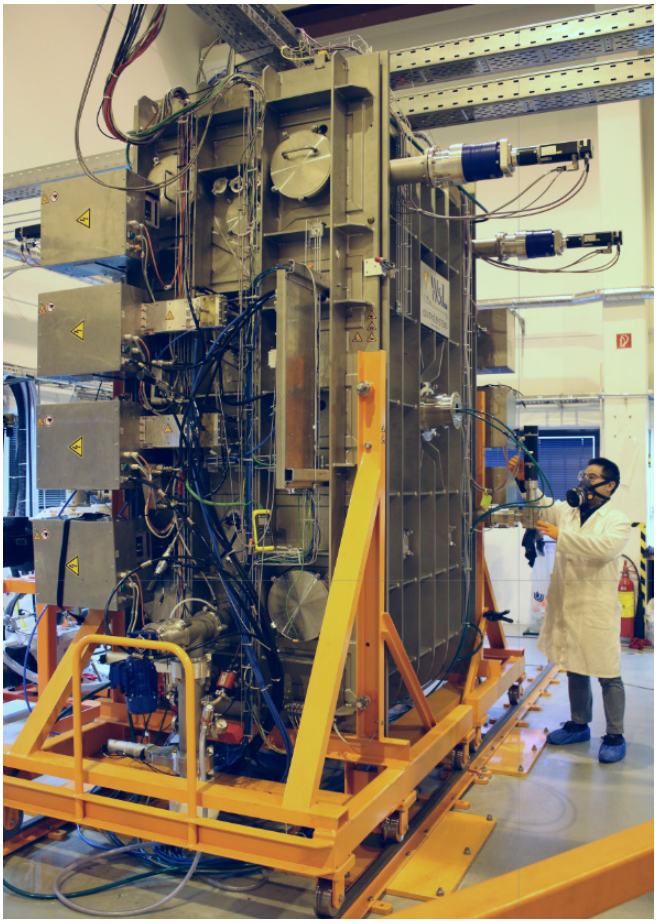

Figure 2: The FORZA Graphene PECVD Production Unit at Cealtech, Stavanger, Norway. Inside the large vacuum chamber there are two motorized metal belts used as substrates for graphene growth. The chamber is equipped with gas reactant controls, microwave plasma generators, a harvesting system and interlock controls.

The graphene deposited on the metal bands can be harvested by mechanical scraping and conveying from the reactor. In addition to controlling the flake sizes, the morphology of the produced graphene can be controlled by varying the process parameters, such as temperatures, total gas pressure, plasma energy, gas compositions, and argon dilution parameters. For on-line analysis, the machine has a probe installed for in-situ Raman spectroscopy measurements. Further, routine characterization of harvested graphene powder is done by Raman mapping.

2.2 Methods for Graphene Characterization and Mechanical Testing of Composite Materials

As part of normal quality control routines, every batch of FORZA graphene is analyzed by means of Raman spectroscopy (Raman). Other techniques such as Scanning Electron Microscopy (SEM), Transmission Electron

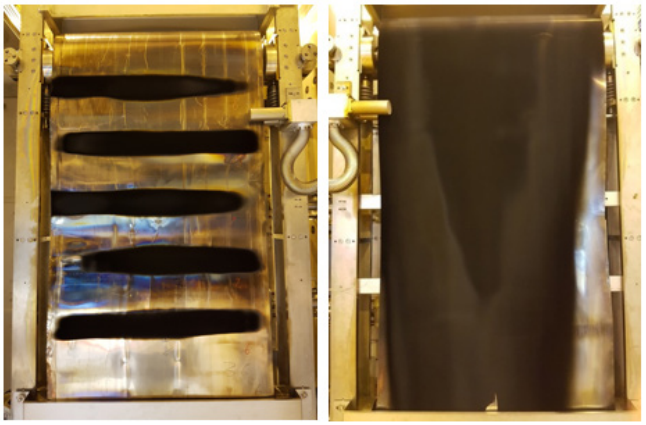

Figure 3: The Graphene (Black Substance) Inside the FORZA Machine Can Be Produced Using Various Processing Parameters. Here is shown a step-mode growth (left) where the belt is kept in a static position, and a dynamic mode growth by moving the substrate at a continuous speed (right). In addition, one can tune the gas composition and temperatures in the FORZA, to produce the desired amounts and graphene qualities and morphologies.

Microscopy (TEM), and Energy Dispersive X-ray Spectroscopy (EDS) are complementary used to ensure the consistency of the product.

Raman spectroscopy (Renishaw inVia, UK) is a preferred tool for characterizing graphene in-situ and as harvested from the production process, as well as during subsequent manipulation for interfacing it in various application matrices. The Raman spectra and analysis give a good indication of the crystallinity and quality and the interaction with host materials.

The morphology and nanostructure of graphene are observed by SEM (Gemini SUPRA 35VP (ZEISS), Germany) and TEM (JEOL-2100 (LaB6 filament) equipped with Energy Dispersive X-ray Spectroscopy (EDS), operating at 200 kV, Japan). Elemental composition and impurity in graphene is identified by EDS. In addition, the TEM provides electron diffraction patterns that give valuable insight into the crystallinity of the honeycomb graphene lattice. The dispersion of graphene in a polymer/elastomer matrix is determined by X-ray diffraction (Bruker's X-ray Diffraction D8).

Tensile strengths of graphene enhanced polymer composites were measured according to the ASTM D3039 standard. Flexural strength (3-points flexure) was measured according to ISO standard 14125. All tests were performed on an Instron Applications Laboratory Model 5985. For each sample, seven specimens were tested to reduce uncertainty on the measurement.

3.0 RESULTS AND DISCUSSION

3.1 Properties of FORZA Graphene

The Raman spectra of neat FORZA graphene, Figure 4, and subsequent analysis, see Figure 5, shows that the graphene produced is very uniform. Furthermore, the neat graphene has a signature suggesting it is functionalized, which is believed to be partially hydrogenated graphene [10].

Figure 4 shows the spectrum before and after annealing the neat graphene in vacuum, and the resulting Raman spectrum looks more like pristine graphene. The neat FORZA graphene goes through some changes, where the most noteworthy is: low total mass losses of <28% as shown by Thermal Gravimetric Analysis (TGA). A significant reduction of D and D' peaks indicate reduction of defects (morphology and/or functionalization). The G peak width is maintained and indicates no deterioration of crystallinity. The significant increase in the 2D peak area, and the 2D/G ratio, as well as a narrower 2D peak width from 78 to 61 $cm^{-1,}$ indicates a reduction of over-all number of layers down to very few layers during the annealing process.

The drastic decrease in D peak in Raman by annealing is correlated to two aspects; the reduction of poor quality graphene content such as graphene with more holes and lower crystallinity, which is mechanically weaker and less thermally stable, and carbon content which is non-graphene such as amorphous carbon or other forms of carbon. This could also contribute to most of the weight loss during thermal process as is found by TGA analysis. Annealing may also reduce hydrogen that is incorporated during PECVD production of graphene in the presence of hydrogen gas. The removal of hydrogen enables the transformation of sp3 to sp2 states in atoms within the partially hydrogenated graphene. This would enhance electron mobility in the graphene sheet, and therefore an increased electrical conductivity. However, it is challenging to quantify the consequence of these two effects and which one of these two plays the most important role in improving graphene quality as seen by Raman, remains to be determined.

Figure 6 shows some of the morphologies obtained as shown by SEM. Using TEM, and subsequent electron diffraction shows that the graphene obtained from the FORZA reactor is of high crystallinity and quality (see Figure 7) with no impurity found (Figure 8).

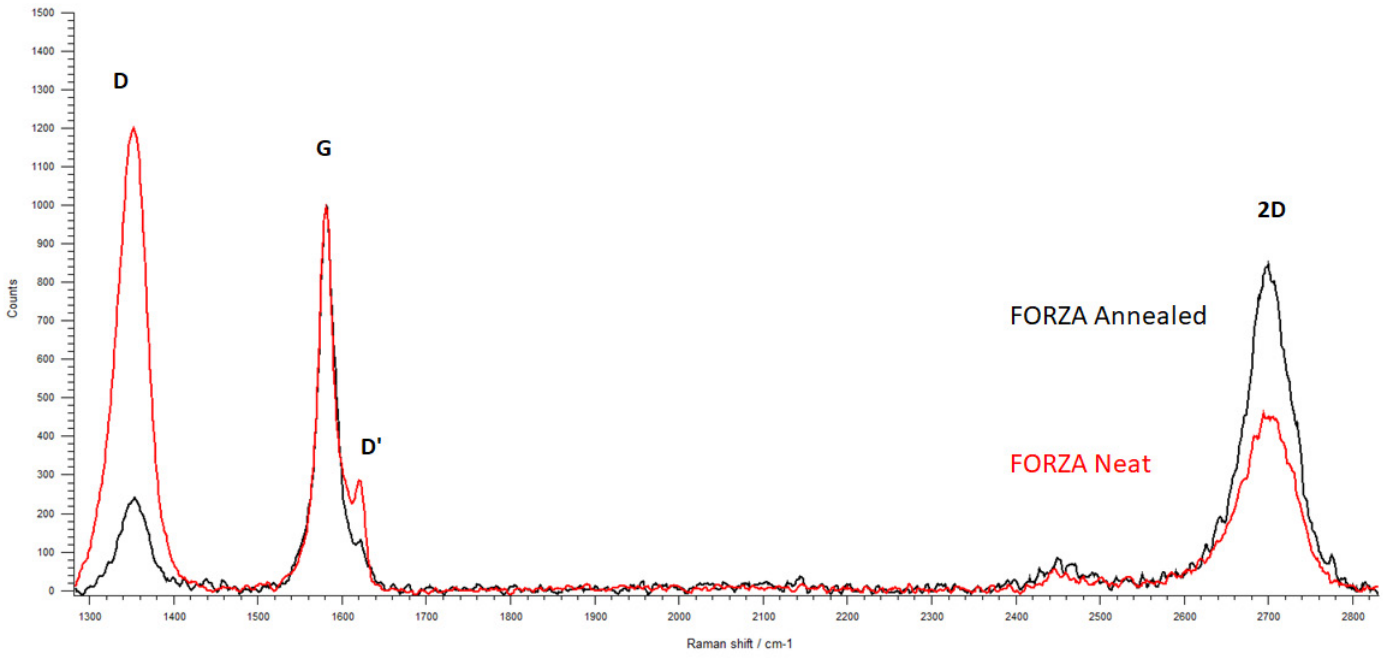

Figure 4: Raman Spectra of FORZA Graphene Before and After Heat Treatment up to 1700°C. For certain applications, the neat FORZA graphene is more suitable for entering various material matrices, while other applications can benefit from the properties of the annealed graphene.

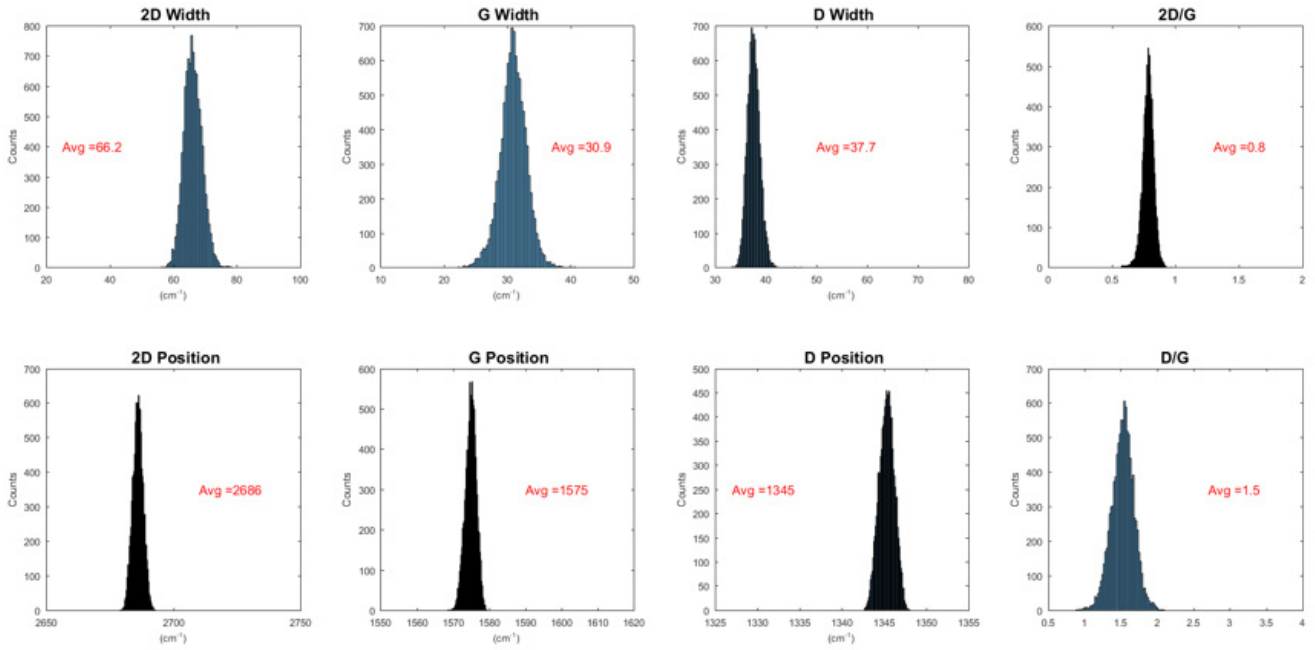

Figure 5: Distribution of Raman Peak Parameters and Peak Relations for a Raman Map of FORZA Graphene.

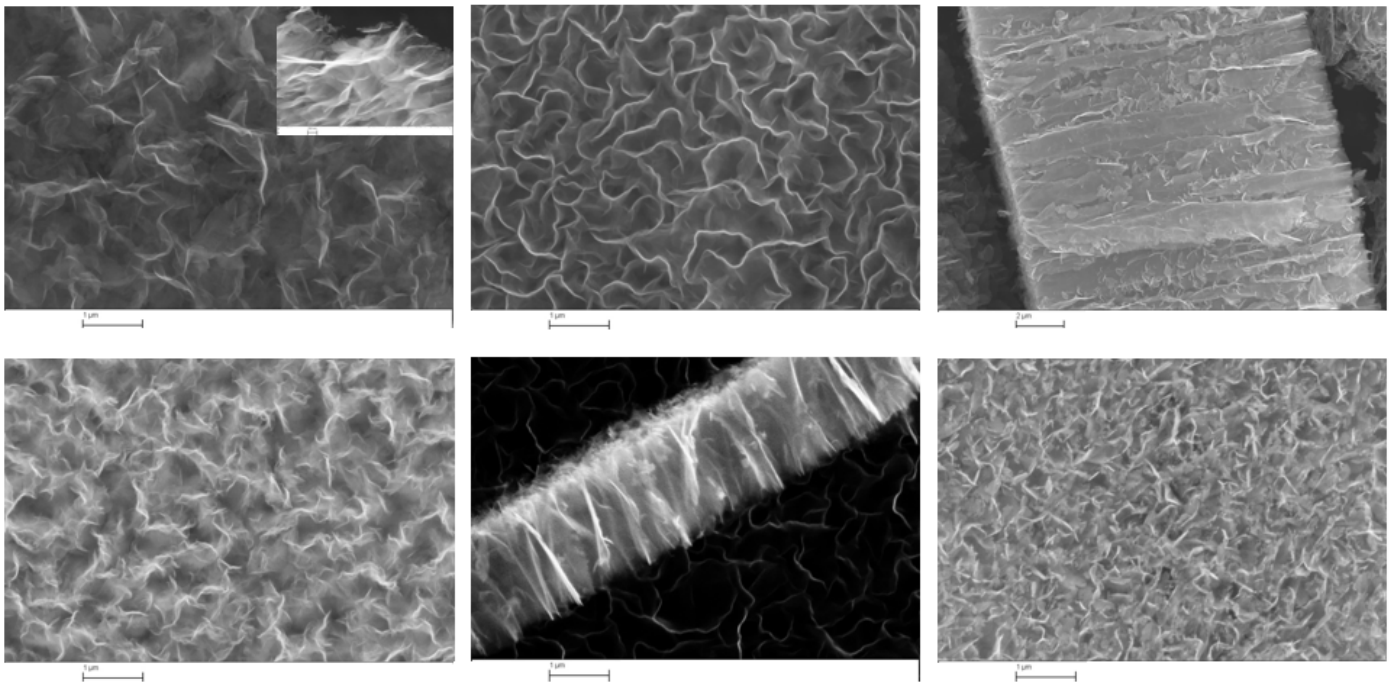

Figure 6: SEM Images from the Graphene Morphologies that Arise from Varying Production Parameters in the FORZA Reactor. By tuning gas compositions, temperatures and plasma power, different morphologies are grown. Here are shown wavy walls, maze-like walls, dense structures, highly branched, and loose branched morphologies (scale bars = 1 μm).

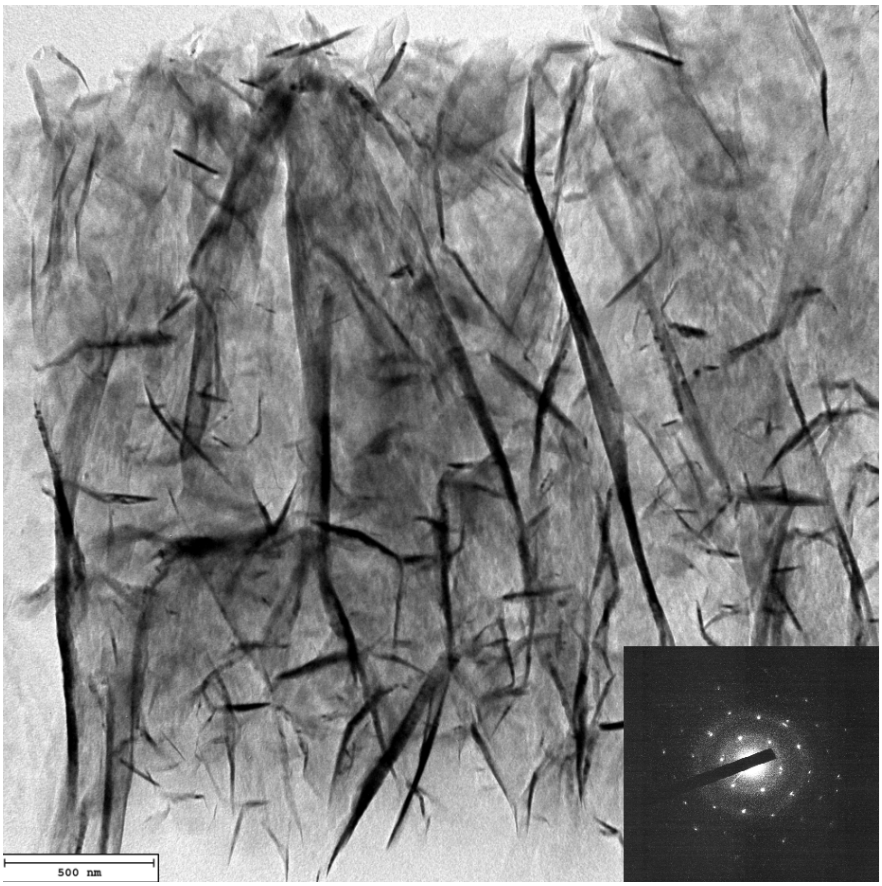

Figure 7: TEM Image of a FORZA Graphene Flake. The inset at the bottom right shows the corresponding electron diffraction peaks from an arbitrary position in the TEM image. The diffraction pattern shows that the graphene has a high degree of crystallinity (scale = 500 nm).

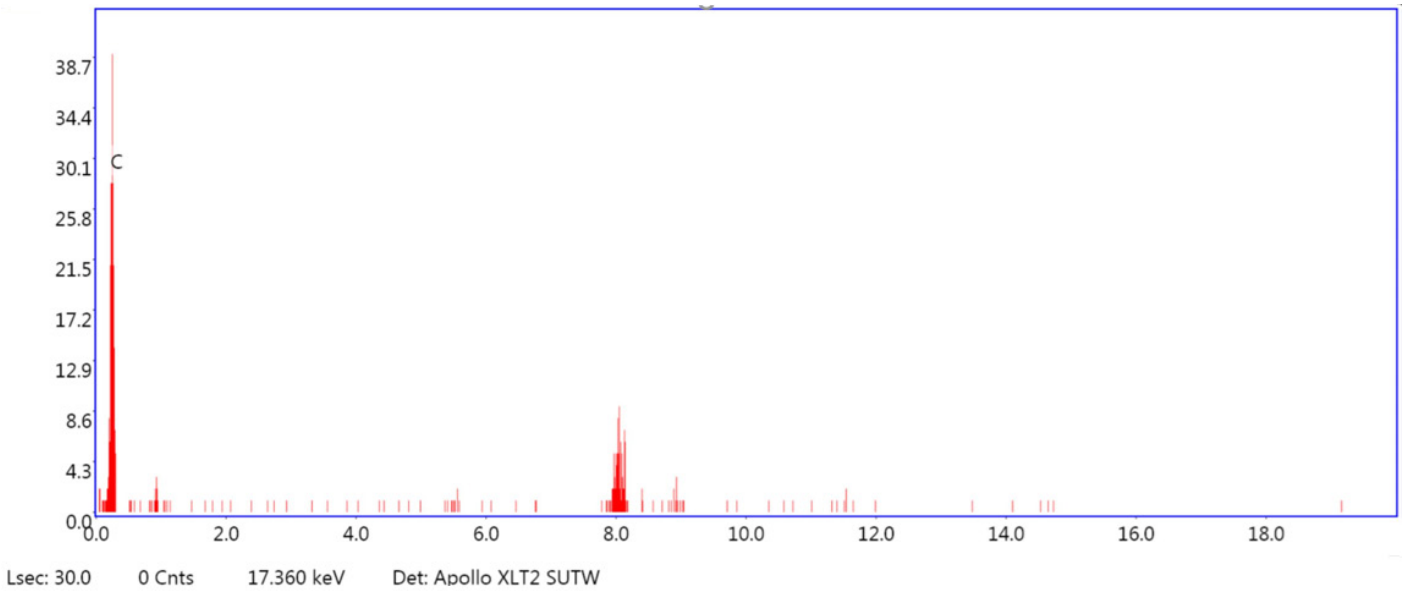

Element	Weight %	Atomic %	Net Int.	Error %	Kratio	Z	A	F
C K	100.00	100.00	7.25	7.98	1.0000	1.0000	1.0000	1.0000

Figure 8: EDS Spectrum of FORZA Graphene. EDS indicates that the graphene contains only carbon without any impurity found (The peak at 8.0 keV refers to copper in the sample holder).

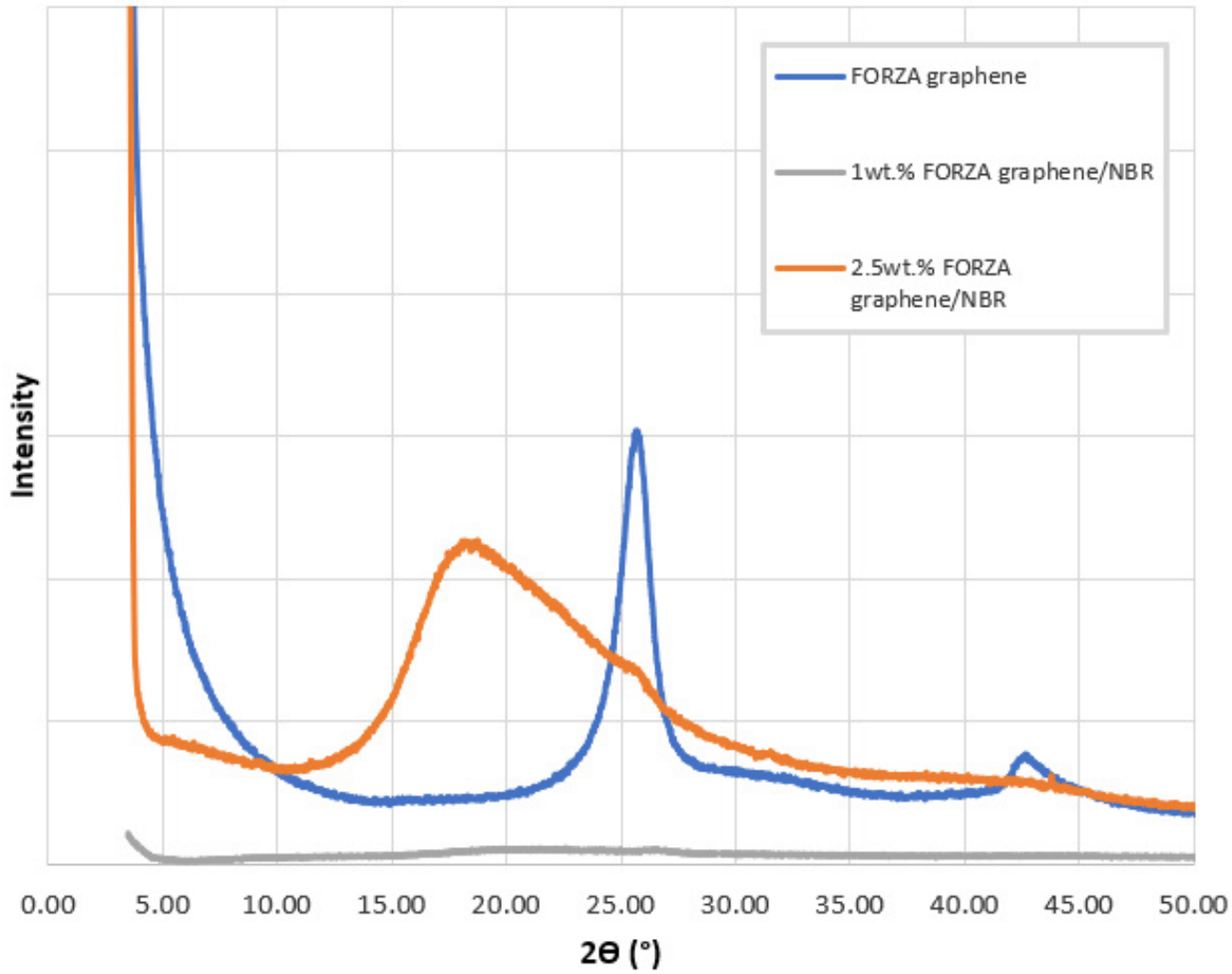

Figure 9: XRD Patterns of FORZA Graphene and FORZA Graphene Enhanced NBR. The XRD pattern of FORZA graphene exhibits a characteristic diffraction peak at 2θ= 26,268° (d = 0.339 nm), which is assigned to the (002) plane of graphene. The interlayer distance will be increased when graphene is intercalated by NBR molecules, leading to intensity decrease and a shift to lower angle or disappearance of this peak. This peak totally disappears in the sample containing only 1 wt % FORZA graphene, indicating complete exfoliation of the graphene layers.

3.2 Implementation of FORZA Graphene in Materials for Applications

The FORZA graphene has been successfully integrated in various polymer matrices, either as produced or annealed or chemically functionalized, as well as mixed with other available graphene-like materials. Some of the applications are of both military and civil interest. In addition to producing graphene in powder form, it can also be deposited directly on large surface areas of various materials. The only limit to direct deposition with the PECVD methodology is for the host material to sustain the conditions, such as temperature and low-pressure growth conditions.

3.2.1 Graphene Enhanced Poly Lactic Acid (PLA) Polymer, Epoxy, Vinyl Esters, and Elastomers

The dispersion of graphene is one of the main challenges for graphene composite applications. CealTech has successfully developed methods to homogeneously disperse FORZA graphene in various material matrices. XRD of one of the samples where graphene is fully exfoliated and homogeneously dispersed in Nitrile Rubber (NBR) is showed in Figure 9. In addition to expected changes in strength of the composite materials, the fatigue performance is expected to be enhanced. Confirming this is part of ongoing research programs.

Table 1: Increased Mechanical Performance by Introducing FORZA Vertical Graphene into Fiber Reinforced Polyester.

Samples	Average Standard Tensile Strength (MPa)	*Increase compared to Ref (%)*	Average E-Modulus (MPa)	*Increase compared to Ref (%)*	Average Standard Maximum Flexure Stress (MPa)	*Increase compared to Ref (%)*
Polyester/ fiberglass (Ref)	100.6(9.6)	-	6598(687)	-	190(11)	-
0.01 wt % FORZA Graphene	114.9(3.0)	*14.2*	7323(686)	*11.0*	205(10)	*7.7*
0.1 wt % FORZA Graphene	124.0(3.9)	*23.2*	7129(441)	*8.1*	200(7)	*4.8*

Significant improvement in these properties, will facilitate early commercialization of various applications of low wt % graphene composites.

In order to improve electrical conductivity as well as terahertz absorption of epoxy composites, FORZA graphene has been homogeneously dispersed in epoxy at various concentrations. Van Rheenen et al. [11] have tested these materials and found that introducing as little as 0.1% graphene in epoxy increased the electrical conductivity by a factor 108 which was further improved by increasing the graphene concentration. The implication is that using graphene enhanced materials as coatings has many possible practical applications due to, e.g., making insulating materials electrically conductive. The capability of enhancing microwave and near infrared absorption makes the material interesting for among others stealth applications.

3.2.2 Graphene Enhanced Fiber Reinforced Polyester

Graphene was homogeneously dispersed in polyester resin via high shear rate mechanical mixing. The resin/graphene mixture was then well mixed with a hardener. Graphene enhanced glass fiber/polyester composites were prepared by hand-lay-up techniques, with 65% polyester resin and 35% fiberglass.

The prepared resin was poured on a stainless steel plate with the surface treated by wax. A piece of fiberglass mat was then placed on the resin mixture and additional resin was spread by brush on the mat. A steel roller was used to press air out of the sample to improve the wetting of the polyester resin in and on the fiberglass mat.

The strength properties of a matrix material modified with graphene changes as a function of the graphene concentrations. For polyester, the tensile strength increases with increasing concentration of graphene, while the E-modulus and maximum flexure strength seem to go through a maximum value at concentrations below 0.1 wt % graphene (see Table 1). For each different matrix, these properties need to be investigated before concluding on suitable graphene concentrations.

3.2.3 Direct Deposition on Carbon Fibers and Other Functional Materials

Graphene coatings have numerous applications in areas of electronics, mechanical wear reduction, and mechanical strength. Perpendicular graphene is strongly light absorbing [12] . Perpendicular graphene coatings can also be combined with polymers and existing commercial carbon materials such as carbon fibers for improved strength.

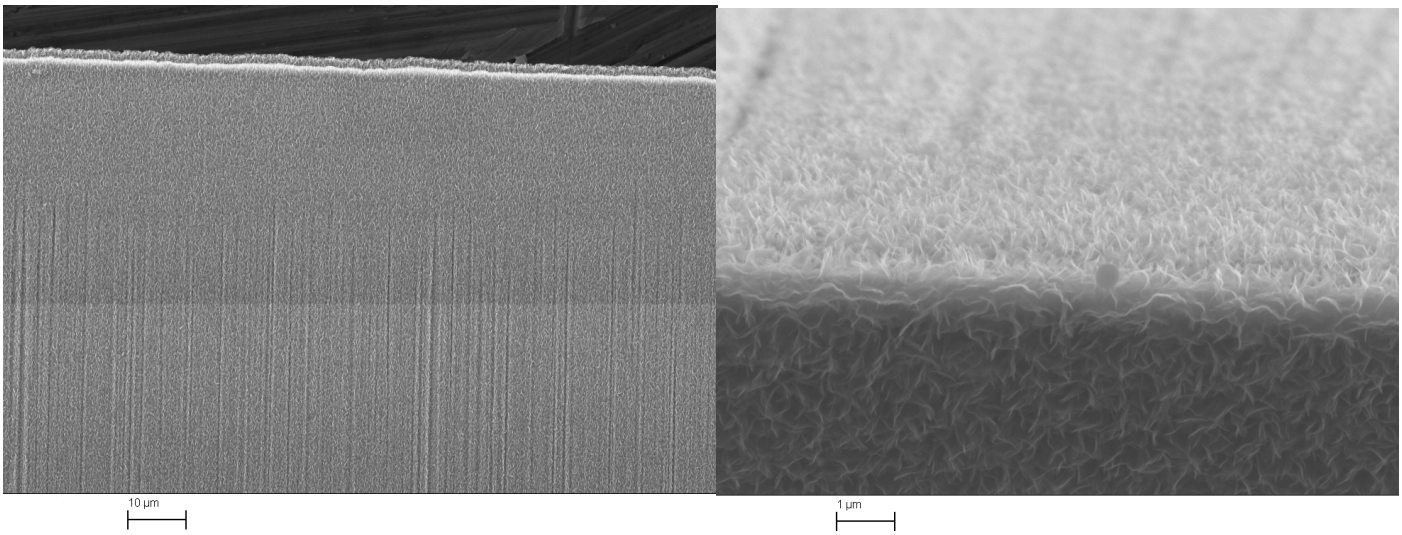

Figure 10: SEM Images of Direct Deposition of FORZA Graphene on a Cr-Based Knife Edge. Left: low resolution side view of the blade, and right: higher resolution image of the edge.

Various substrates, such as metals and ceramics and even organic materials, have been coated with graphene in the FORZA machine. The capability to directly grow and coat up to the 86 cm width of the plasma region makes it possible to produce a large area and uniform coating up to 6.7 m^2 and could be utilized among others in large scale electronics. Figure 10 shows SEM images of graphene growth on a Cr-plated knife blade.

Yao Chi et. al. [13] reported that that the interface strength of composites and carbon fibers were considerably improved (by 173%) by growing graphene nano walls on carbon fibers. To confirm this using the FORZA machine, graphene was grown on carbon fiber bundles (see Figure 11), which is a topic for further investigation towards improving material strength.

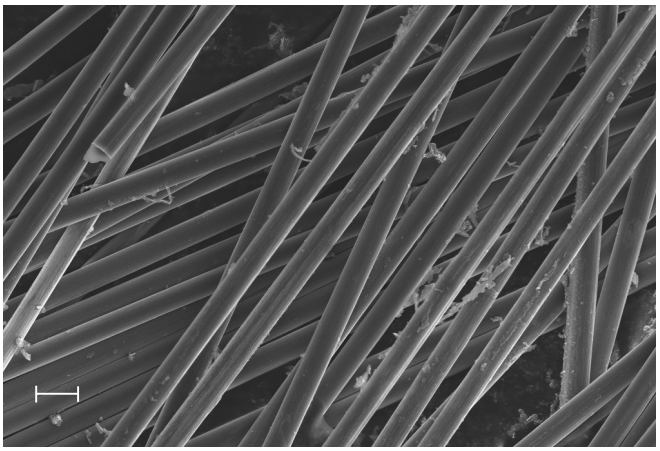

Figure 11: SEM Images of Direct Deposition of FORZA Graphene on Carbon Fiber. Graphene is seen as the paler material that resides on the darker carbon fibers (scale = 10 µm).

3.3 Battery Technology

Batteries are critical for both general society as well as the modern military, and the need for rapid charging may impair operations. The time needed to fully charge devices may be a critical factor. To study the possibility to enhance charging rate FORZA graphene has been incorporated into battery electrodes.

Lithium Ion Battery (LIB) performance includes the aspects of, for example, energy capacity, battery life and safety. The capacity of a LIB is related to the rate of discharge. LIB experiences increasing capacity drop as the discharge rate is increased. Graphene is highly effective in enhancing the capacity as discharge rate increases, which means shorter charging time and higher power output.

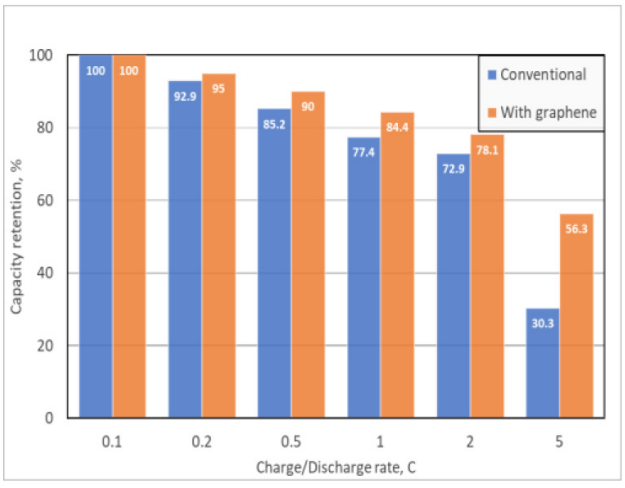

Figure 12: Advantage of Electrodes Which Incorporate Graphene for Fast Charging and Discharging. Conventional electrode discharge capacity (represented as blue columns) drops more drastically than the electrode with graphene (represented as red columns) when the rate of discharge (discharge current) increases from 0.1 C to 5 C.

This is due to higher electrical conductivity and improved ionic transport kinetics provided by graphene [14], [15]. A preliminary study was performed at CealTech (as shown in Figure 12) and demonstrated an improved rate capability of the cathode with graphene. Graphene also helps to increase battery life by mitigating instability of the electrode caused by volume expansion and irreversible phase transitions of the active material [14]. It is also reported that LIB safety can be improved because graphene can confine the growth of lithium dendrites which is a significant cause for shorting the LIB cell and may lead to fire and even explosion [16].

3.4 Other Potential Applications

Graphene-reinforced advanced materials are of military as well as civil importance, to e.g., reduce weight of various types of equipment by using stronger and still lightweight materials. In addition, the enhanced electrical and thermal conductivities of graphene enhanced host materials may be beneficial for smart clothes as well as in aiding anti-fouling and anti-icing properties of aviation machines.

An important area of interest is ballistic protection, and since graphene has been shown to be compatible with materials used as ballistic protection, there are projects ongoing that aim to show improvement of the relevant properties. Potential benefits obtained include increased ballistic performance and/or lighter personnel protection equipment and lighter protection for vehicles.

4.0 CONCLUSION

We have presented a machine for large scale production of high-quality graphene coatings and flakes. The machine is capable of continuous production of graphene flakes as well as coating areas as large as 6.7 m^2. The graphene is found to be of excellent quality.

Dispersion of graphene in a host matrix is essential for successful composites, and CealTech's FORZA graphene has been found to easily disperse in a variety of solvents, polymers, organic compounds, and oils. The FORZA graphene is well suited for composite and energy storage applications. We have explored graphene enhancement of fiber reinforced polymer materials, elastomers, and paints/coatings with regards to improving strength, electrical and thermal conductivity, mechanical and chemical resistance, anti-corrosion, and anti-icing. Perpendicular graphene is an excellent conductor with a high surface area. We have demonstrated direct deposition of graphene on various substrates, and in particular on metal foils for use as electrodes for batteries and supercapacitors. The application areas demonstrated are believed to be relevant for both civil and military use.

5.0 REFERENCES

[1] Chen, L., Zhang, Y., Wu, Q. Effect of graphene coating on the heat transfer performance of a composite anti-/deicing component. Coatings, 7:158, 2017.

[2] Raji, A.O., Varadhachary, T., Nan, K., Wang, T., Lin, J., Ji, Y. et al. Composites of graphene nanoribbon stacks and epoxy for joule heating and deicing of surfaces. .ACS Appl. Mater. Interfaces, 8(5):551-3556, 2016.

[3] Huang, X., Tepylo, N., Pommier-Budinger, V., Budinger, M., Bonaccurso, E., Villedieu, P. et al. A survey of icephobic coatings and their potential use in a hybridcoating/active ice protection system for aerospace applications. Prog. Aerospace Sciences, 105:74-97, 2019.

[4] Backes, C., Abdelkader, A.M., Alonso, C., Andrieux-Ledier, A., Arenal, R., Azpeitia, J. et al. Production and processing of graphene and related materials. 2D Mater. 7:022001, 2020.

[5] Novoselov, K.S., Jiang, D., Schedin, F., Booth, T.J., Khotkevich, V.V., Morozov, S.V. et al. Two-dimensional atomic crystals. Proc. Natl Acad. Sci., 102:10451-10453, 2005.

[6] Sajibul Alam Bhuyan, M., Nizam Uddin, M., Maksudul Islam, M., Alam Bipasha, F., Shafayat Hossain, S. Synthesis of graphene. Int. Nano Lett., 6:65-83, 2016.

[7] Zhang, Y., Zhang, L., Zhou, C. et al., Review of chemical vapor deposition of graphene and related applications. Acc. Chem. Res., 46(10):2329-2339, 2013.

[8] Woehrl, N., Ochedowski, O., Gottlieb, S., Shibasaki, K., Schulz, S. Plasma-enhanced chemical vapor deposition of graphene on copper substrates. AIP Advances, 4:047128, 2014.

[9] Boyd, D.A., Lin, W.-H., Hsu, C.-C., Teague, M.L., Chen, C.-C., Lo, Y.-Y. et al. Single-step deposition of high-mobility graphene at reduced temperatures. Nat. Commun., 6:6620, 2015.

[10] Luo, Z., Yu, T., Ni, Z., Lim, S., Hu, H., Shang, J. et al. Electronic structures and structural evolution of hydrogenated graphene probed by Raman spectroscopy. J. Phys. Chem. C , 115(5):1422-1427, 2011.

[11] van Rheenen, A.D., Johnsen, B.B., Haakestad, M.W., Hoang Dam, A., Knudsen, K.S. Transmission of terahertz waves through graphene/epoxy samples – correlation with electrical conductivity. NATO paper, Trondheim, MP-AVT-304-15, 2019.

[12] Krivchenko, V.A., Evlashin, S. A., Mironovich, K. V., Verbitskiy, N. I., Nefedov, A., Wöll, C. Carbon nanowalls: The next step for physical manifestation of the black body coating. Scientific Reports 3, 3328, 2013.

[13] Chi, Y., Chu, J., Chen, M., Li, C., Mao, W., Piao, M. et al. Directly deposited graphene nanowalls on carbon fiber for improving the interface strength in composites. Appl. Phys. Lett., 108:211601, 2016.

[14] Park, K.H., Lee, D., Kim, J., Song, J., Lee, Y.M., Kim, H.-T., et al. Defect-free, size-tunable graphene for high-performance lithium ion battery. Nano Lett., 14 :4306-4313, 2014.

[15] Brownson, D.A.C., Kampouris, D.K., Banks, C.E. An overview of graphene in energy production and storage applications. Journal of Power Sources, 196:4873-4885, 2011.

[16] Lochala, J.A., Zhang, H., Wang, Y., Okolo, O., Li,X., Xiao, J. Practical challenges in employing graphene for lithium-ion batteries and beyond. Small Methods, 1700099, 2017.

Graphene-Based Ultraviolet Photodetectors Using Zinc Oxide Thin Films

Nicholas A. Charipar, Heungsoo Kim, Kristin M. Charipar, Alberto Piqué
United States Naval Research Laboratory
4555 Overlook Ave. SW, Washington, DC 20375
USA
Email nicholas.charipar@nrl.navy.mil

Keywords: Defense; Graphene; Photodetector; Pulsed Laser Deposition; Ultraviolet; Zinc Oxide.

ABSTRACT

The broadband transparency of graphene from the UV to far-IR makes it an ideal candidate as a transparent electrode for optoelectronic applications. However, the intrinsic photoresponse of graphene is low and, as such, is not alone suitable for photodetection. As a method to improve photoresponse, zinc oxide has been studied extensively for photodetector applications because of its wide bandgap (~3.3 eV) and high exciton binding energy (~60 meV). By combining the advantageous properties of both zinc oxide and graphene, solar blind hybrid photodetectors were demonstrated using pulsed laser deposition for zinc oxide thin film growth. The electrical and optical properties, as well as surface morphology of the zinc oxide thin films as a function of growth pressure and film thickness, were characterized. Additionally, the effect of the zinc oxide thin film growth process on the graphene layer was also investigated. Two device architectures were fabricated and characterized, including zinc oxide graphene hybrid phototransistors and Schottky-type photodiodes.

1.0 INTRODUCTION

From a defense standpoint, there is a strong need for Ultraviolet (UV) detectors as there is an underutilized atmospheric window in the UV region of the electromagnetic spectrum. While there has been a proliferation of optical sensors in the battle space, none has been as pronounced as infrared detectors. While the atmospheric transmission losses are less in the infrared, they are strongly dependent on atmospheric conditions including water vapor. UV propagation on the other hand is less sensitive to water vapor as it is more transparent in the UV. Traditional photodetectors such as silicon have a modest bandgap of ~1 eV and, as such, show a peak sensitivity between the visible and near infrared. Because of this, these photodetectors require extensive filtering to ensure that the sensor is not overwhelmed by visible radiation. Photodetectors that do not respond to the visible portion of the solar spectrum are referred to as solar blind detectors. These solar blind detectors have significantly lower false alarm rates in applications, such as missile warning systems. Wide bandgap semiconductors offer an alternative to solar blind photoelectric detectors as they do not require fragile glass envelopes or vacuum to operate. Traditional photoconductive wide bandgap photodetectors rely on an interdigitated electrode design, which is detrimental to both detection efficiency and response time. These interdigitated electrodes shadow a fraction of the surface decreasing sensitivity. Secondly, the transit time is determined by the distance between the electrodes and the carrier mobility of the underlying material thereby limiting the response time of the detector.

The combination of low sheet resistance and ultralow absorption of 2.3% make graphene ideal as a transparent top conductor for photodetectors. This transparency enables devices with out-of-plane geometries which provide faster response times and lower loss compared to lateral device geometries. Graphene offers additional design freedom because it does not have to be grown directly

on the device of interest. Both wet and dry transfer processes allow for the device to be fabricated by conventional methods, where the graphene layer can be transferred onto the device as the final fabrication step. Alternatively, the device could be directly fabricated on graphene and an associated copper or silicon carbide superstrate. In the case of the silicon carbide superstrate, it is preferred to leave the superstrate in place because it exhibits a large bandgap and exceptional mechanical properties. Because of this, the device is environmentally protected which increases operational lifetime and ultimately reduces cost. On the other hand, a superstrate comprised of copper requires its eventual removal due to its lack of transparency. Depending on the adhesion between the device, graphene, and superstrate, it has been shown that the superstrate can be mechanically removed from the device and graphene layer. Unfortunately, it is not possible to do this in all cases, as the surface energies may not be favorable. Under these conditions it is necessary to remove the copper layer via chemical etching.

Zinc oxide, or ZnO, is a promising material for ultraviolet detection because of its wide direct bandgap of 3.37 eV and high exciton binding energy of 60 meV at room temperature [1]. While there are other wide bandgap semiconductors that exhibit similar properties such as GaN, ZnSe, and ZnS, zinc oxide also has the added advantage of having a higher degree of radiation resistance. The peak responsivity of ZnO can be easily adjusted by tuning the bandgap via doping. For example, the bandgap of ZnO can be tuned by Al-doping which has a direct effect on its transport properties such as conductivity, carrier density and mobility [2]. By adjusting the Al-doping, its mobility can be tuned from ~ 10 to 40 $cm^2V^{-1}s^{-1}$ while the direct band gap increases from 3.3 to 3.8 eV for Al-doped ZnO films. In addition, the bandgap of ZnO can be further increased up to ~6 eV by Mg-doping to extend its responsivity into the deep UV [3]. A photoconductive UV photodetector can be fabricated using a simple implementation comprised of a graphene / ZnO / metal thin film stack. High quality ZnO thin films with a relatively high mobility of ~40 $cm^2V^{-1}s^{-1}$ allow for high speed operation because of the reduced transit times and can be grown onto highly conductive, yet transparent graphene layers.

The graphene-based approach described here is compatible with ZnO based photodiode detectors such as ZnO p-n homojunctions and Schottky barrier photodiodes. Because graphene is ultrathin, these photodetectors can exhibit physical flexibility not achievable using traditional photodetectors such as silicon. This enables the possibility of applications requiring conformal arrays where optoelectronics can be applied to non-planar surfaces. In addition, because the detector is flexible and can be wrapped around a cylinder, it offers the possibility of truly omnidirectional sensing. Graphene as a transparent conductor provides a method of photodetection that is broadband with a fast response time, while highly sensitive at the same time. To demonstrate the aforementioned advantages, both a solar blind graphene / zinc oxide-based UV photodetector and a ZnO/graphene-based phototransistor are presented.

2.0 EXPERIMENTAL METHODS

Pulsed Laser Deposition (PLD) was used to grow ZnO thin films onto various substrates, including quartz, graphene/quartz, and graphene/SiO2/Si. All films were deposited using a KrF excimer laser (Lambda Physik LPX 205, 248 nm, 30 ns FWHM) with a repetition rate of 5 Hz. The pressure (10 – 100 mTorr), temperature (room temperature to 150 °C), and processing gas (O_2 and Ar) were varied to optimize the optical and electrical properties of the ZnO films. The incident laser was focused onto a rotating ZnO target (5 cm diameter) in a vacuum chamber with a laser fluence of 2 J/cm^2. Prior to the deposition, the chamber was evacuated to a base pressure below 10-5 Torr. The target-to-substrate distance was set to the maximum allowable in the system (~9 cm), which allowed for reactive species to thermalize. The number of laser shots was adjusted to yield various thicknesses of ZnO films, ranging from 20 to 100 nm.

Commercial graphene grown on Cu foils by chemical vapor deposition (Graphene Supermarket) was used for all experiments. A wet transfer process [4], [5], [6], [7] was used to fabricate the ZnO/graphene devices.

The commercial graphene/Cu substrate was first spin-coated with poly(methyl methacrylate), or PMMA, (Microchem, 495 PMMA A2), yielding a thickness of ~600 nm, followed by curing on a hot plate at 100°C for 2 min. The sample was then floated onto a solution consisting of 20% HNO_3 acid in water to remove the graphene on the back side of the substrate. It was then floated in a ferric chloride etchant solution for 2 hr to remove the Cu substrate. The PMMA/graphene film was then floated in a bath of deionized water and rinsed several times to clear the solution of any remaining etchant. The sample was then floated on a solution of ~0.2% HCl acid in water to remove any Cu particles that may have adhered to the graphene layer during the etching process. This substrate was then placed in a bath of deionized water where it was ready for transfer onto a receiving substrate. Both highly-doped Si substrates (0.001 – 0.005 Ω·cm) with a 285 nm SiO_2 layer and quartz substrates were used for the wet transfer of graphene. Once transferred, the devices were allowed to air dry. A small droplet of PMMA was then drop casted onto the graphene surface to encourage flattening of the film, followed by a 3 min bake at 60°C on a hot plate. The PMMA was removed in an acetone bath and rinsed in isopropanol and gently dried with nitrogen. ZnO thin films were subsequently grown via PLD on the surface of the graphene devices. As an alternative, ZnO was grown on the as-received graphene/Cu substrates. It was wet transferred following the identical procedure described above, resulting in the congruent transfer of the ZnO and graphene stack. Electrical contacts were fabricated via electron beam evaporation of Ti (5 nm) / Au (100 nm) using a shadow mask so as to avoid further lift-off processes that could contaminate or modify the device surfaces. Because the highly-doped Si substrates have SiO_2 on both sides, the SiO_2 on the backside was removed via laser micromachining so that an electrode can be attached when back-gating the device thereby removing an additional wet etching step. Additionally, because multiple devices were fabricated on each chip, an isolation line was laser micromachined around each individual graphene device.

Optical characterization was performed using an optical microscope (Olympus, BX51) as a first-line inspection. Raman spectroscopy (WITec, alpha300 R), operating at 532 nm (2.33 eV), was used to give insight into the structural and physical properties of both the graphene and ZnO. The optical transmission spectra were collected using a UV/Vis spectrophotometer (JASCO, V670), while surface morphology and roughness were analyzed using atomic force microscopy, or AFM, (Bruker, Dimension Icon). Photoillumination experiments were conducted using a 100 W Hg lamp fed via optical fiber through a spectrometer (Oriel, MS260i). From there, the light was coupled through a 10x microscope objective mounted on a probe station controlled via a semiconductor characterization system (Keithley, 4200). The illumination spot size used for these experiments was ~ 2 mm in diameter, while the intensity was maintained via computer-controlled attenuation.

3.0 RESULTS AND DISCUSSION

3.1 Pulsed Laser Deposition of ZnO Thin Films

A study of the ZnO growth process on various substrates, including quartz, graphene/quartz, graphene/copper, and graphene/SiO_2/Si was performed. The optimization for ZnO growth was first done on quartz substrates because the substrate material is not affected by the PLD process. When depositing ZnO on graphene surfaces, the PLD process must be optimized to reduce oxidation and degradation of the graphene surface. Thus, various different parameters were investigated for PLD of ZnO onto graphene surfaces and will be discussed in the following sections.

3.1.1 Quartz Substrates

ZnO thin films were grown on bare quartz substrates to characterize the processing parameters of the pulsed laser deposition process [8], [9], [10]. To characterize the optical properties of the deposited ZnO films, UV/Vis spectrophotometry was performed. The films were grown at varying temperatures, from room temperature up to 150°C, and at varying pressures, ranging from 1 to 100 mTorr. As the growth pressure increased, an increase in optical transmission was observed in conjunction with an increase in resistivity

[11]. The optical band gaps of 20 nm ZnO films grown at 20 mTorr and 100 mTorr were determined to be 3.29 eV and 3.24 eV, respectively, which can be seen in the Tauc plots in Figure 1.

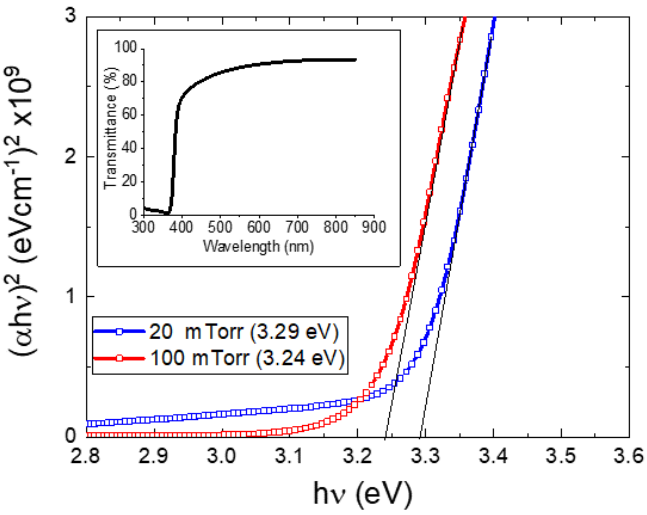

Figure 1: Tauc Plots of ZnO Film on Glass Substrates Grown at 150 ˚C at Both 20 mTorr and 100 mTorr, Showing Band Gaps of ~ 3.29 and 3.24 eV, Respectively. Inset: Transmission spectra (300 to 900 nm) of a typical ZnO film deposited on a quartz substrate.

3.1.2 Graphene/Cu Substrates

Raman spectroscopy was performed on ZnO grown on graphene/Cu substrates. Initial measurements show a strong background signal from the Cu substrate. This observation is due to photoluminescence of copper, which has a maximum peak at ~ 600 nm [12], [13]. Because the Raman measurements were carried out using a 532 nm (2.33 eV) laser, this photoluminescence effect is expected. This background can be subtracted out during analysis to reveal flat spectra. The effect of growth temperature and partial pressure were studied by growing ZnO films at both room temperature and also at 150°C, and by varying the partial pressure growth in an Ar atmosphere (both at 1 and 20 mTorr). While higher temperature processing in an oxygen environment can help grow higher quality ZnO films with fewer defects, these conditions can degrade the graphene through oxidation. The as-received graphene/Cu substrates show distinct peaks at 1580 and 2700 cm^{-1} representing the G and 2D bands, respectively. Because PLD is a high energy process, requiring laser fluences on the order of 2 J/cm^2, the target-to-substrate distance can also affect the quality of the films.

3.1.3 Graphene/Quartz Substrates

In addition to growth of ZnO films onto graphene/Cu substrates, thin film deposition of ZnO films on graphene/quartz substrates was also optimized by varying growth temperature and film thickness. It is known that the temperature greatly affects the quality of the ZnO film where higher growth temperature can help reduce defect density by reducing compressive stress induced in the films as displayed in Figure 2 (note highlighted area inside of yellow circles), where the evolution of cracking throughout the 100 nm film can be seen. This residual stress induced during the growth process is due to the different thermal expansion coefficient between the ZnO and graphene/quartz layers. For comparison, another 100 nm film was grown under similar conditions but at Room Temperature (RT). The morphology of the RT film is significantly

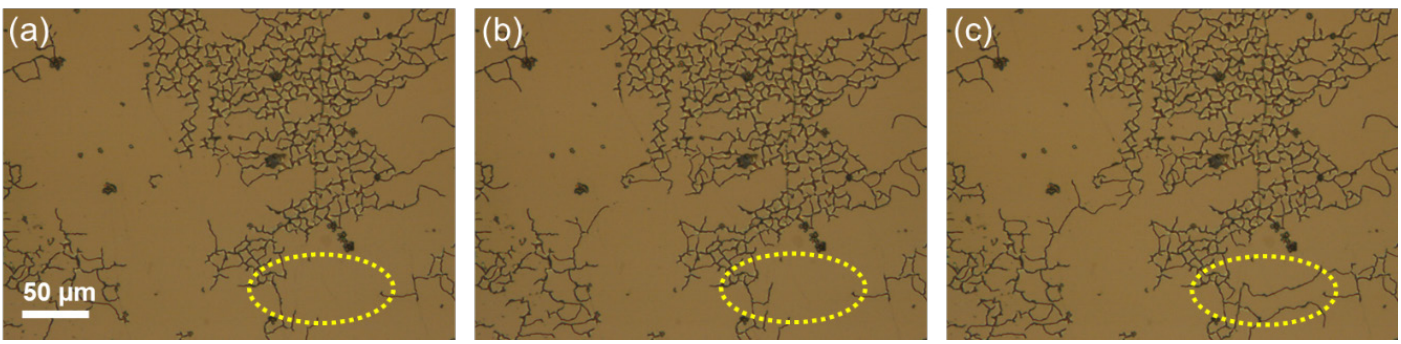

Figure 2: Time Lapse Optical Micrographs of 100 nm Thick ZnO Film (Grown at 100°C) at (a) 0 sec (b) 10 sec and (c) 20 sec Displaying the Evolution of Cracking in the Films. (Yellow circles are guides for the eye.)

different than that of those grown at high temperature; however, the RT film still exhibits wide-scale buckling.

The thickness and residual stress of the 100 nm thick films are likely the cause of the observed cracking and buckling. To determine the effect of film thickness on the quality of the film, two ZnO films (20 nm and 350 nm thick) were grown at room temperature. The 20 nm ZnO film is seen to lack the macroscopic defects, such as wrinkling and cracking, observed in the 100 nm films. The thicker film also appears to be of higher quality compared with the 100 nm films; however, some small areas of cracking are observed. The surface morphology was analyzed by Atomic Force Microscopy (AFM) on the 350 nm thick ZnO film. The measured rms surface roughness was ~ 1.84 nm, indicative of a very smooth film (Figure 3). A similar surface roughness was observed for 20 nm films.

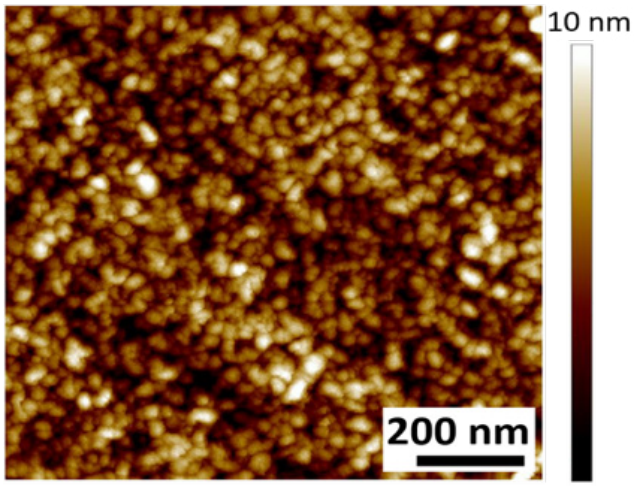

Figure 3: Atomic Force Microscope (AFM) Image of ZnO (350 nm) Film, Showing an rms Roughness of ~1.84 nm.

The high quality 20 nm film that exhibited no cracking or wrinkling was further characterized via Raman spectroscopy. Before deposition, Raman of the graphene/quartz substrates reveals two distinct graphene peaks, at ~ 1606 cm^{-1} and ~ 2684 cm^{-1}, which correspond nicely to expected G and 2D peaks with an additional peak at 440 cm^{-1}, representing the underlying quartz substrate (Figure 4(a)). After the deposition of the 20 nm ZnO film, the Raman data again shows two distinct graphene peaks at 1586 cm^{-1} (G) and 2684 cm^{-1} (2D) (Figure 4(b)). In addition, a broad peak is observed at 474 cm^{-1}, characteristic of a ZnO film with oxygen deficiency, interstitial Zn, or the formation of free carriers [9]. The typical E2 peak, normally observed at 437 cm^{-1} is absent, which is expected for films grown at low or room temperature. Because of the growth temperature and the fluences required for PLD, compressive stress on the ZnO can be induced in addition to the abovementioned defects. The optimization process for growth of ZnO must balance the quality (transmission and resistivity) of the ZnO film with the quality of the underlying graphene film. In other words, to minimize oxidation of the graphene layer during the growth of ZnO, the ZnO deposition temperature must be minimized. The D band peak observed at 1349 cm^{-1} for graphene indicates defects in the graphene film via the formation of graphene oxide. The Raman spectra for ZnO grown on graphene/quartz substrates as well as ZnO grown on graphene/copper substrates followed by a subsequent wet transfer onto a SiO_2/Si substrate are shown in Figures 4(c) and 4(d), respectively.

In addition to studying the effect of ZnO film thickness and growth temperature on the resulting films, the effect of oxygen growth pressure was also investigated. ZnO films were grown at room temperature with a thickness of 20 nm at both 20 mTorr and 100 mTorr onto graphene/quartz substrates. The effect of pressure on bandgap can be seen in Figure 1, where increasing pressure causes a minimal decrease in bandgap from 3.29 to 3.24 eV. In addition, the growth pressure impacts the electrical properties of the film as well as the quality of the underlying graphene layer. Raman spectra can be seen for films grown at both 20 mTorr and 100 mTorr in Figure 5(a) and Figures 5(b), respectively. The ratio of the 2D to G graphene peaks increases from 0.26 to 0.54 (an increase of over 200%) with increasing growth pressure, indicating that defects are reduced at higher pressure. Furthermore, the resistivity of the film grown at higher pressure (0.11 Ω cm) is roughly 10 times higher than that of the film grown at lower pressure (0.012 Ω·cm). This increased resistivity at high pressure is attributed to decreased oxygen vacancies in the film. However, the intensity of the laser produced plasma may be reduced at higher oxygen deposition pressure due to more scattering with oxygen gas molecules

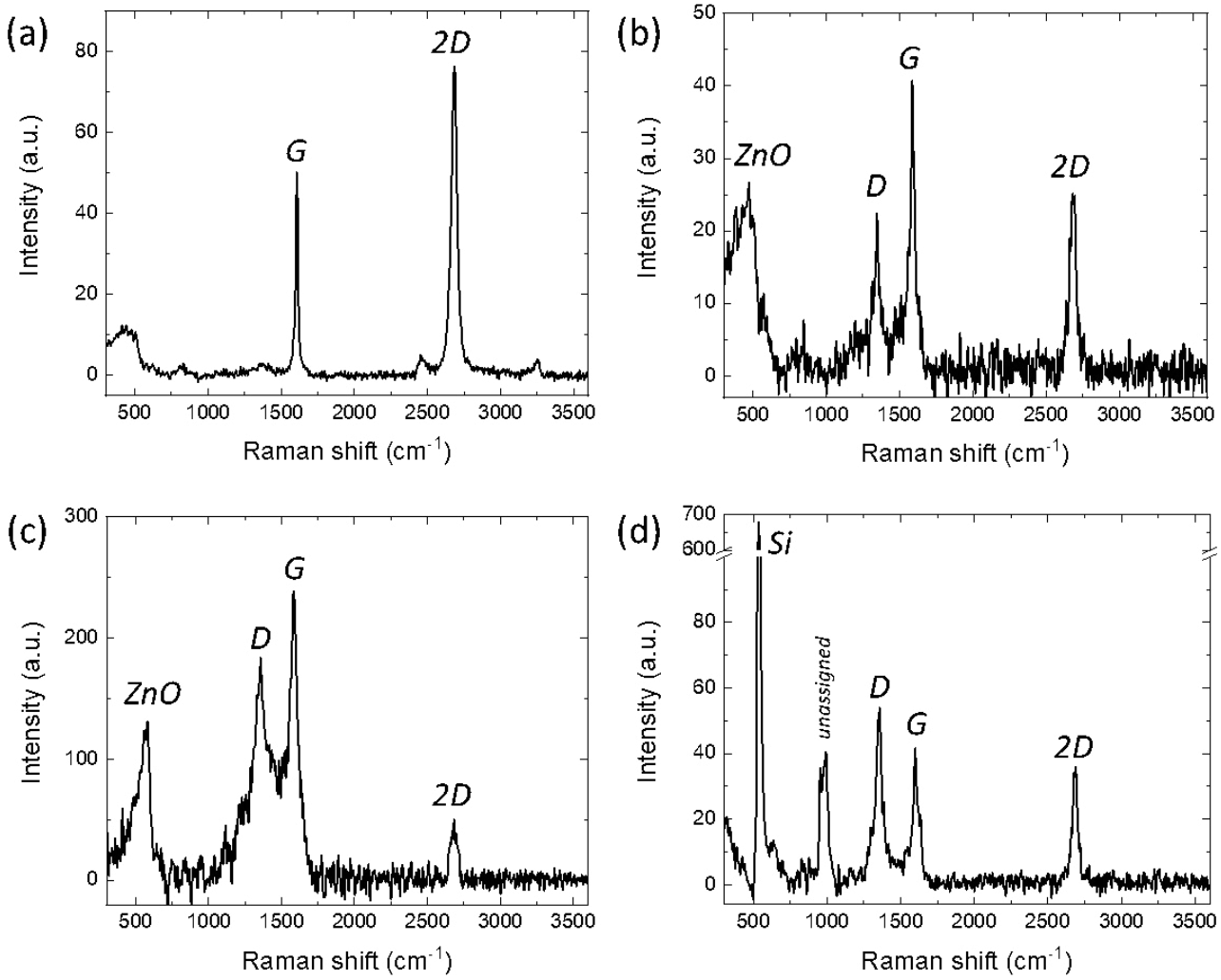

Figure 4: Raman Spectra of (a) Graphene on Quartz, (b) ZnO (20 nm) on Graphene/Quartz, (c) ZnO (20 nm) / Graphene / Cu (Before Wet Transfer), and (d) ZnO (20 nm) / Graphene / SiO2 / Si (After Wet Transfer).

during deposition, resulting in a less damaged graphene layer [14].

In addition to controlling growth temperature, the role of target-to-substrate distance in conjunction with growth gas and pressure plays an important role in the quality of the ZnO films. By increasing the target-to-substrate distance to the maximum allowable in the system, reactive species are allowed to thermalize more before being depositing onto the receiving substrate. The use of a buffer gas, such as oxygen, also allows for energetic species to thermalize before deposition. This is especially important when depositing ZnO films onto graphene layers, where the graphene is susceptible to oxidation and degradation.

3.2 Photodetector Architecture

Because of the synergistic relationship between ZnO and graphene, a wide variety of optoelectronic devices have become possible [15]. ZnO exhibits a wide direct band gap of ~ 3.3 eV and a high exciton binding energy of ~ 60 meV while graphene exhibits high carrier mobility, optical transparency, and both mechanical and chemical stability. By combining the advantages of both materials, ZnO/graphene hybrid photodetectors offer high responsivity, high detectivity and fast response. The architecture of the devices depends on the application, where the ZnO can be nanostructured to further enhance the properties of the device.

3.2.1 Photodetector (ZnO/Graphene/Quartz)

ZnO/graphene heterostructures can be used as Schottky photodiodes, similar to metal-semiconductor Schottky junctions [16], [17]. Lee et al. demonstrate a ZnO/graphene/SiO2/Si Schottky photodiode, where the ZnO (340 nm) was deposited via RF magnetron sputtering. The Schottky barrier height was observed to be 0.684 eV, where the magnitude of the photocurrent is highly dependent on wavelength [18]. Zhang et al. developed a

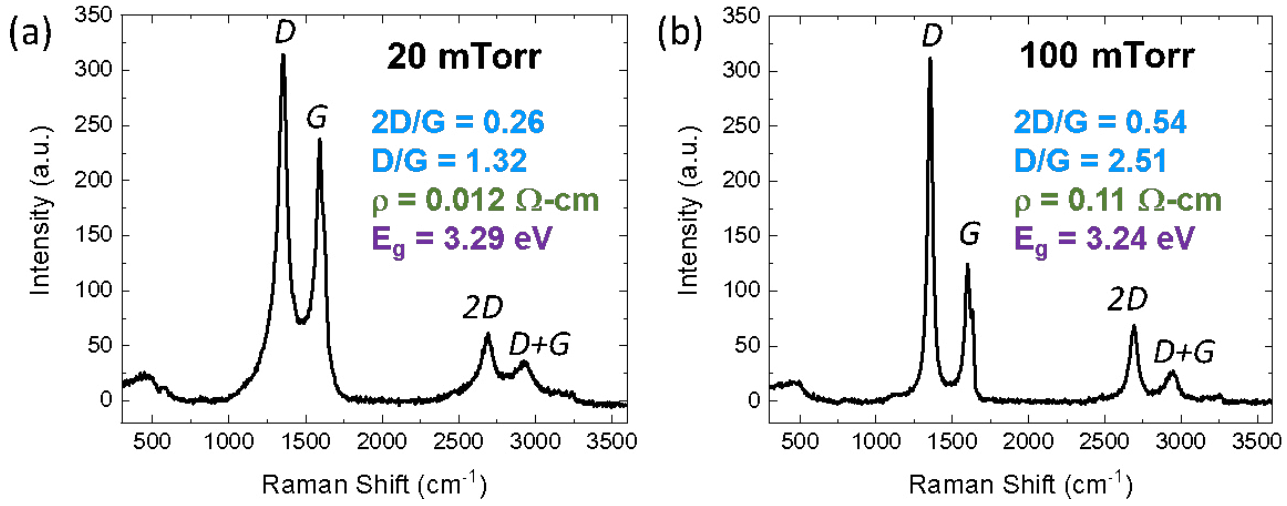

Figure 5: Raman Spectra of 20 nm ZnO Films Grown at Room Temperature via PLD on Graphene/Quartz at both (a) 20 mTorr and (b) 100 mTorr of O2. The corresponding electrical resistivity, optical bandgap values, and both 2D/G and D/G ratio values are also shown.

Schottky photodiode by creating a metal/ZnO/graphene structure, where an electrode is evaporated on the backside of a ZnO wafer and graphene is transferred onto the topside [19]. Because graphene is optically transparent, the graphene acts as the top electrode.

Quartz/graphene/ZnO/Ti/Au photodetectors (Figure 6(a)) fabricated via PLD of ZnO were characterized, showing I-V curves that exhibit a weak Schottky behavior with a signification amount of leakage current. This is expected due to the difficulty in growing high quality ZnO on graphene as discussed previously. The leakage current is likely exacerbated by the thin, 20nm, ZnO which likely has pin hole defects resulting in shorting between the graphene and gold layers. The photoresponse of this structure when illuminated with 365 nm radiation from a Hg-source (after a monochromator) is shown in Figure 6(b). The responsivity of the device was determined to be 2 AW^{-1} at a bias voltage of 5V. The rise time (10 % to 90 %) is 89 sec which is limited by oxygen migration in the ZnO films [14].

3.2.2 Phototransistors (ZnO/Graphene/SiO_2/Si)

In an effort to improve sensitivity, we investigated a graphene hybrid architecture similar to a phototransistor. While this phototransistor geometry does not use graphene as a transparent electrode like the Schottky-type photodetector, it does offer the benefit of higher sensitivity. Graphene/ZnO heterostructures as UV phototransistors have been demonstrated using ZnO nanowires, graphene foams, and quantum dots, to

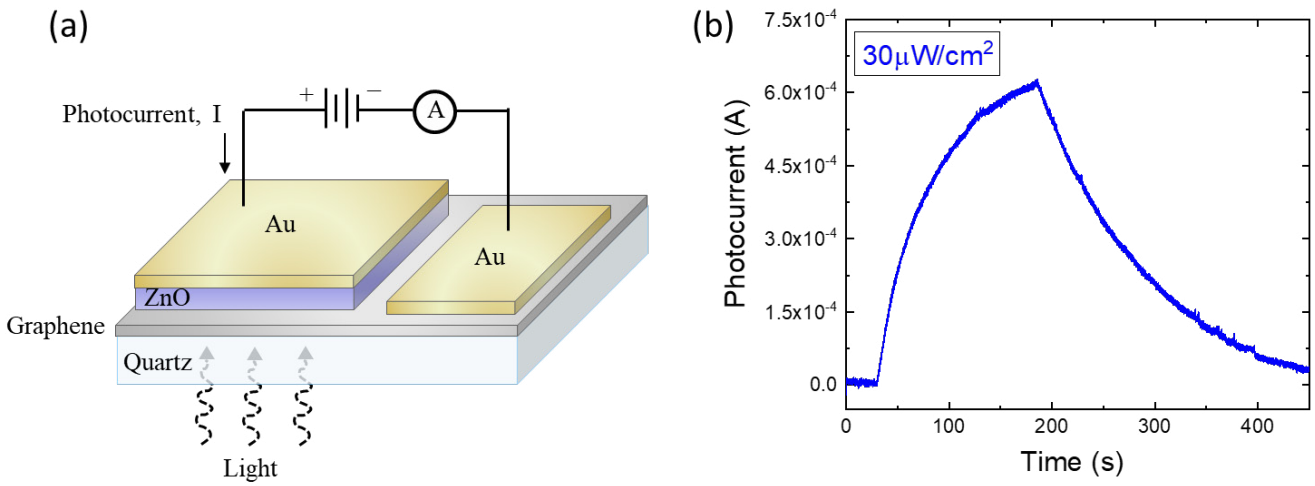

Figure 6: (a) Schematic Diagram and (b) Temporal Photoresponse of Schottky Photodiode (ZnO/Graphene/Quartz).

name a few. Dang et al. demonstrated a UV phototransistor based on ZnO nanorods / graphene heterostructures that showed photocurrent responsivity of 2.5 x 10^6 AW^{-1} with a gain of 8.3 x 10^6 [20], [21]. For the current work, a similar phototransistor architecture was fabricated using PLD-grown ZnO in combination with laser micromachining to pattern individual devices. These devices were fabricated on highly-doped Si substrates with a 285 nm SiO_2 thermal oxide layer using the techniques described earlier in the experimental section. The final ZnO active area was 2 mm x 0.5 mm, where two devices can be seen in an optical micrograph in Figure 7(a). Additionally, a schematic of this phototransistor architecture is seen in Figure 7(b).

The first devices tested consisted of 20 nm ZnO films grown at 20 mTorr, yielding a resistivity of 0.012 Ω·cm and a bandgap of 3.29 eV. The phototransistors were gated from -70 V to 70 V at a drain voltage, V_D, of 1 V at both dark current and an intensity (λ = 365 nm) of 63 μW/cm^2. As seen in Figure 8(a), there is an observed shift in drain current when UV light is applied. Furthermore, transfer characteristics of the devices can be seen in the I-V curves in Figure 3-8(b), where drain voltage, V_D, is varied from -5 V to 5 V, with no gating (V_G = 0 V).

Temporal measurements were conducted over various fluences ranging from 38 μW/ cm^2 up to 1.05 mW/cm^2. These tests yield a responsivity of up to ~ 120 AW-1 at low fluence (38 μW/ cm^2).

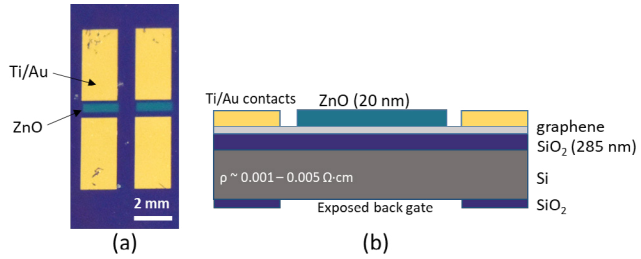

Figure 7: (a) Optical Micrograph and (b) Schematic Diagram of Fabricated ZnO/Graphene Phototransistor Devices.

Other devices were fabricated using a higher growth pressure of 100 mTorr to determine if the films resulted in better performance. These ZnO films yielded a resistivity of 0.11 Ω·cm and a bandgap of 3.24 eV; however, the resulting responsivity was very similar (~117 AW^{-1} at 38 μW/cm^2) to the devices with ZnO grown at 20 mTorr.

The spectral response of the phototransistors was measured as a function of incident wavelength, showing superior solar blind performance, as seen in Figure 9.

4.0 CONCLUSION

In conclusion, both UV Schottky-type photodetectors and phototransistors were fabricated by the direct growth of ZnO thin films onto graphene. It is shown that the effects of PLD growth conditions strongly influence the quality of the underlying graphene via oxidation to graphene oxide. Through process optimization, including studying the effect of film thickness on device performance and

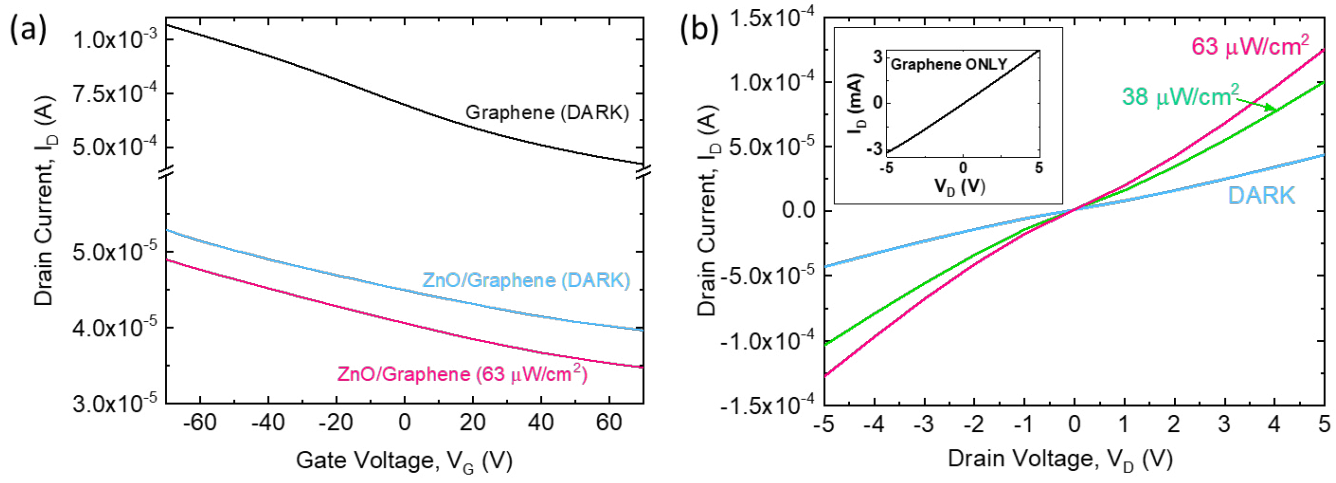

Figure 8: (a) Effect of Voltage Gating on Drain Current for Graphene FET (without UV Illumination) and ZnO/Graphene Phototransistors (with and without UV Illumination) at a Source-Drain Voltage, V_D, of 1 V. (b) I-V Characterization of ZnO/Graphene Phototransistors at UV Fluences Of 0 (DARK), 38, and 63 μw/Cm^2 With V_G Fixed at 0 V. (Inset: I-V Characterization Of Graphene-Only Device Without UV Illumination).

altering the device geometry such as channel width, it is expected that the quality of both the ZnO and graphene can be improved further. A responsivity of 120 AW^{-1} was observed for the phototransistor hybrid devices as well as superior UV spectral selectivity below ~ 400 nm. These UV photodetector architectures illustrate how the use of ZnO/ graphene heterostructures enables the fabrication of new types of photodetectors.

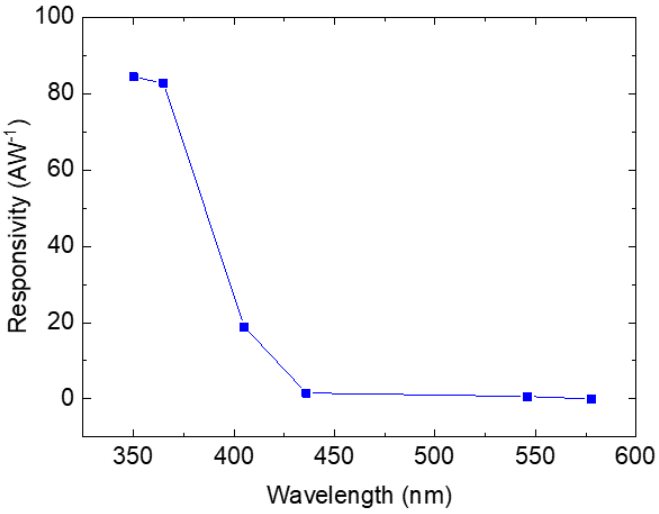

Figure 9: Responsivity of ZnO/Graphene Phototransistors as a Function of Incident Wavelength (V_D = -5 V, V_G = 0 V, and P ~ 50 µw/cm²).

5.0 REFERENCES

[1] Liang, F.-X., Gao, Y., Xie, C., Tong, X.-W., Li, Z.-J., Luo, L.-B. Recent advances in the fabrication of graphene-ZnO heterojunctions for optoelectronic device applications. *Journal of Materials Chemistry C*, 6:3815-3833, 2018.

[2] Kim, H., Piqué, A., Horwitz, J.S., Murata, H., Kafafi, Z.H., Gilmore, C.M., Chrisey, D.B. Effect of aluminium doping on zinc oxide thin films grown by pulsed laser deposition for organic light-emitting diodes. *Thin Solid Films*, 377-378:798-802, 2000.

[3] Bhattacharya, P., Das, R.R., Katiyar, R.S. Fabrication of stable wide-band-gap ZnO/MgO multilayer thin films. *Applied Physics Letters*, 83:2010, 2013.

[4] Suk, J.W., Kitt, A., Magnuson, C.W., Hao, Y., Ahmed, S., An, J., Swan, A.K., Goldberg, B.B., Ruoff, R.S. Transfer of CVD-grown monolayer graphene onto arbitrary substrates. *ACS Nano*, 5:6916-6924, 2011.

[5] Liang, X., Sperling, B.A., Calizo, I., Cheng, G., Hacker, C.A., Zhang, Q., Obeng, Y., Yan, K., Peng, H., Li, Q., Zhu, X., Yuan, H., Hight Walker, A.R., Liu, Z., Peng, L.-M., Richter, C.A. Toward clean and crackles transfer of graphene. *ACS Nano,* 5:9144-9153, 2011.

[6] Li, X., Zhu, Y., Cai, W., Borysiak, M., Han, B., Chen, D., Piner, R.D., Colombo, L., Ruoff, R.S. Transfer of large-area graphene films for high-performance transparent conductive electrodes. *Nano Letters*, 9:4359-4363, 2009.

[7] Li, X., Cai, W., An, J., Kim, S., Nah, J., Yang, D., Piner, R., Velamakanni, A., Jung, I., Tutuc, E., Banerjee, S.K., Colombo, L., Ruoff, R.S. Large-area synthesis of high-quality and uniform graphene films on copper films. *Science*, 324:1312-1314, 2009.

[8] Exarhos, G.J., Sharma S.K. Influence of processing variables on the structure and properties of ZnO films. *Thin Solid Films*, 270:27-32, 1995.

[9] Zeng, J.N., Low, J.K., Ren, Z.M., Liew, T., Lu, Y.F. Effect of deposition conditions on optical and electrical properties of ZnO films prepared by pulsed laser deposition. *Applied Surface Science*, 197:362-367, 2002.

[10] Wisz, G., Virt, I., Sagan, P., Potera, P., Yavorskyi, R. Structural, optical and electrical properties of zinc oxide layers produced by pulsed laser deposition method. *Nanoscale Research Letters*, 12:253, 2017.

[11] Srikant, V., Clarke, D.R. On the optical band gap of zinc oxide. *Journal of Applied Physics*, 83:5447-5451, 1998.

[12] Mooradian, A. Photoluminescence of metals. *Physical Review Letters*, 22:185-187, 1969.

[13] Costa, S.D., Righi, A., Fantini, C., Hao, Y., Magnuson, C., Colombo, L., Ruoff, R.S., Pimenta, M.A. Resonant Raman spectroscopy of graphene grown on copper substrates. *Solid State Communications*, 152:1317-1320, 2012.

[14] Kim, H. Pulsed Laser Deposition of Thin Films. In Pulsed Laser Deposition of Thin Films: Applications-Led Growth of Functional Materials, R. Eason (Ed.), Wiley-Interscience, 239-260, 2006.

[15] Xu, Q., Cheng, Q., Zhong, J., Cai, W., Zhang, Z., Wu, Z., Zhang, F. A metal-semiconductor-metal detector based on ZnO nanowires grown on a graphene layer. *Nanotechnology,* 25:055501, 2014.

[16] Lee, Y., Kim, D.Y., Lee, S. Low-power graphene/ZnO Schottky UV photodiodes with enhanced lateral Schottky barrier homogeneity. *Nanomaterials*, 9:799, 2019.

[17] Lee, S., Lee, Y., Kim, D.Y., Song, E.B., Kim, S.M. Back-gate tuning of Schottky barrier height in graphene/zinc-oxide photodiodes. *Applied Physics Letters*, 102:242114, 2013.

[18] Lee, H., An, N., Jeong, S., Kang, S., Kwon, S., Lee, J., Lee, Y., Kim, D.Y., Lee, S. Strong dependence of photocurrent on illumination-light colors for ZnO/graphene Schottky diode. *Current Applied Physics*, 17:552-556, 2017.

[19] Zhang, T.-F., Wu, G-A., Wang, J.-Z., Yu, Y.-Q., Zhang, D.-Y., Wang, D.-D., Jiang, J.-B., Wang, J.-M., Luo, L.-B. A sensitive ultraviolet light photodiode based on graphene-on-zinc oxide Schottky junction. *Nanophotonics*, 6:1073-1081, 2017.

[20] Dang, V.Q., Trung, T.Q., Duy, L.T., Kim, B.-Y., Siddiqui, S., Lee, W., Lee, N.-E. High-performance flexible ultraviolet (UV) phototransistor using hybrid channel of vertical ZnO nanorods and graphene. *ACS Applied Materials & Interfaces*, 7:11032-11040, 2015.

[21] Dang, V.Q., Trung, T.Q., Kim, D.-I., Duy, L.T., Hwang, B.-U., Lee, D.-W., Kim, B.-Y., Toan, L.D., Lee, N.-E. Ultrahigh responsivity in graphene-ZnO nanorod hybrid UV photodetector. *Small,* 11:3054-3065, 2015.